

# Geometry-Aware Discretization Error of Diffusion Models

Samuel Hurault  
Univ. Gustave Eiffel, CNRS, LIGM  
samuel.hurault@univ-eiffel.fr

Thomas Moreau  
Univ. Paris-Saclay, Inria, CEA  
thomas.moreau@inria.fr

Gabriel Peyré  
CNRS, ENS, PSL Université  
gabriel.peyre@ens.fr

## Abstract

Practical diffusion sampling is a numerical approximation problem: under a fixed inference budget, one must simulate a reverse-time ODE or SDE using only a limited number of denoising steps, so discretization error is often the dominant source of error. Existing non-asymptotic analyses provide convergence guarantees, but are typically too loose and too insensitive to diffusion parameters to guide practical design: broad families of schedules receive the same rates, which depend on coarse worst-case quantities such as the dimension or the drift Lipschitz constant. We take a less ambitious but more informative route. In the exact-score setting, we derive first-order asymptotic expansions of the Euler-Maruyama weak and Fréchet discretization errors. These formulas hold for general smooth reverse diffusions and become fully explicit under Gaussian data. They show how discretization error adapts to the geometry of the data through the covariance spectrum, and how this geometry interacts with key diffusion parameters, including the diffusion schedules and the diffusion-term coefficient. This yields tractable objectives for geometry-aware parameter optimization. Finally, we show that the qualitative predictions of the Gaussian formulas remain robust across diffusion sampling problems with different geometries, including image generation on different datasets and image posterior sampling.

## 1 Introduction

Diffusion and score-based generative models have become a central paradigm for high-dimensional generation [Ho et al., 2020, Song et al., 2021, Dhariwal and Nichol, 2021, Lipman et al., 2022]. Their main practical limit, however, remains sampling time: generating one sample requires integrating a reverse-time ODE or SDE through many sequential denoising steps, each involving an expensive neural network evaluation. Under a fixed inference budget, one is therefore forced to use a coarse time-discretization of the dynamics, and the resulting discretization bias quickly becomes a dominant source of sampling error. The necessity to reduce the number of denoising steps also motivates recent families of fast-generative models [Song et al., 2023, Liu et al., 2022, Deng et al., 2026].

Coarse discretization can favor different parameterizations of the sampling dynamics, which should therefore be adapted to reduce discretization error. This practical question is complicated by the size of the parameter space. A diffusion sampler is specified by many choices: the shape of the noise schedule (e.g. polynomial, exponential), the rescaling schedule (e.g., variance preserving, variance exploding), the level of stochasticity or the stepsize schedule [Karras et al., 2022, Song et al., 2021, Nichol and Dhariwal, 2021]. In practice, guidance on how to tune these parameters remains largely empirical, relying on optimization for specific models and datasets rather than on predictive theory. Existing approaches for coarse-budget adaptation

rely on hand-designed grids [Lu et al., 2022, 2023], adaptive stepsize heuristics [Jolicœur-Martineau et al., 2021, Gao et al., 2023, Xue et al., 2024], or data-driven optimization [Watson et al., 2022, Wang et al., 2023, Li et al., 2023, Xia et al., 2023].

On the theoretical side, most existing analyses of discrete diffusion sampling provide non-asymptotic convergence guarantees [De Bortoli, 2022, Lee et al., 2023, Li et al., 2024a, Benton et al., 2024, Conforti et al., 2025, Beyler and Bach, 2025]. This typically yields bounds that describe how the discretization error scales with the number of steps, the ambient dimension, or regularity parameters of the score. These results are important for consistency and complexity, but they are much less informative for tuning diffusion parameters: different parameterizations often share the same rates, while the constants are driven by coarse worst-case quantities such as the dimension or the drift Lipschitz constant [Chen et al., 2025]. As a consequence, current theory does not sharply explain which schedules or stochasticity levels should be preferred under small sampling budget, and in particular how these choices depend on the specific geometrical properties of the target distribution.

In this paper, we study the Euler–Maruyama discretization error of diffusion sampling in the exact-score setting, with formulas that make the dependence on diffusion parameters explicit. Rather than seeking non-asymptotic control of the full sampling error, we derive small-stepsize expansions for the errors on the first two moments and the resulting Fréchet distance. This restricted objective yields tractable formulas for analyzing how diffusion parameters interact with target geometry.

We next specialize these expansions to Gaussian data, for which the discretization error decouples along covariance eigenspaces. Although the Gaussian case is not our final objective, it yields explicit parameter-design criteria and qualitative predictions that we later compare against non-Gaussian experiments. It is a natural and well-motivated theoretical testbed: recent empirical and theoretical works [Wang and Vastola, 2024, 2023, Li et al., 2024b] suggest that Gaussian or nearly linear score models can provide insight into more general regimes. Pierret and Galerne [2024] already observed this eigenspace decoupling, but do not derive error formulas suitable for parameter optimization. Related scheduler-design approaches also use Gaussian simplifications, either through alternative criteria such as the drift Lipschitz constant [Chen et al., 2025], which depends only on the smallest covariance eigenvalue, or under isotropic covariance assumptions [Sabour et al., 2024]. In contrast, our analysis characterizes how discretization error depends on a full anisotropic covariance spectrum.

Our contributions are the following:

- For general data distributions, we establish a first-order small-stepsize weak-error expansion for Euler–Maruyama discretization. Specializing this expansion yields first-order expressions for the mean and covariance errors, which can be combined into a corresponding Fréchet error.
- For Gaussian data, we make these formulas fully explicit, obtaining closed-form expressions that expose how discretization error depends on the sampling parameters – namely, the diffusion-term coefficient and the noise and rescaling schedules – as well as on the covariance spectrum of the target distribution.
- We use these formulas to derive geometry-aware design principles for the sampling parameters. In particular, we show that the optimal diffusion-term coefficient decreases linearly with the stepsize, with a spectrum-dependent slope; characterize how the optimal rescaling schedule depends on the scale and decay of the covariance power spectrum; and explain why polynomial noise schedules are naturally adapted to anisotropic spectra. We validate these predictions in real image-sampling experiments across different datasets and posterior distributions, showing that the optimal parameters vary as theory predicts from the corresponding covariance spectra.

The paper is organized as follows. Section 2 recalls the diffusion framework, Section 3 derives the general first-order expansions, and Section 4 gives their explicit Gaussian instantiation. Section 5 then uses these formulas for parameter design and compares the predictions with image sampling.

## 2 Preliminaries on diffusion sampling

Diffusion models generate samples from a target distribution  $p_{\text{data}}$  by reversing a forward noising process. We use a unified parameterization with a scale schedule  $\eta_t$  and a noise schedule  $\sigma_t$ , and define the forward process by

$$X_0 \sim p_{\text{data}}, \quad \text{for } t < T, \quad dX_t = \frac{\dot{\eta}_t}{\eta_t} X_t dt + \eta_t \sqrt{2\sigma_t \dot{\sigma}_t} dW_t. \quad (1)$$

The marginal distribution of this linear SDE is [Davis, 1977]  $p_t \propto p_{\text{data}}\left(\frac{\cdot}{\eta_t}\right) * \mathcal{N}(0, (\eta_t \sigma_t)^2 \text{Id})$ . Hence, if  $\mu_{\text{data}}$  and  $\Sigma_{\text{data}}$  denote the mean and covariance of  $p_{\text{data}}$ ,

$$\mu_t := \mathbb{E}[X_t] = \eta_t \mu_{\text{data}}, \quad \Sigma_t := \text{Cov}[X_t] = \eta_t^2 (\Sigma_{\text{data}} + \sigma_t^2 \text{Id}).$$

This unified notation recovers several standard scheduler choices. Variance Preserving diffusion corresponds to  $\eta_t = (1 + \sigma_t^2)^{-1/2}$ , for which the forward process converges to  $\mathcal{N}(0, \text{Id})$  as  $T \rightarrow \infty$ . VE diffusion sets  $\eta_t = 1$ , for which the variance grows with time. The noise schedule  $\sigma_t$  typically starts at  $\sigma_0 = 0$  (or close to 0) and increases sharply as  $t$  approaches  $T$ , reaching a large terminal value  $\sigma_T$ , with geometric [Song et al., 2021] or polynomial [Karras et al., 2022] parametrization. Flow matching and stochastic interpolants [Lipman et al., 2022, Albergo et al., 2023] also fall within this formulation, with  $\eta_t = T - t$  and  $\sigma_t = t/(T - t)$  for linear interpolation. More generally, we use the following assumptions on the schedules  $(\sigma_t, \eta_t)$ :

**Assumption 1.** We assume, denoting  $\beta_t := \frac{\dot{\eta}_t}{\eta_t}$  and  $\xi_t := \eta_t^2 \dot{\sigma}_t \sigma_t$ :

(i)  $\eta, \sigma \in \mathcal{C}([0, T]) \cap \mathcal{C}^\infty((0, T])$ ,  $\eta_t > 0$ ,  $\sigma_t \geq 0$ ,  $\eta_0 = 1$ ,  $\sigma_0 = 0$  and  $\beta_t, \xi_t \in \mathcal{C}^\infty[0, T]$ .

(ii) (**Optional**) Assume for  $t \rightarrow 0$ :  $\beta_0 = 0$  and  $\xi_0 = 0$ , and for  $t = T$ :

$$\text{As } \sigma_T = \sigma_{\max} \rightarrow \infty, \quad \sigma_T^{-(1+\alpha)} \frac{\dot{\eta}_T}{\eta_T} \rightarrow 0, \quad \sigma_T^{-2\alpha} \left( \frac{\dot{\eta}_T}{\eta_T} + \frac{\dot{\sigma}_T}{\sigma_T} \right) \rightarrow 0.$$

Assumption 1(i) ensures integrability of (1). Assumption 1(ii) is only used to simplify the Gaussian error formulas in Proposition 1. In this assumption, the time horizon  $T < \infty$  is kept fixed, and the limit is taken with respect to the terminal noise level  $\sigma_T = \sigma_{\max} \rightarrow \infty$ . It is satisfied, for example, by VP schedules and by VE schedules when  $\alpha > 0$ . We keep it optional because it may fail in some settings, such as flow matching with linear interpolation.

**Continuous diffusion sampling** Sampling is performed by reversing the forward noising process (1). Following Song et al. [2021], we consider the reverse-time dynamics started from  $p_T$ , with marginals  $q_t := p_{T-t}$ . As detailed in Appendix A.1, this backward process follows the SDE:

$$Y_0 \sim p_T, \quad \text{for } t \in [0, T], \quad dY_t = v_t(Y_t)dt + \sqrt{2a_t} dW_t. \quad (2)$$

where the drift term  $v_t$  and the diffusion term  $a_t$  satisfy:

$$\begin{cases} v_t(x) = -\frac{\dot{\eta}_{T-t}}{\eta_{T-t}} x + (1 + \alpha_t) \eta_{T-t}^2 \sigma_{T-t} \dot{\sigma}_{T-t} \nabla \log p_{T-t}(x) \\ a_t = \alpha_t \eta_{T-t}^2 \sigma_{T-t} \dot{\sigma}_{T-t} \end{cases}$$

The parameter  $\alpha_t \geq 0$  controls the magnitude of the diffusion term. When  $\alpha_t = 0$ , the SDE reduces to a non-stochastic ODE. In most of the diffusion sampling literature,  $\alpha_t$  is fixed by default to 1 or to 0 [Song et al., 2021, Ho et al., 2020]. In the rest of the paper, we consider  $\alpha_t = \alpha$  constant in time.

**Discretized diffusion sampling** In practice, the reverse SDE cannot be simulated exactly and must be discretized. In this work, we study the Euler–Maruyama (EM) scheme, which is the standard discretization used in practical samplers, with  $K$  iterations and constant step size  $\gamma = T/K$ :

$$\hat{Y}_0 \sim q_0, \text{ for } k < K \text{ and } t_k := \gamma k, \quad \hat{W}_k \sim \mathcal{N}(0, \text{Id}), \quad \hat{Y}_{k+1} = \hat{Y}_k + \gamma v_{t_k}(\hat{Y}_k) + \sqrt{2\gamma a_{t_k}} \hat{W}_k \quad (3)$$

We prove in Appendix A.3 that using a time-dependent stepsize  $\gamma_t$ , instead of a constant  $\gamma$ , corresponds to a reparameterization of time in the schedules  $\sigma_t$  and  $\eta_t$ . We therefore restrict ourselves to uniform-step discretizations and let the schedules absorb these time changes.

**Other sources of error.** Beyond discretization, sampling also suffers from score-approximation and initialization errors [Hurault et al., 2025, Beyler and Bach, 2025]. Our theoretical results are derived in the exact-score setting, and our experiments use small stepsizes, where discretization bias is expected to dominate. In Appendix A.2, we show that the initialization error vanishes as  $\sigma_T \rightarrow \infty$ , independently of  $\eta_t$ , whereas the discretization error studied here persists in this large-terminal-noise regime, which is adopted here (see Proposition 1).

### 3 First-order asymptotic control of the weak and Fréchet discretization errors

In this section, we derive a first-order expansion, for small stepsize  $\gamma$ , of the Euler–Maruyama discretization error associated with the SDE (2). We first give in Theorem 1 the expansion of the general weak error, defined for a test function  $f$  by  $\mathbb{E}[f(\hat{Y}_k)] - \mathbb{E}[f(Y_{t_k})]$ . We then discuss the ODE case, in which the error has a simple interpretation. Finally, in Corollary 1, we specialize the result to obtain first-order discretization errors for the mean and covariance.

The weak error in Theorem 1 is derived for a general drift  $v_t$  and diffusion coefficient  $a_t$ . We do not aim to establish a minimal regularity framework here. Instead, we assume that  $a_t$  and  $v_t$  are smooth, with  $a_t \geq 0$ , that  $v_t$  has at most linear growth, and that sufficiently many spatial and time derivatives of  $v_t$  are bounded. These assumptions ensure, in particular, that the reverse SDE (2) admits a unique strong solution and that the flow derivatives appearing in the theorem are well defined.

We now introduce the stochastic calculus quantities that appear in the weak-error formula.

**Definition 1** (Flow derivatives and infinitesimal generator). *For  $0 \leq s \leq t \leq T$ , let  $\Phi_{t,s}$  denote the stochastic flow map associated with SDE (2): for each  $x \in \mathbb{R}^d$ ,  $\Phi_{t,s}(x)$  is the value at time  $t$  of the solution started from  $x$  at time  $s$ . Along the trajectory  $(Y_t)_{t \in [0, T]}$ , we define the stochastic Jacobian, Hessian, and Laplacians of the flow by:*

$$J_{t,s}(Y) := \nabla_x \Phi_{t,s}(x)|_{x=Y_s}, \quad H_{t,s}(Y) := \nabla_x^2 \Phi_{t,s}(x)|_{x=Y_s}, \quad \Delta_{t,s}(Y) := (\Delta \Phi_{t,s}(x)|_{x=Y_s})_{i \in \llbracket 1, d \rrbracket}.$$

We also denote by  $\mathcal{L}_s$  the infinitesimal generator of (2), acting on  $f \in \mathcal{C}^2(\mathbb{R}^d, \mathbb{R})$  as

$$\mathcal{L}_s f(y) := v_s(y) \cdot \nabla f(y) + a_s \Delta f(y).$$

Finally, for a third-order tensor  $A \in \mathbb{R}^{d \times d \times d}$  and a matrix  $M \in \mathbb{R}^{d \times d}$ , we use the notation  $[A, M] \in \mathbb{R}^d$  for the contraction over the last two indices of  $A$ .

More heuristically, the Jacobian transports first-order perturbations from time  $s$  to time  $t$ , while the Hessian and Laplacian encode the corresponding second-order sensitivity.  $\mathcal{L}_s$  describes the infinitesimal change of the observable  $f$  along the diffusion. Using these quantities, the next theorem gives the weak error induced by the time discretization, at first order in the stepsize  $\gamma$ .

**Theorem 1** (First-order weak error, proof in Appendix B). *For all  $f \in C^\infty(\mathbb{R}^d, \mathbb{R})$  with polynomial growth, we have, for  $k \in \llbracket 0, K \rrbracket$  and  $t_k = \gamma k$ :*

$$\mathbb{E}[f(\hat{Y}_k)] - \mathbb{E}[f(Y_{t_k})] = \gamma \int_0^{t_k} \mathbb{E} \left[ e_{t_k, s}(Y) \cdot \nabla f(Y_{t_k}) + \langle E_{t_k, s}(Y), \nabla^2 f(Y_{t_k}) \rangle \right] ds + O(\gamma^2)$$

with 
$$\begin{cases} e_{t, s}(Y) := -\frac{1}{2} \left( J_{t, s}(Y) [(\partial_s + \mathcal{L}_s)v_s](Y_s) + \dot{a}_s \Delta_{t, s}(Y) + 2a_s [H_{t, s}(Y), \nabla v_s(Y_s)] \right) \in \mathbb{R}^d \\ E_{t, s}(Y) := -\frac{1}{2} J_{t, s}(Y) \left( a_s (\nabla v_s(Y_s) + \nabla v_s(Y_s)^\top) + \dot{a}_s \text{Id} \right) J_{t, s}(Y)^\top \in \mathbb{R}^{d \times d} \end{cases}$$

The proof follows the expansion strategy from [Talay and Tubaro \[1990\]](#): using the backward Kolmogorov value function, we expand the one-step local Euler error, and sum them along the time grid. Note that the same weak-error approach could be extended to higher-order discretization schemes [[Karras et al., 2022](#), [Lu et al., 2022](#)] at the cost of involving higher derivatives of the flow.

**Interpretation of the terms.** The leading error is the accumulation of local Euler defects, transported from time  $s$  to time  $t$  by the Jacobian  $J_{t, s}(Y)$ . The vector  $e_{t, s}$  represents the local mean error and acts on  $\nabla f(Y_t)$ , while  $E_{t, s}$  is the local covariance error and acts on  $\nabla^2 f(Y_t)$ . More precisely,  $J_{t, s} [(\partial_s + \mathcal{L}_s)v_s](Y_s)$  is the drift-freezing error, since Euler keeps the drift fixed over each step, while the terms involving  $\dot{a}_s$  come from freezing the diffusion term. Finally, the terms involving  $\nabla v_s$  describe the interactions between the discretized Brownian motion and the curvature of the flow.

**ODE sampling** ( $\alpha = 0$ ) This is an instructive special case of the general expansion. In this setting, the diffusion term  $a_s = 0$ , and thus  $E_{t, s}(Y) = 0$ . Note that if  $Y$  solves  $\dot{Y}_s = v_s(Y_s)$ , then  $\frac{d}{ds} v_s(Y_s) = (\partial_s + v_s \cdot \nabla)v_s(Y_s)$ . The discretization weak error then only depends on the drift material derivative  $D_s v_s := (\partial_s + v_s \cdot \nabla)v_s$  (local acceleration) transported by the Jacobian:

$$\mathbb{E}[f(\hat{Y}_k)] - \mathbb{E}[f(Y_{t_k})] = -\frac{\gamma}{2} \int_0^{t_k} \mathbb{E} \left[ J_{t_k, s}(Y) D_s v_s(Y_s) \cdot \nabla f(Y_{t_k}) \right] ds + O(\gamma^2). \quad (4)$$

In particular, the discretization error vanishes when  $D_s v_s = 0$  along the characteristics, i.e., when trajectories remain straight in time [[Liu et al., 2022](#), [Tong et al., 2024](#)]. The relation between this first-order error and Lipschitz-based objectives [[Chen et al., 2025](#)] is discussed in Appendix H.

**Mean and covariance errors** We now apply the above weak-error result to the reverse diffusion sampler introduced in Section 2. Since this process is initialized from  $p_T$ , its exact terminal law satisfies  $\text{Law}(Y_T) = p_{\text{data}}$ , so that  $\mu_{\text{data}} = \mathbb{E}[Y_T]$  and  $\Sigma_{\text{data}} = \text{Cov}[Y_T]$ . We can then derive the first-order error on the mean and covariance, propagated until final sampling step  $K$ :

**Corollary 1** (First-order mean and covariance errors, proof in Appendix C). *With the notations from Theorem 1, we have:*

$$\mathbb{E}[\hat{Y}_K] = \mu_{\text{data}} + \gamma \int_0^T \mathbb{E}[e_{T, s}(Y)] ds + O(\gamma^2) \quad (5)$$

$$\text{Cov}[\hat{Y}_K] = \Sigma_{\text{data}} + \gamma \int_0^T \left( \text{Cov}[e_{T, s}(Y), Y_T] + \text{Cov}[e_{T, s}(Y), Y_T]^\top + 2\mathbb{E}[E_{T, s}(Y)] \right) ds + O(\gamma^2) \quad (6)$$

In the rest of the document, we focus on the errors in these first two moments, which become especially tractable when the drift is linear, as detailed in Section 4. We show in Appendix D that these moment errors can be combined into a first-order expansion of the Fréchet distance (FD), defined as the sum of the squared  $L^2$  distance between means and of the squared Bures distance between covariances. For Gaussian data, FD coincides with the Wasserstein-2 distance.

## 4 Explicit formulas under Gaussian data

We now specialize the general discretization-error expansions to Gaussian data. This yields explicit *geometry-aware* formulas that depend on the covariance spectrum of the target distribution. In Section 5, we use these formulas to optimize the diffusion parameters  $(\sigma_t, \eta_t, \alpha)$  with respect to this spectrum, and compare the resulting predictions on non-Gaussian image sampling problems.

For Gaussian data  $p_{\text{data}} \sim \mathcal{N}(\mu_{\text{data}}, \Sigma_{\text{data}})$ , the score is affine and reads, using the notations from Section 2,  $\nabla \log p_t = -\Sigma_t^{-1}(x - \mu_t)$ . The generative SDE (2) thus has linear drift

$$v_t(x) = H_t x + r_t \quad \text{where for } t \leq T \quad \begin{cases} H_{T-t} := -\frac{\dot{\eta}_t}{\eta_t} \text{Id} - (1 + \alpha)\eta_t^2 \dot{\sigma}_t \sigma_t \Sigma_t^{-1} \\ r_{T-t} := (1 + \alpha)\eta_t^2 \dot{\sigma}_t \sigma_t \Sigma_t^{-1} \mu_t. \end{cases} \quad (7)$$

In Appendix E, we specialize the *first-order* mean and covariance error formulas from Corollary 1 to general affine drifts, and additionally derive their *second-order* expansions in  $\gamma$ . Instantiating these formulas with  $v_t$  from (7) yields Proposition 1. In this Gaussian setting, each eigendirection evolves independently in the data eigenbasis  $\Sigma_{\text{data}} = U \text{Diag}(\lambda_i) U^\top$ , so the discretization error decomposes by eigendirection  $\lambda_i$ . By abuse of notation, we sometimes write  $\lambda$  for  $\lambda_i$ ; all such expressions are understood componentwise in this eigenbasis.

**Proposition 1** (Gaussian data mean and covariance errors, proof in Appendix F). *Assume Gaussian data  $p_{\text{data}} \sim \mathcal{N}(\mu_{\text{data}}, \Sigma_{\text{data}})$  and Assumption 1(i) on the schedules. Then the mean and covariance discretization errors decouple in the eigenbasis of the data covariance  $\Sigma_{\text{data}} = U \text{Diag}(\lambda_i) U^\top$ :*

$$\begin{aligned} \mathbb{E}[\hat{Y}_K] &= \mu_{\text{data}} + U \text{Diag}(\Delta^\mu(\lambda_i)) U^\top \mu_{\text{data}}, \\ \text{Cov}[\hat{Y}_K] &= \Sigma_{\text{data}} + U \text{Diag}(\Delta^\Sigma(\lambda_i)) U^\top. \end{aligned}$$

For both per-eigendirection defects  $\Delta^\mu(\lambda_i)$  and  $\Delta^\Sigma(\lambda_i)$ , we derive explicit first- and second-order small-stepsize expansions of the form

$$\Delta(\lambda) = \gamma \Delta^{[1]}(\lambda) + \gamma^2 \Delta^{[2]}(\lambda) + O(\gamma^3),$$

In particular, denoting

$$A_s := \frac{\dot{\eta}_s}{\eta_s}, \quad B_s(\lambda) := \frac{\sigma_s \dot{\sigma}_s}{\lambda + \sigma_s^2}, \quad N_s(\lambda) := \frac{\lambda}{\lambda + \sigma_s^2}$$

the first-order coefficients are

$$\Delta^{\mu, [1]}(\lambda) = -\frac{1}{2} \int_0^T N_s(\lambda)^{\frac{1+\alpha}{2}} A_s (A_s + (1 + \alpha)B_s(\lambda)) ds - \frac{1}{2} \left[ N_s(\lambda)^{\frac{1+\alpha}{2}} A_s \right]_0^T \quad (8)$$

$$\Delta^{\Sigma, [1]}(\lambda) = -\lambda \int_0^T N_s(\lambda)^\alpha \left[ (A_s + B_s(\lambda))^2 - \alpha^2 B_s(\lambda)^2 \right] ds - \left[ \lambda N_s(\lambda)^\alpha (A_s + B_s(\lambda)) \right]_0^T. \quad (9)$$

Under Assumption 1(ii), the boundary terms  $[\cdot]_0^T$  in both expansions vanish as  $\sigma_T = \sigma_{\max} \rightarrow \infty$ . The expressions of the second-order coefficients are given in Appendix F equations (64) and (66).

**ODE sampling** ( $\alpha = 0$ ) In this case, the first-order coefficients considerably simplify: the covariance error only depends on the eigendecomposition of the drift matrix  $H_s = U \text{Diag}(\Delta_s^H) U^\top$ :

$$\Delta^{\Sigma, [1]}(\lambda) = -\lambda \int_0^T (\Delta_s^H(\lambda))^2 ds + \lambda \left[ \Delta_s^H(\lambda) \right]_0^T$$

This error is *geometry-aware*: it controls the full drift spectrum rather than only its Lipschitz constant as in [Chen et al., 2025] and in non-asymptotic error analyses; see details in Appendix H.

**Typical rescaling schedules** Appendix F.1 specializes the above error terms for usual rescaling schedules, including VE, VP, and FM; see Section 2. We state here the VE case, which corresponds to  $\eta_t = 1$ . Then, the first and second-order terms in the mean error vanish:  $\mathbb{E}[\hat{Y}_K] = \mu_{\text{data}} + O(\gamma^3)$ . For the covariance error term (9), when  $\alpha > 0$  and if  $\sigma_t = O(t)$  as  $t \rightarrow 0$ , Assumption 1(ii) holds and for large terminal noise  $\sigma_T = \sigma_{\text{max}}$ :

$$\Delta^{\Sigma, [1]}(\lambda) = (\alpha^2 - 1)\lambda^{\alpha+1} \int_0^T \frac{(\sigma_s \dot{\sigma}_s)^2}{(\lambda + \sigma_s^2)^{\alpha+2}} ds + o_{\sigma_{\text{max}} \rightarrow \infty}(1) \quad (10)$$

For example, in the case of the *polynomial schedule*  $\sigma_t = \sigma_{\text{max}} \left(\frac{t}{T}\right)^\beta$ ,  $\beta > \frac{1}{2}$  (B the Beta function):

$$\Delta^{\Sigma, [1]}(\lambda) = (\alpha^2 - 1) \frac{\beta}{2T} \lambda^{1-\frac{1}{2\beta}} \text{B}\left(2 - \frac{1}{2\beta}, \alpha + \frac{1}{2\beta}\right) \sigma_{\text{max}}^{1/\beta} + o(\sigma_{\text{max}}^{1/\beta}). \quad (11)$$

**Fréchet distance expansion for Gaussian data** Using Proposition 1, we obtain an explicit expansion for small stepsize of the Fréchet distance. Using the fact that the covariance error is diagonal in the covariance eigenbasis, the Bures distance between covariances decomposes nicely as a single sum over  $\lambda_i$ -dependent terms (proof in Appendix D.1):

$$\text{FD}(p_{\text{data}}, \text{Law}(\hat{Y}_K)) = \gamma^2 \sum_{i=1}^d \Delta^{\mu, [1]}(\lambda_i)^2 (u_i^\top \mu_{\text{data}})^2 + \frac{\gamma^2}{4} \sum_{i=1}^d \frac{\Delta^{\Sigma, [1]}(\lambda_i)^2}{\lambda_i} + o(\gamma^2) \quad (12)$$

In Appendix D.1, a third-order expansion in  $\gamma$  is derived using the second-order terms  $\Delta^{\mu, [2]}$  and  $\Delta^{\Sigma, [2]}$  from Proposition 1. In Section 5, we use this Fréchet objective for parameter design.

## 5 Optimal diffusion sampling parameters

The Gaussian formulas above yield explicit objectives for choosing diffusion parameters, namely the diffusion-term parameter  $\alpha$  and the noise  $\sigma_t$  and rescaling  $\eta_t$  schedules. By minimizing the leading order Fréchet discretization error, we derive geometry-aware optimality criteria, expressed through the covariance spectrum, and test whether the resulting predictions extend beyond Gaussians.

In particular, we compare with image sampling using pretrained score models [Karras et al., 2022] on CIFAR-10, ImageNet, and FFHQ. For empirical curves, we calculate FID (Fréchet Distance computed in *Inception-v3* feature space) from 30k generated images. For theoretical curves, we plot the Gaussian Fréchet Distance (FD) from (12), with  $\mu_{\text{data}}$  and  $\Sigma_{\text{data}}$  estimated empirically from each dataset in image space. Experimental details are given in Appendix I.1.

**Optimal diffusion-term parameter  $\alpha$**  We first study the diffusion-term parameter  $\alpha$  for fixed noise schedules  $\sigma_t$  in the Variance Exploding setting (VE;  $\eta_t = 1$ ). The first-order Gaussian theory (11) gives a clean reference:  $\alpha = 1$  cancels the first-order mean and covariance errors in every eigendirection. This is exactly the choice of  $\alpha$  used in the original SDE-based diffusion work [Song et al., 2021]. More precisely, the covariance shift  $\Delta^{\Sigma, [1]}$  increases with  $\alpha$ : it is negative for  $\alpha < 1$  and positive for  $\alpha > 1$ . Thus, small  $\alpha$  underestimates variance in every eigendirection, while large  $\alpha$  overestimates it. This is visually reflected in the samples shown in Figure I.3. This variance reduction at  $\alpha = 0$  can be leveraged to improve posterior mean estimation with diffusion models (see Appendix I.4).

Figure 1(a) shows that, for real image sampling, the  $\alpha^*$  minimizing the FID decreases below 1 as the number of discretization steps  $K$  decreases. This decrease is approximately linear in the stepsize  $\gamma = T/K$ , as shown in Figure 1(c). We now show that this shift is well captured by our *second-order* theoretical error

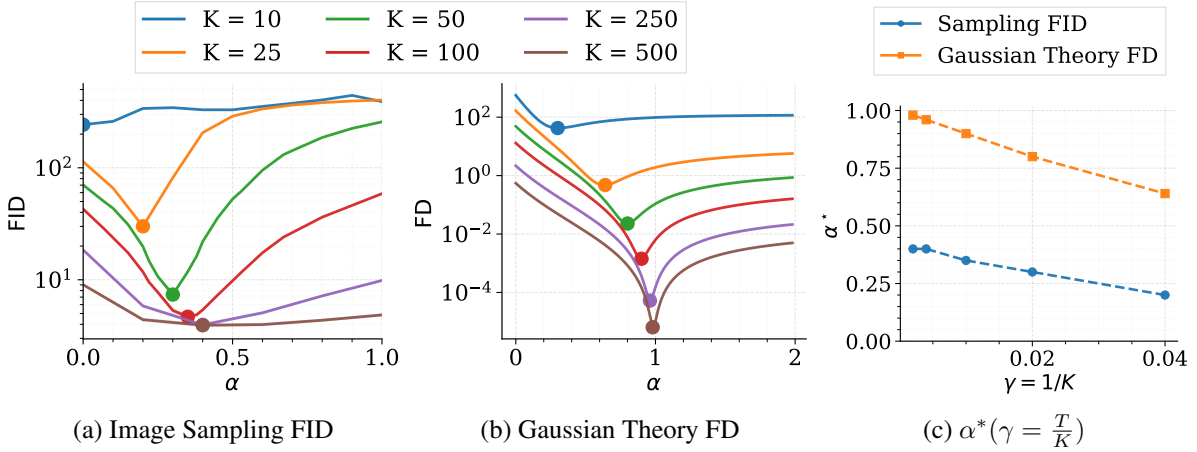


Figure 1: Empirical FID for FFHQ sampling (a) and Gaussian-theory Fréchet Distance (FD) using the empirical FFHQ covariance (b) versus  $\alpha$ , for several step counts  $K$ . Using  $\eta_t = 1$  (VE) and  $\sigma_t = \sigma_{\max}(t/T)^5$ . (c) shows the minimizer  $\alpha^*$  of each curve as a function of  $\gamma = T/K$ .

from Proposition 1, represented in Figure 1(b). Proposition 2 makes the linear evolution of  $\alpha^*$  explicit in terms of the spectrum of  $\Sigma_{\text{data}}$ .

**Proposition 2** (Proof in Appendix G.1). *For  $p_{\text{data}} \sim \mathcal{N}(\mu_{\text{data}}, \Sigma_{\text{data}})$  and VE schedule with  $\sigma_t = \sigma_{\max}(\frac{t}{T})^\beta$ ,  $\beta > 1$ , the  $\alpha$  minimizing the third-order Gaussian Fréchet expansion (34), satisfies:*

$$\alpha^*(\gamma) = 1 - \gamma \left( \frac{\sigma_{\max}^{\frac{1}{\beta}}}{T} \sum_{i=1}^d w_{\beta,i} \lambda_i^{-\frac{1}{2\beta}} + o\left(\sigma_{\max}^{\frac{1}{\beta}}\right) \right) + o(\gamma), \quad w_{\beta,i} = C_\beta \frac{\lambda_i^{1-\frac{1}{\beta}}}{\sum_{j=1}^d \lambda_j^{1-\frac{1}{\beta}}} > 0$$

In particular, the leading  $O(\gamma)$  term predicts the slope of the linear  $\alpha^*(\gamma)$  trend in Figure 1(c). This suggests that a few coarse-step experiments can be used to fit the theoretical scaling law and extrapolate the optimal  $\alpha^*$  to smaller  $\gamma$ .

The expression for  $\alpha^*(\gamma)$  in Proposition 2 is eigendirection-dependent: directions with smaller variance  $\lambda_i$  favor smaller values of  $\alpha^*$ . In Appendix I.3, we show that this spectral inhomogeneity also appears in image sampling by decomposing FID along the covariance eigenbasis.

**Optimal rescaling schedule  $\eta_t$**  We now optimize the rescaling schedule  $\eta_t$ , for a given diffusion parameter  $\alpha$  and noise schedule  $\sigma_t$ . In the large final noise regime of Proposition 1, both first-order mean (8) and covariance (9) errors in one eigendirection of variance  $\lambda$  are canceled by

$$\frac{\dot{\eta}_s}{\eta_s} + (1 + \alpha) \frac{\sigma_s \dot{\sigma}_s}{\lambda + \sigma_s^2} = 0 \quad \Leftrightarrow \quad \eta_t^*(\lambda) = \left( \frac{\lambda}{\lambda + \sigma_t^2} \right)^{\frac{\alpha+1}{2}}. \quad (13)$$

For ODE sampling ( $\alpha = 0$ ), since  $\text{Cov}(X_t) = \eta_t^2(\Sigma_{\text{data}} + \sigma_t^2 \text{Id})$ , the above  $\eta_t^*(\lambda)$  exactly preserves variance along eigendirection  $\lambda$  during sampling, and precisely coincides with VP when  $\Sigma_{\text{data}} = \text{Id}$ . For anisotropic data, however, it cannot be imposed in all directions simultaneously. Note that if  $\alpha > 0$ , the forward process (1) then converges to  $\text{dirac } 0 : \eta_t^*(\lambda)^2(\Sigma_{\text{data}} + \sigma_t^2 \text{Id}) \rightarrow 0$  as  $\sigma_t \rightarrow \infty$ .

In the following, we thus keep  $\alpha = 0$  and replace  $\lambda$  with a scalar parameter  $c_\eta > 0$ , which is chosen by minimizing the leading-order Gaussian Fréchet objective (12) for  $\mu_{\text{data}} = 0$ :

$$\eta_t(c) = \left( \frac{c_\eta}{c_\eta + \sigma_t^2} \right)^{1/2}, \quad c_\eta^* \in \arg \min_{c>0} \sum_{i=1}^d \frac{\Delta^{\Sigma, [1]}(\lambda_i; c_\eta)^2}{\lambda_i}. \quad (14)$$

The forward process (1) with  $\eta_t = \eta_t(c_\eta)$  then converges to  $\mathcal{N}(0, c_\eta \text{Id})$ , so  $c_\eta$  controls the variance of the backward initialization:  $c_\eta = 1$  gives VP, while  $c_\eta \gg \sigma_T^2$  approaches VE. For a finite anisotropic spectrum  $(\lambda_i)_{i \leq d}$ ,  $c_\eta^*$  does not admit a closed-form expression. Given that empirical image spectra are close to power laws (see Appendix Figure I.1), we consider  $\lambda_i = \lambda_{\max} i^{-p}$ . Proposition 3 then describes the structure of the corresponding leading-order minimizer.

**Proposition 3** (Optimal  $c_\eta$  parameter for power-law spectra, proof in Appendix G.2). *In dimension  $d \geq 2$ , assume a power-law spectrum  $\lambda_i = \lambda_{\max} i^{-p}$  with  $p > 0$  and a polynomial noise schedule  $\sigma_t = \sigma_{\max}(t/T)^\beta$ . For large  $\sigma_{\max}$  and  $\beta$ , the leading-order minimizer of (14) satisfies:*

$$c_\eta^*(\lambda_{\max}, p) = \lambda_{\max} \tau_p^*, \text{ for } \tau_p^* \in (0, 1) \text{ minimizing } \sum_{i=1}^d i^{-p} g(\tau i^p) \text{ with } g(z) = \left[ \frac{z+1}{z-1} \log z - 2 \right]^2.$$

The evolution of  $\tau_p^*$  with  $p$  is further described and plotted in Appendix G.2.

Figure 2 (top) confirms the prediction  $c_\eta^*(\lambda_{\max}, p) = \lambda_{\max} \tau_p^*$  from Proposition 3 on CIFAR, FFHQ and ImageNet sampling with  $K = 100$  steps. Figure 2 compares, for each dataset, the empirical sampling FID (a) with the theoretical Gaussian Fréchet error (b), computed from (12) using an empirical estimation of each covariance spectrum. Across datasets, the fitted exponent  $p$  changes only mildly, with limited impact on  $\tau_p$ , while  $\lambda_{\max}$  changes substantially. Correspondingly, both empirical FID and Gaussian FD are minimized at a  $c_\eta^*$  value increasing with  $\lambda_{\max}$ .

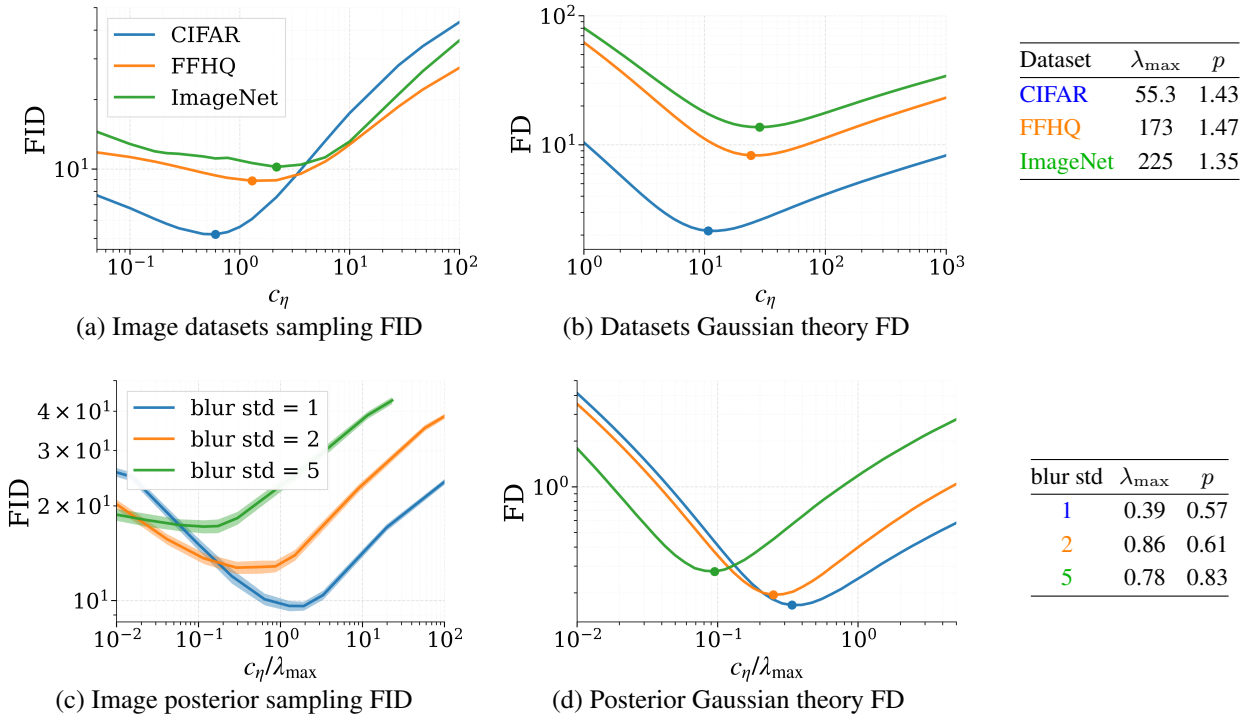


Figure 2: Empirical FID and theoretical Fréchet Distance (FD) for image sampling across datasets (top) and for deblurring posteriors (bottom), using  $K = 100$  steps,  $\alpha = 0$  and  $\sigma_t = \sigma_{\max} \left(\frac{t}{T}\right)^5$ . Power-law parameters fitted on empirical spectrum (Figure I.1) are reported in the tables. Per-eigendirection error curves are given in Appendix I.5.

To isolate the role of  $p$ , we also study image deblurring posteriors  $p(x | y)$  with  $y = k * x + w$ , varying the Gaussian blur standard deviation in kernel  $k$ . Larger blur yields faster spectral decay of  $\text{Cov}[x|y]$  and thus larger  $p$  (Figure 2, table). Using the moment-matching approximation [Rozet et al., 2024] (exact for Gaussian data; Appendix I.2), Figure 2 again compares FID (c) with theoretical Gaussian FD (d). After rescaling by

$\lambda_{\max}$ , the remaining variation is due to  $p$ : both empirical and theoretical errors have similar shapes, and their minimizers  $\tau_p^* = c_\eta^*/\lambda_{\max}$  shift to smaller values as  $p$  increases. As detailed at the end of Appendix G.2, this behavior is consistent with Proposition 3: Figure G.1 predicts a decrease of  $\tau_p^*$  over the range of  $p$  values representing these posterior distributions.

**Optimal noise schedule**  $\sigma_t$  Finally, we propose to optimize the noise schedule  $\sigma_t$  for fixed diffusion parameter  $\alpha$  and rescaling  $\eta_t$ . As in previous cases, we start with the one-dimensional problem: for one eigendirection of variance  $\lambda$ , the following proposition gives the optimal choice of  $\sigma_t^*$  that minimizes the first-order Fréchet error (12) for VE (Appendix G.4 shows an analogous formula for VP).

**Proposition 4** (Single-eigendirection optimal noise schedule in the variance exploding case, proof in Appendix G.3). *Fix one eigendirection of variance  $\lambda$ , let  $\eta_t = 1$  (VE), and define  $q_\alpha := 1 - 2\alpha - \alpha^2$ . The following schedule cancels the first-order one-dimensional Fréchet error:*

$$\sigma_t^*(\lambda)^2 = \begin{cases} \lambda \left[ \left( 1 + \frac{\sigma_{\max}^2}{\lambda} \right)^{t/T} - 1 \right], & q_\alpha = 0, \\ \lambda \left[ \left( 1 + \frac{t}{T} \left( \left( 1 + \frac{\sigma_{\max}^2}{\lambda} \right)^{q_\alpha/2} - 1 \right) \right)^{2/q_\alpha} - 1 \right], & q_\alpha \neq 0. \end{cases} \quad (15)$$

In multiple dimensions, the Fréchet objective sums eigendirection-wise errors and no single closed-form global minimizer exists. We can use (15) as a surrogate family by replacing  $\lambda$  with a tunable scalar proxy  $c_\sigma$ . However, we observe that this parametrized schedule performs poorly for sampling highly anisotropic data such as images, because small and large eigenvalues favor incompatible values of  $c_\sigma$ . Figure 3 demonstrates this effect on two 100-dimensional Gaussian mixture models with different covariance spectra. For mild anisotropy, one choice of  $c_\sigma$  lets the above one-dimensional optimal family outperform polynomial schedules, consistent with Proposition 4. For strong anisotropy, however, no single  $c_\sigma$  fits the whole spectrum, and polynomial schedules perform better.

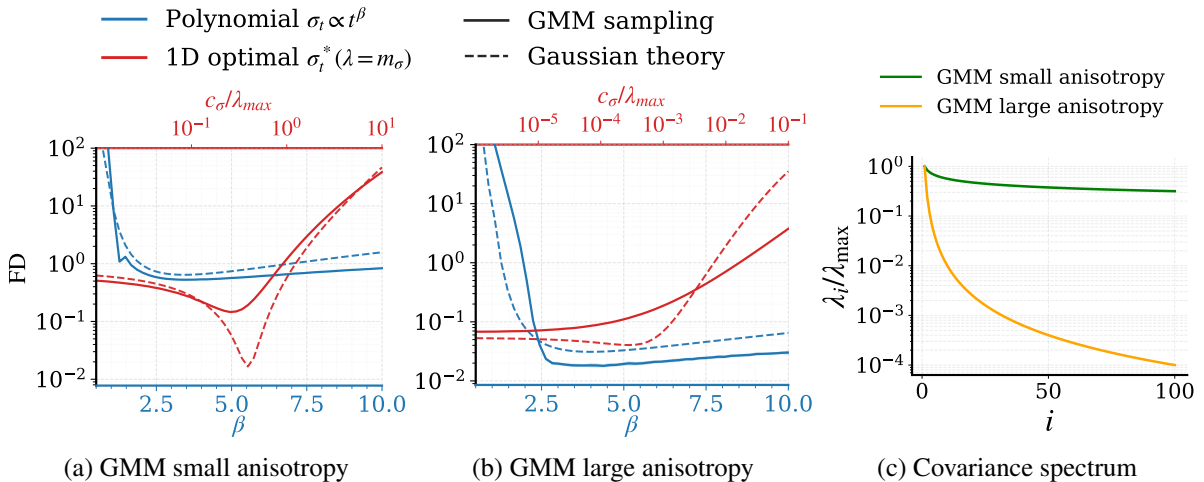


Figure 3: Fréchet error for sampling a 100-dimensional Gaussian mixture model with 10 centers and covariance rescaled to follow two different power spectra shown in (c). Using  $\alpha = 0.25$  and  $K = 50$ . Figures (a) and (b) compare two noise schedule families: the one-dimensional optimal schedule (15)  $\sigma_t^*(c_\sigma)$  as a function of  $c_\sigma$  (top axis), and the polynomial schedules  $\sigma_t = \sigma_{\max}(t/T)^\beta$  as a function of  $\beta$  (bottom axis). Solid curves show empirical FID and dashed curves Gaussian theory.

Polynomial schedules  $\sigma_t = \sigma_{\max}(t/T)^\beta$  with moderately large  $\beta$  have indeed been empirically shown to be effective for sampling highly anisotropic data such as images, [Karras et al. \[2022\]](#) recommending  $\beta = 7$ . Our theory explains this robustness: in the VE case (11), the Gaussian Fréchet error (12) along one eigendirection of variance  $\lambda$  satisfies  $\text{FD}_\lambda(\beta) \propto \lambda^{1-1/\beta}$ . Hence, for two eigenvalues  $\lambda_1$  and  $\lambda_2$ :

$$\frac{d}{d\beta} \log \left( \frac{\text{FD}_{\lambda_2}(\beta)}{\text{FD}_{\lambda_1}(\beta)} \right) = \frac{1}{\beta^2} \log \left( \frac{\lambda_2}{\lambda_1} \right).$$

For large enough  $\beta$ , this derivative depends only weakly on the  $\lambda$  quotient, so the shape of  $\text{FD}_\lambda(\beta)$  varies little across eigendirections. This explains why a single polynomial exponent can remain robust for the full Gaussian Fréchet objective  $\text{FD}(\beta) = \sum_i \text{FD}_{\lambda_i}(\beta)$  even under strong anisotropy. This behavior is confirmed for real image datasets in [Figure I.6](#): the optimal  $\beta^*$  remains unchanged across datasets, and the per-eigendirection error curves vary only mildly across eigenvalues  $\lambda_i$ .

## 6 Conclusion

We studied how the discretization error of diffusion models depends on the parameters of the dynamics. Starting from general weak and Fréchet error expansions, we derived explicit discretization error formulas under Gaussian data, revealing how the covariance spectrum controls the effect of the diffusion coefficient  $\alpha$ , and the diffusion schedules  $\eta_t$  and  $\sigma_t$ . These formulas predict several practical trends observed in experiments, including the decrease of the optimal  $\alpha$  under tighter discretization budgets, the dependence of the optimal rescaling  $\eta_t$  on spectral anisotropy, and the robustness of polynomial noise schedules  $\sigma_t$  for image-like spectra. Overall, our results provide a simple spectral perspective on diffusion sampler design and a theoretical basis for important empirical heuristics.

**Limitations.** Our parameter-design analysis relies on Gaussian approximations, which capture useful global trends but remain far from the true distribution of natural images. Hence, it does not take into account discretization error effects due to multimodality. Another limitation is that we ignore score-estimation error, analyzed in a Gaussian setting by [Hurault et al. \[2025\]](#); this may introduce tradeoffs with discretization error when optimizing sampling parameters. Extending the analysis beyond the Gaussian case using our general error [Theorem 1](#) and incorporating score-estimation error into parameter optimization are natural next steps.

## 7 Acknowledgments

This work was supported by the European Research Council (ERC project WOLF) and the French government under the management of Agence Nationale de la Recherche as part of the “France 2030” program, reference ANR-23-IACL-0008 (PRAIRIE-PSAI). This work was performed using HPC resources from GENCI–IDRIS (Grant 2025-AD011015483R1).

## References

- Michael S Albergo, Nicholas M Boffi, and Eric Vanden-Eijnden. Stochastic interpolants: A unifying framework for flows and diffusions, 2023. URL <https://arxiv.org/abs/2303.08797>, 3:1, 2023.
- Joe Benton, Valentin De Bortoli, Arnaud Doucet, and George Deligiannidis. Nearly  $d$ -linear convergence bounds for diffusion models via stochastic localization. *International Conference on Learning Representations*, 2024.

- Eliot Beyler and Francis Bach. Convergence of deterministic and stochastic diffusion-model samplers: A simple analysis in wasserstein distance. *arXiv preprint arXiv:2508.03210*, 2025.
- Yochai Blau and Tomer Michaeli. The perception-distortion tradeoff. In *Proceedings of the IEEE conference on computer vision and pattern recognition*, pages 6228–6237, 2018.
- Yifan Chen, Eric Vanden-Eijnden, and Jiawei Xu. Lipschitz-guided design of interpolation schedules in generative models. *arXiv preprint arXiv:2509.01629*, 2025.
- Giovanni Conforti, Alain Durmus, and Marta Gentiloni Silveri. Kl convergence guarantees for score diffusion models under minimal data assumptions. *SIAM Journal on Mathematics of Data Science*, 7(1):86–109, 2025.
- M. H. A. Davis. *Linear Estimation and Stochastic Control*. Chapman and Hall, 1977.
- Valentin De Bortoli. Convergence of denoising diffusion models under the manifold hypothesis. *arXiv preprint arXiv:2208.05314*, 2022.
- Mingyang Deng, He Li, Tianhong Li, Yilun Du, and Kaiming He. Generative modeling via drifting. *arXiv preprint arXiv:2602.04770*, 2026.
- Prafulla Dhariwal and Alexander Nichol. Diffusion models beat gans on image synthesis. In *Advances in Neural Information Processing Systems*, 2021.
- Yansong Gao, Zhihong Pan, Xin Zhou, Le Kang, and Pratik Chaudhari. Fast diffusion probabilistic model sampling through the lens of backward error analysis. *arXiv preprint arXiv:2304.11446*, 2023.
- Jonathan Ho, Ajay Jain, and Pieter Abbeel. Denoising diffusion probabilistic models. In *Advances in Neural Information Processing Systems*, 2020.
- Samuel Hurault, Matthieu Terris, Thomas Moreau, and Gabriel Peyré. From score matching to diffusion: A fine-grained error analysis in the gaussian setting. *arXiv preprint arXiv:2503.11615*, 2025.
- Alexia Jolicoeur-Martineau, Ke Li, Rémi Piché-Taillefer, Tal Kachman, and Ioannis Mitliagkas. Gotta go fast when generating data with score-based models. 2021.
- Tero Karras, Miika Aittala, Timo Aila, and Samuli Laine. Elucidating the design space of diffusion-based generative models. In *Advances in Neural Information Processing Systems*, 2022.
- Bahjat Kawar, Gregory Vaksman, and Michael Elad. Stochastic image denoising by sampling from the posterior distribution. In *Proceedings of the IEEE/CVF international conference on computer vision*, pages 1866–1875, 2021.
- Holden Lee, Jianfeng Lu, and Yixin Tan. Convergence of score-based generative modeling for general data distributions. In *International Conference on Algorithmic Learning Theory*, pages 946–985. PMLR, 2023.
- Gen Li, Yuting Wei, Yuxin Chen, and Yuejie Chi. Towards non-asymptotic convergence for diffusion-based generative models. In *The Twelfth International Conference on Learning Representations*, 2024a.
- Lijiang Li, Huixia Li, Xiawu Zheng, Jie Wu, Xuefeng Xiao, Rui Wang, Min Zheng, Xin Pan, Fei Chao, and Rongrong Ji. Autodiffusion: Training-free optimization of time steps and architectures for automated diffusion model acceleration. In *Proceedings of the IEEE/CVF International Conference on Computer Vision*, 2023.

- Xiang Li, Yixiang Dai, and Qing Qu. Understanding generalizability of diffusion models requires rethinking the hidden gaussian structure. *Advances in neural information processing systems*, 37:57499–57538, 2024b.
- Yaron Lipman, Ricky TQ Chen, Heli Ben-Hamu, Maximilian Nickel, and Matt Le. Flow matching for generative modeling. *arXiv preprint arXiv:2210.02747*, 2022.
- Xingchao Liu, Chengyue Gong, and Qiang Liu. Flow straight and fast: Learning to generate and transfer data with rectified flow. *arXiv preprint arXiv:2209.03003*, 2022.
- Cheng Lu, Yuhao Zhou, Fan Bao, Jianfei Chen, Chongxuan Li, and Jun Zhu. Dpm-solver: A fast ode solver for diffusion probabilistic model sampling in around 10 steps. *Advances in neural information processing systems*, 35:5775–5787, 2022.
- Cheng Lu, Yuhao Zhou, Fan Bao, Jianfei Chen, Chongxuan Li, and Jun Zhu. Dpm-solver++: Fast solver for guided sampling of diffusion probabilistic models. 2023.
- Luigi Malago, Luigi Montrucchio, and Giovanni Pistone. Wasserstein riemannian geometry of positive definite matrices. *arXiv preprint arXiv:1801.09269*, 2018.
- Alexander Quinn Nichol and Prafulla Dhariwal. Improved denoising diffusion probabilistic models. In *International conference on machine learning*, pages 8162–8171. PMLR, 2021.
- Emile Pierret and Bruno Galerne. Diffusion models for gaussian distributions: Exact solutions and wasserstein errors. *arXiv preprint arXiv:2405.14250*, 2024.
- François Rozet, G r me Andry, Fran ois Lanusse, and Gilles Louppe. Learning diffusion priors from observations by expectation maximization. *Advances in Neural Information Processing Systems*, 37: 87647–87682, 2024.
- Amirmojtaba Sabour, Sanja Fidler, and Karsten Kreis. Align your steps: Optimizing sampling schedules in diffusion models. In *International Conference on Machine Learning*, pages 42947–42975, 2024.
- Yang Song and Stefano Ermon. Generative modeling by estimating gradients of the data distribution. In *Advances in Neural Information Processing Systems*, 2019.
- Yang Song, Jascha Sohl-Dickstein, Diederik P Kingma, Abhishek Kumar, Stefano Ermon, and Ben Poole. Score-based generative modeling through stochastic differential equations. In *International Conference on Learning Representations*, 2021.
- Yang Song, Prafulla Dhariwal, Mark Chen, and Ilya Sutskever. Consistency models. In *International Conference on Machine Learning*, pages 32211–32252. PMLR, 2023.
- Juli n Tachella, Matthieu Terris, Samuel Hurault, Andrew Wang, Dongdong Chen, Minh-Hai Nguyen, Maxime Song, Thomas Davies, Leo Davy, Jonathan Dong, et al. Deepinverse: A python package for solving imaging inverse problems with deep learning. *arXiv preprint arXiv:2505.20160*, 2025.
- Denis Talay and Luciano Tubaro. Expansion of the global error for numerical schemes solving stochastic differential equations. *Stochastic analysis and applications*, 8(4):483–509, 1990.
- Alexander Tong, Kilian Fatras, Nikolay Malkin, Guillaume Hugu t, Yanlei Zhang, Jarrid Rector-Brooks, Guy Wolf, and Yoshua Bengio. Improving and generalizing flow-based generative models with minibatch optimal transport. *Transactions on Machine Learning Research*, 2024. ISSN 2835-8856. URL <https://openreview.net/forum?id=CD9Snc73AW>. Expert Certification.

- Binxu Wang and John J Vastola. The hidden linear structure in score-based models and its application. *arXiv preprint arXiv:2311.10892*, 2023.
- Binxu Wang and John J Vastola. The unreasonable effectiveness of gaussian score approximation for diffusion models and its applications. *arXiv preprint arXiv:2412.09726*, 2024.
- Yunke Wang, Xiyu Wang, Anh-Dung Dinh, Bo Du, and Charles Xu. Learning to schedule in diffusion probabilistic models. In *Proceedings of the 29th ACM SIGKDD Conference on Knowledge Discovery and Data Mining*, 2023.
- Daniel Watson, William Chan, Jonathan Ho, and Mohammad Norouzi. Learning fast samplers for diffusion models by differentiating through sample quality. In *International Conference on Learning Representations*, 2022.
- Mengfei Xia, Yujun Shen, Changsong Lei, Ran Zhou, Ran Yi, Deli Zhao, Wenping Wang, and Yongjin Liu. Towards more accurate diffusion model acceleration with a timestep aligner. *arXiv preprint arXiv:2310.09469*, 2023.
- Shuchen Xue, Zhaoqiang Liu, Fei Chen, Shifeng Zhang, Tianyang Hu, Enze Xie, and Zhenguo Li. Accelerating diffusion sampling with optimized time steps. In *Proceedings of the IEEE/CVF Conference on Computer Vision and Pattern Recognition*, pages 8292–8301, 2024.

## A Introduction details

### A.1 Backward diffusion SDE

Let  $(X_t)_{t \geq 0}$  be the stochastic process in  $\mathbb{R}^d$  defined as the solution to the stochastic differential equation:

$$dX_t = -\beta_t(X_t) dt + \sqrt{2\xi_t} dW_t,$$

where  $\beta_t : \mathbb{R}^d \rightarrow \mathbb{R}^d$  is a measurable drift field, and  $\xi_t > 0$  is a time-dependent diffusion coefficient.

We assume throughout that the drift  $\beta_t$ , the diffusion coefficient  $\xi_t$ , and the densities  $p_t$  are sufficiently regular. In particular,  $\xi_t$  is positive and bounded away from zero, the coefficients are smooth enough to ensure well-posedness of the SDE and Fokker-Planck equation, and the densities are smooth, positive, and sufficiently decaying at infinity. Under these assumptions, all scores and integrations by parts appearing below are well-defined.

First, the law  $p_t$  of  $X_t$  admits a smooth density that evolves according to the Fokker-Planck equation:

$$\partial_t p_t(x) = \operatorname{div}(\beta_t(x) p_t(x)) + \xi_t \Delta p_t(x),$$

Equivalently, using the identity

$$\Delta p_t(x) = \operatorname{div}(\nabla \log p_t(x) \cdot p_t(x)),$$

this equation can be rewritten in conservative form:

$$\partial_t p_t(x) = -\operatorname{div}(f_t(x, p_t) p_t(x)),$$

where the effective velocity field  $f_t$  is given by:

$$f_t(x, p_t) = -\beta_t(x) - \xi_t \nabla \log p_t(x).$$

Let us consider the reverse process  $q_t = p_{T-t}$ . We have  $\partial_t q_t = -\partial_t p_{T-t}$  and the following Fokker-Planck equation for  $q_t$ :

$$\partial_t q_t(x) = -\operatorname{div}(\beta_{T-t}(x) q_t(x)) - \xi_{T-t} \Delta q_t$$

As the diffusion term is negative, this equation is unstable. We can make it positive by using, for some  $\alpha_t \geq 0$ :

$$-\Delta q_t = \alpha_t \Delta q_t - (1 + \alpha_t) \operatorname{div}(q_t \nabla \log q_t)$$

to get

$$\partial_t q_t(x) = -\operatorname{div}(((1 + \alpha_t) \xi_{T-t} \nabla \log q_t + \beta_{T-t}(x)) q_t(x)) + \alpha_t \xi_{T-t} \Delta q_t$$

for which the corresponding SDE is

$$dY_t = [(1 + \alpha_t) \xi_{T-t} \nabla \log q_t(Y_t) + \beta_{T-t}(Y_t)] dt + \sqrt{2\alpha_t \xi_{T-t}} dW_t.$$

## A.2 Initialization error

Under Gaussian data, we quantify the error induced by replacing the exact terminal law

$$p_T \propto p_{\text{data}} \left( \frac{1}{\eta_T} \cdot \right) * \mathcal{N} \left( 0, (\eta_T \sigma_T)^2 \text{Id} \right)$$

by the Gaussian initialization  $q_0 = \mathcal{N}(0, (\eta_T \sigma_T)^2 \text{Id})$ .

**Proposition 5.** *Assume Gaussian data  $p_{\text{data}} = \mathcal{N}(\mu_{\text{data}}, \Sigma_{\text{data}})$ . Let  $\tilde{Y}_t$  be the solution of the reverse generative SDE (2) initialized using  $q_0 = \mathcal{N}(0, (\eta_T \sigma_T)^2 \text{Id})$  instead of the exact terminal law  $p_T$ . At final sampling time, the Fréchet error between  $\text{Law}(\tilde{Y}_T)$  and  $p_{\text{data}}$  satisfies, for any choice of rescaling schedule  $\eta_t$ :*

$$\text{FD}(p_{\text{data}}, \text{Law}(\tilde{Y}_T)) = O\left(\sigma_T^{-2(1+\alpha)}\right) \quad \text{as } \sigma_T \rightarrow \infty.$$

Moreover, if the data are centered,  $\mu_{\text{data}} = 0$ , then:

$$\text{FD}(p_{\text{data}}, \text{Law}(\tilde{Y}_T)) = O\left(\sigma_T^{-4(1+\alpha)}\right).$$

*Proof.* Assuming Gaussian data  $p_{\text{data}} = \mathcal{N}(\mu_{\text{data}}, \Sigma_{\text{data}})$ , the solution of the forward noising process (1) at time  $T$  is

$$p_T = \mathcal{N}(\eta_T \mu_{\text{data}}, \eta_T^2 (\Sigma_{\text{data}} + \sigma_T^2 \text{Id})).$$

Instead of initializing from  $p_T$ , we initialize from the Gaussian distribution  $q_0 = \mathcal{N}(0, (\eta_T \sigma_T)^2 \text{Id})$ . Therefore, at initialization, the mean and covariance errors are

$$\delta m_0 := \mathbb{E}[X_T] - \mathbb{E}[\tilde{Y}_0] = \eta_T \mu_{\text{data}} \quad \delta \Sigma_0 := \text{Cov}[X_T] - \text{Cov}[\tilde{Y}_0] = \eta_T^2 \Sigma_{\text{data}}$$

We now study how this initial error on the mean and covariance propagates during continuous diffusion sampling via (2). Let  $Y_t$  be the solution of (2) with exact initialization  $Y_0 \sim p_T$ , and let  $\tilde{Y}_t$  be the solution with approximate initialization  $\tilde{Y}_0 \sim q_0$ . As detailed in Section 4, for Gaussian data the drift in the generative SDE (2) is affine and is given by

$$v_t(x) = H_t x + r_t \quad \text{with} \quad \begin{cases} H_{T-t} := -\frac{\dot{\eta}_t}{\eta_t} \text{Id} - (1 + \alpha) \eta_t^2 \dot{\sigma}_t \sigma_t \Sigma_t^{-1} \\ r_{T-t} := (1 + \alpha) \eta_t^2 \dot{\sigma}_t \sigma_t \Sigma_t^{-1} \mu_t. \end{cases} \quad (16)$$

We use  $J_{t,s}$ , the Jacobian of the flow map between time  $s$  and time  $t$  (or fundamental matrix) introduced in Section 3, which is the unique solution of the equation

$$\frac{d}{dt} J_{t,s} = H_t J_{t,s} \quad J_{s,s} = \text{Id}$$

Using the variation-of-constants formula,  $Y_t$  following the affine SDE (2) has the explicit Itô solution at time  $t$ :

$$Y_t = J_{t,0} Y_0 + \int_0^t J_{t,s} r_s ds + \int_0^t J_{t,s} \sqrt{2a_s} dW_s$$

The last two terms do not depend on the initialization law. Therefore, taking mean and covariance on  $Y_t$  and  $\tilde{Y}_t$  we easily get the exact propagation formulas for the mean and covariance:

$$\begin{aligned} \delta m_t &= \mathbb{E}[Y_t] - \mathbb{E}[\tilde{Y}_t] = J_{t,0} \delta m_0 \\ \delta \Sigma_t &= \text{Cov}[Y_t] - \text{Cov}[\tilde{Y}_t] = J_{t,0} \delta \Sigma_0 J_{t,0}^\top \end{aligned}$$

Note that similar propagation equations can be derived in the non-Gaussian case, but we keep it Gaussian here for simplicity. We prove in Section F (equation 61) that the Jacobian  $J_{T,0}$  verifies (at time  $T$ ) in the Gaussian data case:

$$J_{T,0} = \eta_T^{-1} \Sigma_{\text{data}}^{\frac{1+\alpha}{2}} (\Sigma_{\text{data}} + \sigma_T^2 \text{Id})^{-\frac{1+\alpha}{2}}.$$

We thus get, after replacing  $\delta m_0$  and  $\delta \Sigma_0$ , that the mean and covariance errors, at final diffusion time  $T$ , due to initialization bias, are:

$$\begin{aligned} \delta m_T &= \Sigma_{\text{data}}^{\frac{1+\alpha}{2}} (\Sigma_{\text{data}} + \sigma_T^2 \text{Id})^{-\frac{1+\alpha}{2}} \mu_{\text{data}} \\ \delta \Sigma_T &= \Sigma_{\text{data}}^{2+\alpha} (\Sigma_{\text{data}} + \sigma_T^2 \text{Id})^{-(1+\alpha)} \end{aligned}$$

which rewrites, using the eigendecomposition of the data covariance  $\Sigma_{\text{data}} = U \text{Diag}(\lambda_i) U^\top$ :

$$\begin{aligned} \delta m_T &= U \text{Diag} \left( \left( \frac{\lambda_i}{\lambda_i + \sigma_T^2} \right)^{\frac{\alpha+1}{2}} \right) U^\top \mu_{\text{data}} \\ \delta \Sigma_T &= U \text{Diag} \left( \lambda_i \left( \frac{\lambda_i}{\lambda_i + \sigma_T^2} \right)^{\alpha+1} \right) U^\top \end{aligned}$$

First note that the propagated initialization error is independent of the choice of the rescaling schedule  $\eta_t$ . In particular, it is the same for both Variance Exploding and Variance Preserving.

The mean and covariance biases can be used to evaluate the Fréchet distance between  $p_{\text{data}} = \text{Law}(Y_T)$  and  $q_T = \text{Law}(\tilde{Y}_T)$ :

$$\begin{aligned} \text{FD}(p_{\text{data}}, q_T) &= \text{FD}(\text{Law}(Y_T), \text{Law}(\tilde{Y}_T)) \\ &= \|\delta m_T\|^2 + \mathcal{B}^2(\Sigma_{\text{data}}, \Sigma_{\text{data}} - \delta \Sigma_T) \\ &= \sum_{i=1}^d \left( \frac{\lambda_i}{\lambda_i + \sigma_T^2} \right)^{\alpha+1} (U^\top \mu_{\text{data}})_i^2 + \sum_{i=1}^d \left( \sqrt{\lambda_i} - \sqrt{\lambda_i - \lambda_i \left( \frac{\lambda_i}{\lambda_i + \sigma_T^2} \right)^{\alpha+1}} \right)^2 \end{aligned}$$

When  $\sigma_T \rightarrow \infty$ , the first term is  $O(\sigma_T^{-2(\alpha+1)})$  and after expanding the square-root, the second term is  $O(\sigma_T^{-4(\alpha+1)})$ .  $\square$

### A.3 Equivalences between schedulers

**Relation between time stepsize schedules  $\gamma_t$  and diffusion schedules  $(\eta_t, \sigma_t)$**  The following lemma makes precise how a time reparameterization of the reverse SDE induces a corresponding reparameterization of the diffusion schedules, and how this relates to a change of variable-step Euler–Maruyama scheme.

**Proposition 6** (Time change of the reverse SDE). *Let  $\varphi : [0, S] \rightarrow [0, T]$  be an increasing  $\mathcal{C}^1$  bijection and define  $\psi(s) := T - \varphi(S - s)$  for  $s \in [0, S]$ . If  $(Y_t)$  solves (2) and  $Z_s := Y_{\varphi(s)}$ , then  $(Z_s)$  follows the reverse SDE associated with the forward schedules  $(\eta_{\psi(s)}, \sigma_{\psi(s)})$  on horizon  $S$ , namely*

$$Z_0 \sim p_{\psi(S)} = p_T, \quad dZ_s = v_s^\psi(Z_s) ds + \sqrt{2a_s^\psi} dW_s, \quad s \in [0, S], \quad (17)$$

where

$$\begin{aligned} v_s^\psi(x) &:= -\frac{\dot{\eta}_{\psi(S-s)}}{\eta_{\psi(S-s)}}x + (1 + \alpha)(\eta_{\psi(S-s)}^\psi)^2 \dot{\sigma}_{\psi(S-s)} \sigma_{\psi(S-s)} \nabla \log p_{\psi(S-s)}(x), \\ a_s^\psi &:= \alpha(\eta_{\psi(S-s)}^\psi)^2 \dot{\sigma}_{\psi(S-s)} \sigma_{\psi(S-s)}. \end{aligned}$$

In particular,  $Z_s$  has marginals  $p_{S-s}^\psi = p_{T-\varphi(s)}$ . Moreover, the Euler–Maruyama discretization of (17) with constant step  $\gamma$  corresponds to a variable-step Euler–Maruyama discretization of (2) for  $Y$ , with local stepsizes  $\gamma_k = \varphi'(\gamma k)\gamma$ .

**Remark 1.** Standard Variable-step EM is more commonly defined using  $\gamma_k = t_{k+1} - t_k = \varphi(s_{k+1}) - \varphi(s_k)$  which agrees with  $\gamma_k = \gamma\varphi'(s_k)$  up to  $O(\gamma^2)$ .

*Proof.* By the time-change formula,

$$dZ_s = \varphi'(s)v_{\varphi(s)}(Z_s)ds + \sqrt{2\varphi'(s)a_{\varphi(s)}} dW_s.$$

First note that Euler discretization of  $Z_s$  with constant stepsize  $\gamma$  (on the uniform grid  $s_k = k\gamma$ ) gives

$$\hat{Z}_{k+1} = \hat{Z}_k + \gamma\varphi'(s_k)v_{\varphi(s_k)}(\hat{Z}_k) + \sqrt{2\gamma\varphi'(s_k)a_{\varphi(s_k)}} W_k.$$

This is the same stochastic process as the EM discretization of the original SDE (2) on  $Y_t$  with stepsizes  $\gamma_k = \varphi'(s_k)\gamma$ :

$$\hat{Y}_{k+1} = \hat{Y}_k + \gamma_k v_{t_k}(\hat{Y}_k) + \sqrt{2\gamma_k a_{t_k}} W_k$$

Second, since  $\psi(S-s) = T - \varphi(s)$  and  $\dot{\psi}(S-s) = \varphi'(s)$ , we have, denoting  $\eta_s^\psi = \eta_{\psi_s}$ ,  $\sigma_s^\psi = \sigma_{\psi_s}$  and  $p_s^\psi = p_{\psi_s}$ ,

$$\eta_{S-s}^\psi = \eta_{T-\varphi(s)}, \quad \sigma_{S-s}^\psi = \sigma_{T-\varphi(s)}, \quad p_{S-s}^\psi = p_{T-\varphi(s)},$$

and

$$\dot{\eta}_{S-s}^\psi = \dot{\eta}_{T-\varphi(s)}\varphi'(s), \quad \dot{\sigma}_{S-s}^\psi = \dot{\sigma}_{T-\varphi(s)}\varphi'(s).$$

Substituting these identities into the definitions of  $v_t$  and  $a_t$  in (2) gives

$$\varphi'(s)v_{\varphi(s)} = v_s^\psi, \quad \varphi'(s)a_{\varphi(s)} = a_s^\psi,$$

□

In the rest of the paper, we thus consider a uniform stepsize discretization schedule, and allow for different choices of diffusion schedules  $(\eta_t, \sigma_t)$ .

**Equivalence between scale schedules  $\eta_t$  in the continuous setting.** In the continuous (non-discretized) setting, for fixed noise schedule  $\sigma_t$ , any choice of scale schedule  $\eta_t$  is equivalent, up to a change of variable. Therefore, the choice of  $\eta_t$  (Variance Exploding, Variance Preserving, or any other) does not affect the sampling performance of the continuous SDE (2). However, once discretized, this equivalence is lost and the choice of  $\eta_t$  influences the performance of the generative process (3).

## B Proof of Theorem 1

*Proof.* We denote  $\mathcal{F}$  the class of functions  $f : \mathbb{R}^d \rightarrow \mathbb{R}$  that are  $C^\infty$  and with polynomial growth i.e. there is  $k \in \mathbb{N}, C > 0$  such that:

$$\forall x \in \mathbb{R}^d, \quad |f(x)| \leq C(1 + |x|^k)$$

For  $f \in \mathcal{F}$ , we define the backward value function

$$u_s(x) := \mathbb{E}[f(Y_t) \mid Y_s = x] = \mathbb{E}[f(Y_t^{s,x})], \quad 0 \leq s \leq t. \quad (18)$$

where  $Y_t^{s,x} = \Phi_{t,s}(x)$  is the solution at time  $t$  of the SDE that started at time  $s$  from the point  $x$ . Note that the expectation is here taken only with respect to the Brownian motion (not initialization). Then  $u_s$  solves the backward Kolmogorov PDE

$$(\partial_s + \mathcal{L}_s)u_s(\cdot) = 0, \quad u_{t_k}(\cdot) = f. \quad (19)$$

where we recall that  $\mathcal{L}_s f(y) := v_s(y) \cdot \nabla f(y) + a_s \Delta f(y)$ .

We first compute the local weak defect of one Euler–Maruyama step, with time coefficients frozen, for small stepsize  $\gamma$ . For a fixed time  $s \in [0, T]$  and  $x \in \mathbb{R}^d$ , let

$$\bar{Y}_{s+\gamma}^{s,x} = x + \gamma v_s(x) + \sqrt{2\gamma a_s} \xi, \quad \xi \sim \mathcal{N}(0, I_d),$$

**Lemma 1** (One-step weak defect).

$$\mathbb{E}[u_{s+\gamma}(\bar{Y}_{s+\gamma}^{s,x})] - u_s(x) = \gamma^2 \psi_s(x) + O(\gamma^3),$$

where

$$\psi_s(x) = -\frac{1}{2}((\partial_s + \mathcal{L}_s)v_s)(x) \cdot \nabla u_s(x) - a_s \langle \nabla v_s(x), \nabla^2 u_s(x) \rangle - \frac{1}{2} \dot{a}_s \Delta u_s(x).$$

*Proof.* We start the proof of this lemma by a Taylor expansion of  $\mathbb{E}[u_{s+\gamma}(\bar{Y}_{s+\gamma}^{s,x})]$ . We directly state here the final form of the expansion with the following Lemma. Because the proof of the lemma is technical but quite straightforward, it is deferred to the end of the section.

**Lemma 2.** *By a Taylor expansion in time and space,*

$$\begin{aligned} \mathbb{E}[u_{s+\gamma}(\bar{Y}_{s+\gamma}^{s,x})] &= u_s(x) + \gamma(\partial_s u_s + v_s \cdot \nabla u_s + a_s \Delta u_s)(x) \\ &\quad + \gamma^2 \left[ \frac{1}{2} \partial_{ss} u_s + v_s \cdot \nabla \partial_s u_s + a_s \Delta \partial_s u_s + \frac{1}{2} v_s^\top \nabla^2 u_s v_s \right. \\ &\quad \left. + a_s v_s \cdot \nabla \Delta u_s + \frac{1}{2} a_s^2 \Delta^2 u_s \right](x) + O(\gamma^3). \end{aligned} \quad (20)$$

Now, using the backward Kolmogorov equation

$$(\partial_s + \mathcal{L}_s)u_s = 0$$

the first order term of (20) vanishes. Moreover, differentiating  $\partial_s u_s = -\mathcal{L}_s u_s$  with respect to  $s$  gives

$$\partial_{ss} u_s = -(\partial_s \mathcal{L}_s)u_s - \mathcal{L}_s \partial_s u_s.$$

Hence, using again  $\partial_s u_s = -\mathcal{L}_s u_s$ ,

$$\frac{1}{2} \partial_{ss} u_s + \mathcal{L}_s \partial_s u_s = -\frac{1}{2} (\partial_s \mathcal{L}_s)u_s - \frac{1}{2} \mathcal{L}_s^2 u_s.$$

Thus, the second-order term simplifies to:

$$\begin{aligned} & \frac{1}{2}\partial_{ss}u_s + \mathcal{L}_s\partial_s u_s + \frac{1}{2}v_s^\top \nabla^2 u_s v_s + a_s v_s \cdot \nabla \Delta u_s + \frac{1}{2}a_s^2 \Delta^2 u_s \\ &= -\frac{1}{2}(\partial_s \mathcal{L}_s)u_s - \frac{1}{2}\mathcal{L}_s^2 u_s + \frac{1}{2}v_s^\top \nabla^2 u_s v_s + a_s v_s \cdot \nabla \Delta u_s + \frac{1}{2}a_s^2 \Delta^2 u_s. \end{aligned}$$

Since  $\mathcal{L}_s u_s = v_s \cdot \nabla u_s + a_s \Delta u_s$ , we have

$$\mathcal{L}_s^2 u_s = (v_s \cdot \nabla)(v_s \cdot \nabla u_s) + a_s \Delta(v_s \cdot \nabla u_s) + a_s v_s \cdot \nabla \Delta u_s + a_s^2 \Delta^2 u_s.$$

We now expand the two first terms:

$$(v_s \cdot \nabla)(v_s \cdot \nabla u_s) = ((v_s \cdot \nabla)v_s) \cdot \nabla u_s + v_s^\top \nabla^2 u_s v_s.$$

and

$$\Delta(v_s \cdot \nabla u_s) = (\Delta v_s) \cdot \nabla u_s + 2\langle \nabla v_s, \nabla^2 u_s \rangle + v_s \cdot \nabla \Delta u_s.$$

Therefore,

$$\mathcal{L}_s^2 u_s = ((v_s \cdot \nabla)v_s + a_s \Delta v_s) \cdot \nabla u_s + v_s^\top \nabla^2 u_s v_s + 2a_s v_s \cdot \nabla \Delta u_s + 2a_s \langle \nabla v_s, \nabla^2 u_s \rangle + a_s^2 \Delta^2 u_s.$$

Moreover,

$$(\partial_s \mathcal{L}_s)u_s = (\partial_s v_s) \cdot \nabla u_s + \dot{a}_s \Delta u_s.$$

Therefore the second-order coefficient finally simplifies to

$$-\frac{1}{2}((\partial_s + \mathcal{L}_s)v_s) \cdot \nabla u_s - a_s \langle \nabla v_s, \nabla^2 u_s \rangle - \frac{1}{2}\dot{a}_s \Delta u_s,$$

which proves the claim.  $\square$

We now sum these local defects along the Euler trajectory from time 0 to time  $t_k > 0$ . Since  $u_{t_k}(x) = \mathbb{E}[f(Y_k^{t_k, x})] = f(x)$ ,

$$\mathbb{E}[f(\hat{Y}_k)] = \mathbb{E}[u_{t_k}(\hat{Y}_k)].$$

Moreover, by the definition of  $u_0$ ,  $u_0(x) = \mathbb{E}[f(Y_t^{0, x})]$ , and therefore, using  $Y_{t_k}^{0, Y_0} = Y_{t_k}$ ,

$$\mathbb{E}[f(Y_{t_k})] = \mathbb{E}[u_0(Y_0)].$$

We get:

$$\mathbb{E}[f(\hat{Y}_k)] - \mathbb{E}[f(Y_{t_k})] = \sum_{\ell=0}^{k-1} \mathbb{E}\left[u_{t_{\ell+1}}(\hat{Y}_{\ell+1}) - u_{t_\ell}(\hat{Y}_\ell)\right].$$

Applying Lemma 1 gives

$$\mathbb{E}[f(\hat{Y}_k)] - \mathbb{E}[f(Y_{t_k})] = \gamma^2 \sum_{\ell=0}^{k-1} \mathbb{E}[\psi_{t_\ell}(\hat{Y}_\ell)] + O(\gamma^2).$$

With our assumptions,  $\psi_s \in \mathcal{F}$  and the first-order weak consistency of the Euler scheme [Talay and Tubaro, 1990, Theorem 1] implies

$$\left| \mathbb{E}[\psi_{t_\ell}(\hat{Y}_\ell)] - \mathbb{E}[\psi_{t_\ell}(Y_{t_\ell})] \right| \leq C\gamma.$$

Therefore,

$$\gamma^2 \sum_{\ell=0}^{k-1} \mathbb{E}[\psi_{t_\ell}(\widehat{Y}_\ell)] = \gamma^2 \sum_{\ell=0}^{k-1} \mathbb{E}[\psi_{t_\ell}(Y_{t_\ell})] + O(\gamma^2).$$

Moreover, since  $s \mapsto \mathbb{E}[\psi_s(Y_s)]$  is smooth,

$$\gamma^2 \sum_{\ell=0}^{k-1} \mathbb{E}[\psi_{t_\ell}(Y_{t_\ell})] = \gamma \int_0^{t_k} \mathbb{E}[\psi_s(Y_s)] ds + O(\gamma^2).$$

At first order in  $\gamma$ , the sum can thus be replaced by the corresponding integral along the exact process, which gives

$$\mathbb{E}[f(\widehat{Y}_k)] - \mathbb{E}[f(Y_{t_k})] = \gamma \int_0^{t_k} \mathbb{E}[\psi_s(Y_s)] ds + O(\gamma^2).$$

It remains to rewrite  $\psi_s(Y_s)$  in terms of derivatives of  $f$  at the final time  $t_k$ .

Let  $J_{t,s}(x) = \nabla_y Y_t^{s,x}$  the Jacobian, at time  $t$ , of the process starting from  $x$  at time  $s$ ; as well as  $H_{t,s}(x) := \nabla_y^2 Y_t^{s,x}$  the Hessian process, which is a 3-tensor and the Laplacian process  $\Delta_{t,s}(x) := (\Delta_y(Y_t^{s,x})_i)_{i \in \llbracket 1, d \rrbracket}$ . By differentiating  $u_s(x) = \mathbb{E}[f(Y_t^{s,x})]$  w.r.t the initial condition  $x$  we get:

$$\nabla u_s(x) = \mathbb{E}\left[J_{t,s}(x)^\top \nabla f(Y_t^{s,x})\right] \quad (21)$$

$$\nabla^2 u_s(x) = \mathbb{E}\left[H_{t,s}(x) [\nabla f(Y_t^{s,x})] + J_{t,s}(x)^\top \nabla^2 f(Y_t^{s,x}) J_{t,s}(x)\right] \quad (22)$$

where we denote for the 3-tensor  $H_{t,s}$  and  $v \in \mathbb{R}^d$ , the contraction  $H_{t,s}[v] \in \mathbb{R}^{d \times d}$  with  $(H_{t,s}[v])_{k,l} = \sum_{i=1}^d (H_{t,s})_{ikl} v_i$ .

$$\Delta u_s(x) = \mathbb{E}\left[\Delta_{t,s}(x) \cdot \nabla f(Y_t^{s,x}) + \langle J_{t,s}(x) J_{t,s}(x)^\top, \nabla^2 f(Y_t^{s,x}) \rangle\right] \quad (23)$$

Substituting (21), (22) and (23) into the expression of  $\psi_s$  gives

$$\begin{aligned} \psi_s(x) = & -\frac{1}{2} \mathbb{E}\left[\left(J_{t,s}(x) [(\partial_s + \mathcal{L}_s)v_s](x) + 2a_s [H_{t,s}(x), \nabla v_s(x)] + \dot{a}_s \Delta_{t,s}(x)\right) \cdot \nabla f(Y_t^{s,x})\right] \\ & - a_s \mathbb{E}\left[\langle \nabla v_s(x), J_{t,s}(x)^\top \nabla^2 f(Y_t^{s,x}) J_{t,s}(x) \rangle\right] - \frac{1}{2} \dot{a}_s \mathbb{E}\left[\langle J_{t,s}(x) J_{t,s}(x)^\top, \nabla^2 f(Y_t^{s,x}) \rangle\right]. \end{aligned} \quad (24)$$

Using that for a matrix  $A \in \mathbb{R}^{d \times d}$

$$\langle \nabla v_s(x), J_{t,s}(x)^\top A J_{t,s}(x) \rangle = \langle J_{t,s}(x) \nabla v_s(x) J_{t,s}(x)^\top, A \rangle,$$

and the fact that, since  $\nabla^2 f(Y_t^{s,x})$  is symmetric, only the symmetric part of  $J_{t,s}(x) \nabla v_s(x) J_{t,s}(x)^\top$  contributes, we get

$$\langle J_{t,s}(x) \nabla v_s(x) J_{t,s}(x)^\top, \nabla^2 f(Y_t^{s,x}) \rangle = \langle E_{t,s}(x), \nabla^2 f(Y_t^{s,x}) \rangle,$$

where we set

$$e_{t,s}(x) := -\frac{1}{2} J_{t,s}(x) [(\partial_s + \mathcal{L}_s)v_s](x) - a_s [H_{t,s}(x), \nabla v_s(x)] - \frac{1}{2} \dot{a}_s \Delta_{t,s}(x) \in \mathbb{R}^d, \quad (25)$$

$$E_{t,s}(x) := -\frac{1}{2} J_{t,s}(x) \left( a_s (\nabla v_s(x) + \nabla v_s(x)^\top) + \dot{a}_s I_d \right) J_{t,s}(x)^\top \in \mathbb{R}^{d \times d}. \quad (26)$$

Hence (24) rewrites as

$$\psi_s(x) = \mathbb{E} \left[ e_{t,s}(x) \cdot \nabla f(Y_t^{s,x}) + \langle E_{t,s}(x), \nabla^2 f(Y_t^{s,x}) \rangle \right]. \quad (27)$$

We now replace the deterministic initial condition  $x$  by the random state  $Y_s$ . Denoting by  $\mathcal{F}_s$  the natural filtration of the process,  $Y_s$  is  $\mathcal{F}_s$ -measurable and the future Brownian increments are independent of  $\mathcal{F}_s$ . Therefore, (27) yields

$$\psi_s(Y_s) = \mathbb{E} \left[ e_{t,s}(Y_s) \cdot \nabla f(Y_t^{s,Y_s}) + \langle E_{t,s}(Y_s), \nabla^2 f(Y_t^{s,Y_s}) \rangle \middle| \mathcal{F}_s \right].$$

Using the flow property  $Y_t^{s,Y_s} = Y_t$ , and the notations

$$J_{t,s}(Y) := J_{t,s}(Y_s), \quad H_{t,s}(Y) := H_{t,s}(Y_s), \quad \Delta_{t,s}(Y) := \Delta_{t,s}(Y_s),$$

we obtain

$$\psi_s(Y_s) = \mathbb{E} \left[ e_{t,s}(Y) \cdot \nabla f(Y_t) + \langle E_{t,s}(Y), \nabla^2 f(Y_t) \rangle \middle| \mathcal{F}_s \right].$$

Taking expectation gives

$$\mathbb{E}[\psi_s(Y_s)] = \mathbb{E} \left[ e_{t,s}(Y) \cdot \nabla f(Y_t) + \langle E_{t,s}(Y), \nabla^2 f(Y_t) \rangle \right]. \quad (28)$$

and finally:

$$\mathbb{E}[f(\hat{Y}_k)] - \mathbb{E}[f(Y_{t_k})] = \gamma \int_0^{t_k} \mathbb{E} \left[ e_{t_k,s}(Y) \cdot \nabla f(Y_{t_k}) + \langle E_{t_k,s}(Y), \nabla^2 f(Y_{t_k}) \rangle \right] ds + O(\gamma^2),$$

which concludes the proof.  $\square$

We finally give here the proof of the Taylor expansion (20) from Lemma 2.

*Proof of Lemma 2.* Set

$$\delta_\gamma := \gamma v_s(x) + \sqrt{2\gamma a_s} \xi$$

so that

$$\bar{Y}_{s+\gamma}^{s,x} = x + \delta_\gamma.$$

We Taylor expand  $u_{s+\gamma}(x + \delta_\gamma)$  around  $(s, x)$  in both space (at order 4) and time (at order 2) to keep terms up to  $O(\gamma^2)$ :

$$\begin{aligned} u_{s+\gamma}(x + \delta_\gamma) &= u_s(x) + \gamma \partial_s u_s(x) + \nabla u_s(x) \cdot \delta_\gamma \\ &\quad + \frac{\gamma^2}{2} \partial_{ss} u_s(x) + \gamma \nabla \partial_s u_s(x) \cdot \delta_\gamma + \frac{1}{2} \delta_\gamma^\top \nabla^2 u_s(x) \delta_\gamma \\ &\quad + \frac{\gamma}{2} \delta_\gamma^\top \nabla^2 \partial_s u_s(x) \delta_\gamma + \frac{1}{6} \nabla^3 u_s(x) [\delta_\gamma, \delta_\gamma, \delta_\gamma] \\ &\quad + \frac{1}{24} \nabla^4 u_s(x) [\delta_\gamma, \delta_\gamma, \delta_\gamma, \delta_\gamma] + O(\gamma^3). \end{aligned}$$

We now calculate the expectation of each term with respect to the noise  $\xi \sim \mathcal{N}(0, \text{Id})$ . Since  $\mathbb{E}[\delta_\gamma] = \gamma v_s(x)$ , we have

$$\mathbb{E}[\nabla u_s(x) \cdot \delta_\gamma] = \gamma v_s(x) \cdot \nabla u_s(x).$$

Moreover,  $\mathbb{E}[\delta_\gamma \delta_\gamma^\top] = \gamma^2 v_s(x) v_s(x)^\top + 2\gamma a_s I_d$ , and hence

$$\frac{1}{2} \mathbb{E}[\delta_\gamma^\top \nabla^2 u_s(x) \delta_\gamma] = \gamma a_s \Delta u_s(x) + \frac{\gamma^2}{2} v_s(x)^\top \nabla^2 u_s(x) v_s(x).$$

Similarly,

$$\gamma \mathbb{E}[\nabla \partial_s u_s(x) \cdot \delta_\gamma] = \gamma^2 v_s(x) \cdot \nabla \partial_s u_s(x),$$

and

$$\frac{\gamma}{2} \mathbb{E}[\delta_\gamma^\top \nabla^2 \partial_s u_s(x) \delta_\gamma] = \gamma^2 a_s \Delta \partial_s u_s(x) + O(\gamma^3).$$

For the cubic term, after taking expectation, the only non-zero term of order  $\gamma^2$  comes from one factor  $\gamma v_s(x)$  and two Gaussian factors  $\sqrt{2\gamma a_s} \xi$ . In coordinates:

$$\mathbb{E}[\delta_{\gamma,i} \delta_{\gamma,j} \delta_{\gamma,k}] = 2\gamma^2 a_s (v_{s,i}(x) \delta_{jk} + v_{s,j}(x) \delta_{ik} + v_{s,k}(x) \delta_{ij}) + O(\gamma^3).$$

Thus, by symmetry over indexes

$$\begin{aligned} \frac{1}{6} \sum_{i,j,k} \partial_{ijk} u_s(x) \mathbb{E}[\delta_{\gamma,i} \delta_{\gamma,j} \delta_{\gamma,k}] &= \frac{1}{6} \sum_{i,j,k} \partial_{ijk} u_s(x) 2\gamma^2 a_s (v_{s,i} \delta_{jk} + v_{s,j} \delta_{ik} + v_{s,k} \delta_{ij}) \\ &= \gamma^2 a_s \sum_i v_{s,i} \partial_i \Delta u_s(x). \end{aligned}$$

That is to say

$$\frac{1}{6} \mathbb{E}[\nabla^3 u_s(x) [\delta_\gamma, \delta_\gamma, \delta_\gamma]] = \gamma^2 a_s v_s(x) \cdot \nabla \Delta u_s(x) + O(\gamma^3).$$

For the quartic term, after taking expectation, the only non-zero term of order  $\gamma^2$  comes from the fourth moment of the Gaussian part. Since

$$\mathbb{E}[\xi_i \xi_j \xi_k \xi_\ell] = \delta_{ij} \delta_{kl} + \delta_{ik} \delta_{jl} + \delta_{il} \delta_{jk},$$

we obtain, again by symmetry over indices

$$\frac{1}{24} (2\gamma a_s)^2 \sum_{i,j,k,\ell} \partial_{ijk\ell} u_s(x) (\delta_{ij} \delta_{kl} + \delta_{ik} \delta_{jl} + \delta_{il} \delta_{jk}) = \frac{1}{2} \gamma^2 a_s^2 \Delta^2 u_s(x).$$

i.e.

$$\frac{1}{24} \mathbb{E}[\nabla^4 u_s(x) [\delta_\gamma, \delta_\gamma, \delta_\gamma, \delta_\gamma]] = \frac{1}{2} \gamma^2 a_s^2 \Delta^2 u_s(x) + O(\gamma^3).$$

□

## C Proof of Corollary 1

*Proof. Error on the mean.* For  $i \in \llbracket 1, d \rrbracket$ , we apply Theorem 1 with  $f^{(i)}(x) = x_i$  to get, in vector form,

$$\mathbb{E}[\hat{Y}_k] - \mathbb{E}[Y_{t_k}] = \gamma \int_0^{t_k} \mathbb{E}[e_{t_k,s}(Y)] ds + O(\gamma^2) \quad (29)$$

The corollary directly applies the above result at final iteration  $K$  i.e.  $t_k = T$ , for which  $\mathbb{E}[Y_T] = \mu_{\text{data}}$ .

**Error on the covariance.** For  $i, j \in \llbracket 1, d \rrbracket$ , we now apply the above result with  $f^{(i,j)}(x) = x_i x_j$ . Then  $\nabla f^{(i,j)}(x) = x_j e_i + x_i e_j$  and  $\nabla^2 f^{(i,j)}(x) = E_{ij} + E_{ji}$ . Applying Theorem 1 componentwise gives

$$\begin{aligned} & \mathbb{E}[(\hat{Y}_k)_i (\hat{Y}_k)_j] - \mathbb{E}[(Y_{t_k})_i (Y_{t_k})_j] \\ &= \gamma \int_0^{t_k} \mathbb{E} \left[ e_{t_k,s}(Y) \cdot \nabla f^{(i,j)}(Y_{t_k}) + \langle E_{t_k,s}(Y), \nabla^2 f^{(i,j)}(Y_{t_k}) \rangle \right] ds + O(\gamma^2). \end{aligned}$$

Using that  $E_{t_k,s}(Y)$  is symmetric,

$$\langle E_{t_k,s}(Y), \nabla^2 f^{(i,j)}(Y_{t_k}) \rangle = 2 \langle E_{t_k,s}(Y), E_{i,j} \rangle = 2(E_{t_k,s}(Y))_{ij}.$$

In matrix form:

$$\mathbb{E}[\hat{Y}_k \hat{Y}_k^\top] - \mathbb{E}[Y_{t_k} Y_{t_k}^\top] = \gamma \int_0^{t_k} \mathbb{E} \left[ e_{t_k,s}(Y) Y_{t_k}^\top + Y_{t_k} e_{t_k,s}(Y)^\top + 2E_{t_k,s}(Y) \right] ds$$

We now deduce the error on the covariance. Denoting  $m_t = \mathbb{E}[Y_t]$  and  $K_t = \mathbb{E}[Y_t Y_t^\top]$ , as well as  $\hat{m}_k = \mathbb{E}[\hat{Y}_k]$  and  $\hat{K}_k := \mathbb{E}[\hat{Y}_k \hat{Y}_k^\top]$ , the covariance verifies  $\text{Cov}(Y_t) = K_t - m_t m_t^\top$  and  $\text{Cov}(\hat{Y}_k) = \hat{K}_k - \hat{m}_k \hat{m}_k^\top$ . Then:

$$\text{Cov}(\hat{Y}_k) - \text{Cov}(Y_{t_k}) = (\hat{K}_k - K_{t_k}) - (\hat{m}_k \hat{m}_k^\top - m_{t_k} m_{t_k}^\top). \quad (30)$$

Using

$$m_{t_k} m_{t_k}^\top - \hat{m}_k \hat{m}_k^\top = (m_{t_k} - \hat{m}_k) m_{t_k}^\top + m_{t_k} (m_{t_k} - \hat{m}_k)^\top - (m_{t_k} - \hat{m}_k) (m_{t_k} - \hat{m}_k)^\top,$$

and the fact that  $m_{t_k} - \hat{m}_k = O(\gamma)$ , we have:

$$m_{t_k} m_{t_k}^\top - \hat{m}_k \hat{m}_k^\top = (m_{t_k} - \hat{m}_k) m_{t_k}^\top + m_{t_k} (m_{t_k} - \hat{m}_k)^\top + o(\gamma)$$

Thus, using (5), the first order discretization error on the covariance writes

$$\text{Cov}[\hat{Y}_k] - \text{Cov}[Y_{t_k}] = \gamma \int_0^{t_k} \left( \text{Cov} \left[ e_{t_k,s}(Y), Y_{t_k} \right] + \text{Cov} \left[ e_{t_k,s}(Y), Y_{t_k} \right]^\top + 2\mathbb{E} \left[ E_{t_k,s}(Y) \right] \right) ds \quad (31)$$

The corollary directly applies the above result at final iteration  $K$  i.e.  $t_k = T$ , for which  $\text{Cov}[Y_T] = \Sigma_{\text{data}}$ .  $\square$

## D Fréchet distance expansions

The first-order errors on the mean and on the covariance calculated in Corollary 1 can be combined into a first-order expansion of the Fréchet distance to the target distribution. The Fréchet distance compares the first and second order moments of two distributions, and is defined by

$$\text{FD}(p_{\text{data}}, \text{Law}(y)) = \left\| \mu_{\text{data}} - \mathbb{E}[y] \right\|^2 + \mathcal{B}^2 \left( \Sigma_{\text{data}}, \text{Cov}[y] \right) \quad (32)$$

with the Bures distance between covariances:

$$\mathcal{B}^2(\Sigma_{\text{data}}, \Sigma) = \text{Tr} \left( \Sigma_{\text{data}} + \Sigma - 2(\sqrt{\Sigma_{\text{data}}} \Sigma \sqrt{\Sigma_{\text{data}}})^{1/2} \right). \quad (33)$$

With the following result, we consider the Fréchet sampling error between the distribution of the final iterate  $\text{Law}(\hat{Y}_K)$  and the data distribution  $p_{\text{data}}$ . We express this Fréchet error with respect to the errors on the mean and covariance calculated in Corollary 1, namely:

$$d_k^\mu = \mathbb{E}[\hat{Y}_k] - \mathbb{E}[Y_{t_k}] = \gamma d_k^{\mu,[1]} + o(\gamma) \quad \text{and} \quad D_k^\Sigma = \text{Cov}[\hat{Y}_k] - \text{Cov}[Y_{t_k}] = \gamma D_k^{\Sigma,[1]} + o(\gamma)$$

We also simplify the final expression making use of the eigendecomposition of the data covariance  $\Sigma_{\text{data}} = U \text{Diag}(\lambda_i) U^\top$ .

**Proposition 7** (Fréchet distance expansion). *With the previous notations:*

$$\text{FD}(p_{\text{data}}, \text{Law}(\hat{Y}_K)) = \gamma^2 \left\| d_K^{\mu, [1]} \right\|^2 + \frac{\gamma^2}{2} \sum_{i,j=1}^d \frac{\left( u_i^\top D_K^{\Sigma, [1]} u_j \right)^2}{\lambda_i + \lambda_j} + o(\gamma^2).$$

*Proof.* Malago et al. [2018] give the first order expansion of the Bures distance: for  $\Sigma_0 \in \text{Sym}^{++}(d)$ , and  $\Sigma_1 \in \text{Sym}(d)$  such that for small enough  $\varepsilon$ ,  $\Sigma_0 \pm \varepsilon \Sigma_1 \in \text{Sym}^+(d)$ ,

$$\mathcal{B}^2(\Sigma_0, \Sigma_0 + \varepsilon \Sigma_1) = \frac{\varepsilon^2}{2} \text{Tr} \left( \Sigma_1 L_{\Sigma_0}^{-1} [\Sigma_1] \right) + o(\varepsilon^2)$$

where we used the matrix Lyapunov operator, defined for a real matrix  $C$  by  $L_C[X] = CX + XC^\top$ .

Using  $\text{Cov}[\hat{Y}_K] = \text{Cov}[Y_T] + \gamma D_K^{\Sigma, [1]} + o(\gamma)$  and  $\text{Cov}[Y_T] = \Sigma_{\text{data}}$ , we get

$$\mathcal{B}^2 \left( \Sigma_{\text{data}}, \text{Cov}[\hat{Y}_K] \right) = \mathcal{B}^2 \left( \Sigma_{\text{data}}, \Sigma_{\text{data}} + \gamma D_K^{\Sigma, [1]} \right) = \frac{\gamma^2}{2} \text{Tr} \left( D_K^{\Sigma, [1]} L_{\Sigma_{\text{data}}}^{-1} \left[ D_K^{\Sigma, [1]} \right] \right)$$

We can then use the decomposition of the inverse Lyapunov operator  $L_C^{-1}$  in the eigenbasis of the data covariance, given in the following Lemma:

**Lemma 3.** *For  $C \in \text{Sym}^{++}(d)$ , denoting  $C = U \text{Diag}(\lambda_i)_{1 \leq i \leq d} U^\top$  the diagonalization of  $C$  in its eigenbasis, the inverse operator of  $L_C[X]$  decomposes as*

$$(L_C)^{-1}[X] = U \left( U^\top X U \odot \left( \frac{1}{\lambda_i + \lambda_j} \right)_{1 \leq i, j \leq d} \right) U^\top.$$

The proof follows directly from  $L_C^{-1}[Z] = X \Leftrightarrow U^\top(CX + XC^\top)U = U^\top ZU$ . When applied to our  $L_{\Sigma_{\text{data}}}^{-1} \left[ D_K^{\Sigma, [1]} \right]$ , it gives:

$$L_{\Sigma_{\text{data}}}^{-1} \left[ D_K^{\Sigma, [1]} \right] = U \left( U^\top D_K^{\Sigma, [1]} U \odot \left( \frac{1}{\lambda_i + \lambda_j} \right)_{1 \leq i, j \leq p} \right) U^\top$$

We can finally deduce:

$$\frac{\gamma^2}{2} \text{Tr} \left( D_K^{\Sigma, [1]} L_{\Sigma_{\text{data}}}^{-1} \left[ D_K^{\Sigma, [1]} \right] \right) = \frac{\gamma^2}{2} \sum_{i,j} \frac{(U^\top D_K^{\Sigma, [1]} U)_{i,j}^2}{\lambda_i + \lambda_j}$$

□

## D.1 For Gaussian data

**First-order expansion** Using the above notations, under Gaussian data  $p_{\text{data}} \sim \mathcal{N}(\mu_{\text{data}}, \Sigma_{\text{data}})$ , Proposition 1 gives the mean and covariance errors decomposed along the eigenspace of the data covariance  $\Sigma_{\text{data}} = U \text{Diag}(\lambda_i) U^\top$ :

$$\begin{aligned} d_K^{\mu, [1]} &= U \text{Diag} \left( \Delta_K^{\mu, [1]}(\lambda_i) \right) U^\top \mu_{\text{data}} \\ D_K^{\Sigma, [1]} &= U \text{Diag} \left( \Delta_K^{\Sigma, [1]}(\lambda_i) \right) U^\top \end{aligned}$$

Applying the above Proposition 7 gives directly

$$\text{FD}(p_{\text{data}}, \text{Law}(\hat{Y}_K)) = \gamma^2 \sum_{i=1}^d \Delta^{\mu, [1]}(\lambda_i)^2 (u_i^\top \mu_{\text{data}})^2 + \frac{\gamma^2}{4} \sum_{i=1}^d \frac{\Delta^{\Sigma, [1]}(\lambda_i)^2}{\lambda_i} + o(\gamma^2)$$

Instead of passing by the general decomposition of Proposition 7, one could also simply use the per-eigenvalue decomposition of the Bures distance, as used below.

**Higher order expansion** In Proposition 1, we have seen that the mean and covariance errors fully decompose in the eigenbasis of  $\Sigma_{\text{data}} = U \text{Diag}(\lambda_i) U^\top$  as:

$$\begin{aligned} \mathbb{E}[\hat{Y}_K] &= \mu_{\text{data}} + U \text{Diag} \left( \Delta^\mu(\lambda_i) \right) U^\top \mu_{\text{data}}, \\ \text{Cov}[\hat{Y}_K] &= \Sigma_{\text{data}} + U \text{Diag} \left( \Delta^\Sigma(\lambda_i) \right) U^\top. \end{aligned}$$

The Fréchet distance (32) simplifies directly to:

$$\begin{aligned} \text{FD}(p_{\text{data}}, \text{Law}(y)) &= \left\| U \text{Diag} \left( \Delta^\mu(\lambda_i) \right) U^\top \mu_{\text{data}} \right\|^2 + \mathcal{B}^2 \left( U \text{Diag}(\lambda_i) U^\top, U \text{Diag} \left( \lambda_i + \Delta^\Sigma(\lambda_i) \right) U^\top \right) \\ &= \sum_{i=1}^d \Delta^\mu(\lambda_i)^2 (u_i^\top \mu_{\text{data}})^2 + \sum_{i=1}^d \left( \sqrt{\lambda_i} - \sqrt{\lambda_i + \Delta^\Sigma(\lambda_i)} \right)^2 \end{aligned}$$

Proposition 1 also gives a second-order expansions of the mean and covariance defects:

$$\begin{aligned} \Delta^\mu(\lambda) &= \gamma \Delta^{\mu, [1]}(\lambda) + \gamma^2 \Delta^{\mu, [2]}(\lambda) + O(\gamma^3) \\ \Delta^\Sigma(\lambda) &= \gamma \Delta^{\Sigma, [1]}(\lambda) + \gamma^2 \Delta^{\Sigma, [2]}(\lambda) + O(\gamma^3) \end{aligned}$$

Expanding the square for the mean term,

$$\Delta^\mu(\lambda_i)^2 = \gamma^2 \left( \Delta^{\mu, [1]}(\lambda_i) \right)^2 + 2\gamma^3 \Delta^{\mu, [1]}(\lambda_i) \Delta^{\mu, [2]}(\lambda_i) + O(\gamma^4).$$

For the covariance term, using the square-root expansion

$$\left( \sqrt{\lambda + \delta} - \sqrt{\lambda} \right)^2 = \frac{\delta^2}{4\lambda} - \frac{\delta^3}{8\lambda^2} + O(\delta^4),$$

we get

$$\begin{aligned} \left( \sqrt{\lambda_i} - \sqrt{\lambda_i + \Delta^\Sigma(\lambda_i)} \right)^2 &= \frac{\gamma^2}{4\lambda_i} \left( \Delta^{\Sigma, [1]}(\lambda_i) \right)^2 \\ &\quad + \gamma^3 \left[ \frac{\Delta^{\Sigma, [1]}(\lambda_i) \Delta^{\Sigma, [2]}(\lambda_i)}{2\lambda_i} - \frac{\left( \Delta^{\Sigma, [1]}(\lambda_i) \right)^3}{8\lambda_i^2} \right] + O(\gamma^4). \end{aligned}$$

Therefore,

$$\text{FD}(p_{\text{data}}, \text{Law}(\hat{Y}_K)) = \gamma^2 \mathcal{E}^{[0]} + \gamma^3 \mathcal{E}^{[1]} + O(\gamma^4), \quad (34)$$

where

$$\begin{aligned} \mathcal{E}^{[0]} &:= \sum_{i=1}^d \left( \Delta^{\mu, [1]}(\lambda_i) \right)^2 (u_i^\top \mu_{\text{data}})^2 + \frac{1}{4} \sum_{i=1}^d \frac{\left( \Delta^{\Sigma, [1]}(\lambda_i) \right)^2}{\lambda_i}, \\ \mathcal{E}^{[1]} &:= 2 \sum_{i=1}^d \Delta^{\mu, [1]}(\lambda_i) \Delta^{\mu, [2]}(\lambda_i) (u_i^\top \mu_{\text{data}})^2 + \sum_{i=1}^d \left[ \frac{\Delta^{\Sigma, [1]}(\lambda_i) \Delta^{\Sigma, [2]}(\lambda_i)}{2\lambda_i} - \frac{\left( \Delta^{\Sigma, [1]}(\lambda_i) \right)^3}{8\lambda_i^2} \right]. \end{aligned}$$

## E Affine drift mean and covariance expansions

**Proposition 8** (Affine drift mean and covariance errors). *Under the affine drift  $v_t(x) = H_t x + r_t$ , the mean and covariance biases admit the expansions*

$$\mathbb{E}[\hat{Y}_k] - \mathbb{E}[Y_{t_k}] = \gamma d_{t_k}^{\mu,[1]} + \gamma^2 d_{t_k}^{\mu,[2]} + O(\gamma^3), \quad (35)$$

$$\text{Cov}[\hat{Y}_k] - \text{Cov}[Y_{t_k}] = \gamma D_{t_k}^{\Sigma,[1]} + \gamma^2 D_{t_k}^{\Sigma,[2]} + O(\gamma^3), \quad (36)$$

where, denoting  $m_s := \mathbb{E}[Y_s]$  and  $C_s := \text{Cov}(Y_s)$ ,

$$d_{t_k}^{\mu,[1]} = -\frac{1}{2} \int_0^{t_k} J_{t_k,s} \ddot{m}_s ds, \quad (37)$$

$$D_{t_k}^{\Sigma,[1]} = -\int_0^{t_k} J_{t_k,s} \left( \frac{1}{2} \ddot{C}_s - H_s C_s H_s^\top \right) J_{t_k,s}^\top ds, \quad (38)$$

$$d_{t_k}^{\mu,[2]} = \int_0^{t_k} J_{t_k,s} \left[ -\frac{1}{2} (\dot{H}_s + H_s^2) d_s^{\mu,[1]} + \frac{1}{4} H_s \ddot{m}_s + \frac{1}{12} \ddot{m}_s \right] ds, \quad (39)$$

$$D_{t_k}^{\Sigma,[2]} = \int_0^{t_k} J_{t_k,s} \begin{bmatrix} -\frac{1}{2} (\dot{H}_s + H_s^2) D_s^{\Sigma,[1]} - \frac{1}{2} D_s^{\Sigma,[1]} (\dot{H}_s^\top + (H_s^\top)^2) \\ + \frac{1}{4} H_s \ddot{C}_s + \frac{1}{4} \ddot{C}_s H_s^\top + \frac{1}{12} \ddot{C}_s \\ - \frac{1}{2} \dot{H}_s C_s H_s^\top - \frac{1}{2} H_s C_s \dot{H}_s^\top \\ - H_s^2 C_s H_s^\top - H_s C_s (H_s^\top)^2 - a_s H_s H_s^\top \end{bmatrix} J_{t_k,s}^\top ds. \quad (40)$$

*Proof.* We consider the affine drift  $v_s(x) = H_s x + r_s$ . The Jacobian  $J_{t,s}$  then verifies

$$\frac{dJ_{t,s}}{dt} = H_t J_{t,s}, \quad J_{s,s} = \text{Id},$$

and is deterministic. Moreover, the Hessian and Laplacian of the flow vanish:

$$H_{t,s}(Y) = 0, \quad \Delta_{t,s}(Y) = 0.$$

The quantities  $e_{t,s}$  and  $E_{t,s}$  from Theorem 1 simplify to:

$$e_{t,s}(Y) = -\frac{1}{2} J_{t,s} [\dot{H}_s Y_s + \dot{r}_s + H_s (H_s Y_s + r_s)], \quad (41)$$

$$E_{t,s}(Y) = -\frac{1}{2} J_{t,s} [a_s (H_s + H_s^\top) + \dot{a}_s \text{Id}] J_{t,s}^\top. \quad (42)$$

**First order coefficients** For the first order error we specialize Corollary 1 to the linear drift. Note that the mean  $m_s := \mathbb{E}[Y_s]$  and covariance  $C_s := \text{Cov}(Y_s)$  along the continuous SDE (2) follow the ODEs:

$$\dot{m}_s = H_s m_s + r_s, \quad (43)$$

$$\dot{C}_s = H_s C_s + C_s H_s^\top + 2a_s \text{Id}. \quad (44)$$

Differentiating (43) gives

$$\ddot{m}_s = \dot{H}_s m_s + H_s (H_s m_s + r_s) + \dot{r}_s$$

Therefore, applying (29) with (41) gives

$$\begin{aligned}\mathbb{E}[\hat{Y}_k] - \mathbb{E}[Y_{t_k}] &= \gamma \int_0^{t_k} \mathbb{E}[e_{t_k,s}(Y)] ds + O(\gamma^2) \\ &= -\frac{\gamma}{2} \int_0^{t_k} J_{t_k,s} [\dot{H}_s m_s + \dot{r}_s + H_s (H_s m_s + r_s)] ds + O(\gamma^2) \\ &= -\frac{\gamma}{2} \int_0^{t_k} J_{t_k,s} \ddot{m}_s ds + O(\gamma^2),\end{aligned}$$

which proves (37).

For the covariance error, we specialize (31) for affine drift. Using the variation-of-constants formula [Davis, 1977], the solution of the SDE (2) with linear drift takes the form

$$Y_t = J_{t,s} Y_s + b_{t,s}.$$

Thus  $\text{Cov}(Y_s, Y_t) = C_s J_{t,s}^\top$  and using (41):

$$\text{Cov}[e_{t_k,s}(Y), Y_{t_k}] = -\frac{1}{2} J_{t_k,s} [\dot{H}_s + H_s^2] C_s J_{t_k,s}^\top.$$

The covariance error (31) becomes

$$\begin{aligned}\text{Cov}[\hat{Y}_k] - \text{Cov}[Y_{t_k}] &= -\gamma \int_0^{t_k} J_{t_k,s} \left[ +\frac{1}{2} (\dot{H}_s + H_s^2) \Sigma_s + \frac{1}{2} \Sigma_s (\dot{H}_s^\top + (H_s^\top)^2) \right. \\ &\quad \left. + a_s (H_s + H_s^\top) + \dot{a}_s \text{Id} \right] J_{t_k,s}^\top ds + O(\gamma^2).\end{aligned}$$

Moreover, differentiating the covariance ODE (44) gives

$$\frac{1}{2} \ddot{C}_s - H_s C_s H_s^\top = \frac{1}{2} (\dot{H}_s + H_s^2) C_s + \frac{1}{2} C_s (\dot{H}_s^\top + (H_s^\top)^2) + a_s (H_s + H_s^\top) + \dot{a}_s \text{Id},$$

which proves (38).

**Second-order coefficients.** For the second-order coefficients, we need to re-write the expansion of the mean and covariance from scratch in the linear-drift setting. Recall that the exact mean  $m_s = \mathbb{E}[Y_s]$  and covariance  $C_s = \text{Cov}[Y_s]$  follow the ODEs

$$\dot{m}_s = H_s m_s + r_s, \tag{45}$$

$$\dot{C}_s = H_s C_s + C_s H_s^\top + 2a_s \text{Id}. \tag{46}$$

We can write similar equations for the mean  $\hat{m}_k = \mathbb{E}[\hat{Y}_k]$  and covariance  $\hat{C}_k = \text{Cov}[\hat{Y}_k]$  of the discretized process. Taking expectations in (3) with affine drift:

$$\hat{Y}_{k+1} = \hat{Y}_k + \gamma (H_{t_k} \hat{Y}_k + r_{t_k}) + \sqrt{2\gamma a_{t_k}} \xi_k, \quad \xi_k \sim \mathcal{N}(0, I),$$

gives

$$\hat{m}_{k+1} = \hat{m}_k + \gamma (H_{t_k} \hat{m}_k + r_{t_k}). \tag{47}$$

Similarly, taking covariance:

$$\hat{C}_{k+1} = (I + \gamma H_{t_k}) \hat{C}_k (I + \gamma H_{t_k})^\top + 2\gamma a_{t_k} \text{Id}. \tag{48}$$

Moreover, Taylor expanding the exact mean and covariance at time  $t_k$  gives

$$m_{t_{k+1}} = m_{t_k} + \gamma \dot{m}_{t_k} + \frac{\gamma^2}{2} \ddot{m}_{t_k} + \frac{\gamma^3}{6} m_{t_k}^{(3)} + O(\gamma^4), \quad (49)$$

$$C_{t_{k+1}} = C_{t_k} + \gamma \dot{C}_{t_k} + \frac{\gamma^2}{2} \ddot{C}_{t_k} + \frac{\gamma^3}{6} C_{t_k}^{(3)} + O(\gamma^4). \quad (50)$$

*Second-order mean error.* We look for an expansion of the form

$$d_k^\mu := \mathbb{E}[\hat{Y}_k] - \mathbb{E}[Y_{t_k}] = \gamma d_{t_k}^{\mu,[1]} + \gamma^2 d_{t_k}^{\mu,[2]} + \gamma^3 d_{t_k}^{\mu,[3]} + O(\gamma^4).$$

We subtract the above Taylor expansion (49) from the recursion (47):

$$d_{k+1}^\mu = (I + \gamma H_{t_k}) d_k^\mu - \frac{\gamma^2}{2} \ddot{m}_{t_k} - \frac{\gamma^3}{6} m_{t_k}^{(3)} + O(\gamma^4). \quad (51)$$

We also Taylor expand  $d_{t_{k+1}}^{\mu,[1]}$  and  $d_{t_{k+1}}^{\mu,[2]}$ :

$$\begin{aligned} d_{t_{k+1}}^{\mu,[1]} &= d_{t_k}^{\mu,[1]} + \gamma \dot{d}_{t_k}^{\mu,[1]} + \frac{1}{2} \gamma^2 \ddot{d}_{t_k}^{\mu,[1]} + O(\gamma^3) \\ d_{t_{k+1}}^{\mu,[2]} &= d_{t_k}^{\mu,[2]} + \gamma \dot{d}_{t_k}^{\mu,[2]} + O(\gamma^2), \end{aligned}$$

to get:

$$d_{k+1}^\mu = \gamma d_{t_k}^{\mu,[1]} + \gamma^2 (\dot{d}_{t_k}^{\mu,[1]} + d_{t_k}^{\mu,[2]}) + \gamma^3 (\frac{1}{2} \ddot{d}_{t_k}^{\mu,[1]} + \dot{d}_{t_k}^{\mu,[2]} + d_{t_k}^{\mu,[3]}) + O(\gamma^4), \quad (52)$$

We then compare the coefficients of  $\gamma^2$  and  $\gamma^3$  in (51) and (52):

$$\begin{aligned} \dot{d}_s^{\mu,[1]} &= H_s d_s^{\mu,[1]} - \frac{1}{2} \ddot{m}_s, & d_0^{\mu,[1]} &= 0, \\ \dot{d}_s^{\mu,[2]} &= H_s d_s^{\mu,[2]} - \frac{1}{2} \ddot{d}_s^{\mu,[1]} - \frac{1}{6} m_s^{(3)}, & d_0^{\mu,[2]} &= 0. \end{aligned}$$

Differentiating the first equation above gives

$$\begin{aligned} \ddot{d}_s^{\mu,[1]} &= \dot{H}_s d_s^{\mu,[1]} + H_s \dot{d}_s^{\mu,[1]} - \frac{1}{2} m_s^{(3)} \\ &= (\dot{H}_s + H_s^2) d_s^{\mu,[1]} - \frac{1}{2} H_s \ddot{m}_s - \frac{1}{2} m_s^{(3)}. \end{aligned}$$

We use this identity into  $\dot{d}_s^{\mu,[2]}$  to get

$$\dot{d}_s^{\mu,[2]} = H_s d_s^{\mu,[2]} - \frac{1}{2} (\dot{H}_s + H_s^2) d_s^{\mu,[1]} + \frac{1}{4} H_s \ddot{m}_s + \frac{1}{12} m_s^{(3)},$$

and conclude by variation of constants to finally get (39).

*Second-order covariance error.* We follow the exact same steps for the covariance error. We look for the expansion of

$$D_k^\Sigma = \text{Cov}[\hat{Y}_k] - \text{Cov}[Y_{t_k}] = \gamma D_{t_k}^{\Sigma,[1]} + \gamma^2 D_{t_k}^{\Sigma,[2]} + \gamma^3 D_{t_k}^{\Sigma,[3]} + O(\gamma^4).$$

We get for  $D_{k+1}^\Sigma$ , using Taylor expansions:

$$\begin{aligned} D_{k+1}^\Sigma &= \gamma D_{t_{k+1}}^{\Sigma,[1]} + \gamma^2 D_{t_{k+1}}^{\Sigma,[2]} + \gamma^3 D_{t_{k+1}}^{\Sigma,[3]} + O(\gamma^4) \\ &= \gamma D_{t_k}^{\Sigma,[1]} + \gamma^2 (\dot{D}_{t_k}^{\Sigma,[1]} + D_{t_k}^{\Sigma,[2]}) + \gamma^3 (\frac{1}{2} \ddot{D}_{t_k}^{\Sigma,[1]} + \dot{D}_{t_k}^{\Sigma,[2]} + D_{t_k}^{\Sigma,[3]}) + O(\gamma^4), \end{aligned} \quad (53)$$

On the other side, combining (50) and (48):

$$D_{k+1}^\Sigma = (I + \gamma H_{t_k}) D_k^\Sigma (I + \gamma H_{t_k})^\top - \gamma^2 \left( \frac{1}{2} \ddot{\Sigma}_{t_k} - H_{t_k} \Sigma_{t_k} H_{t_k}^\top \right) - \frac{\gamma^3}{6} \Sigma_{t_k}^{(3)} + O(\gamma^4). \quad (54)$$

We define  $\Lambda_s := \frac{1}{2} \ddot{\Sigma}_s - H_s \Sigma_s H_s^\top$  and compare the coefficients of  $\gamma^2$  and  $\gamma^3$  in (53) and (54):

$$\begin{aligned} \dot{D}_s^{\Sigma, [1]} &= H_s D_s^{\Sigma, [1]} + D_s^{\Sigma, [1]} H_s^\top - \Lambda_s, & D_0^{\Sigma, [1]} &= 0, \\ \dot{D}_s^{\Sigma, [2]} &= H_s D_s^{\Sigma, [2]} + D_s^{\Sigma, [2]} H_s^\top + H_s D_s^{\Sigma, [1]} H_s^\top - \frac{1}{6} \Sigma_s^{(3)} - \frac{1}{2} \ddot{D}_s^{\Sigma, [1]}, & D_0^{\Sigma, [2]} &= 0. \end{aligned}$$

To replace  $\ddot{D}_s^{\Sigma, [1]}$  in the equation above, we differentiate the first-order equation:

$$\begin{aligned} \ddot{D}_s^{\Sigma, [1]} &= \dot{H}_s D_s^{\Sigma, [1]} + D_s^{\Sigma, [1]} \dot{H}_s^\top + H_s (H_s D_s^{\Sigma, [1]} + D_s^{\Sigma, [1]} H_s^\top - \Lambda_s) \\ &\quad + (H_s D_s^{\Sigma, [1]} + D_s^{\Sigma, [1]} H_s^\top - \Lambda_s) H_s^\top - \dot{\Lambda}_s \\ &= (\dot{H}_s + H_s^2) D_s^{\Sigma, [1]} + D_s^{\Sigma, [1]} (\dot{H}_s^\top + (H_s^\top)^2) + 2H_s D_s^{\Sigma, [1]} H_s^\top - H_s \Lambda_s - \Lambda_s H_s^\top - \dot{\Lambda}_s. \end{aligned}$$

Since

$$\Lambda_s = \frac{1}{2} \ddot{\Sigma}_s - H_s \Sigma_s H_s^\top, \quad H_s \Lambda_s + \Lambda_s H_s^\top = \frac{1}{2} H_s \ddot{\Sigma}_s + \frac{1}{2} \ddot{\Sigma}_s H_s^\top - H_s^2 \Sigma_s H_s^\top - H_s \Sigma_s (H_s^\top)^2,$$

and

$$\dot{\Lambda}_s = \frac{1}{2} \dot{\Sigma}_s^{(3)} - \dot{H}_s \Sigma_s H_s^\top - H_s \dot{\Sigma}_s H_s^\top - H_s \Sigma_s \dot{H}_s^\top,$$

using  $\dot{\Sigma}_s = H_s \Sigma_s + \Sigma_s H_s^\top + 2a_s \text{Id}$ , this becomes

$$\begin{aligned} \ddot{D}_s^{\Sigma, [1]} &= (\dot{H}_s + H_s^2) D_s^{\Sigma, [1]} + D_s^{\Sigma, [1]} (\dot{H}_s^\top + (H_s^\top)^2) + 2H_s D_s^{\Sigma, [1]} H_s^\top \\ &\quad - \frac{1}{2} H_s \ddot{\Sigma}_s - \frac{1}{2} \ddot{\Sigma}_s H_s^\top - \frac{1}{2} \Sigma_s^{(3)} + \dot{H}_s \Sigma_s H_s^\top + H_s \Sigma_s \dot{H}_s^\top \\ &\quad + 2H_s^2 \Sigma_s H_s^\top + 2H_s \Sigma_s (H_s^\top)^2 + 2a_s H_s H_s^\top. \end{aligned}$$

Substituting this into the equation for  $\dot{D}_s^{\Sigma, [2]}$  yields the integrand in (40), and variation of constants gives the claimed formula.

**Equivalent form for the first-order errors** Recall that the Jacobian satisfies

$$\frac{dJ_{t,s}}{ds} = -J_{t,s} H_s.$$

Using  $\dot{m}_s = H_s m_s + r_s$ , we get

$$\frac{d}{ds} \left( J_{t_k, s} (H_s m_s + r_s) \right) = -J_{t_k, s} H_s (H_s m_s + r_s) + J_{t_k, s} \dot{m}_s.$$

Plugging this identity into (35) gives

$$\mathbb{E}[\hat{Y}_k] - \mathbb{E}[Y_{t_k}] = -\frac{\gamma}{2} \left[ J_{t_k, s} (H_s m_s + r_s) \right]_0^{t_k} - \frac{\gamma}{2} \int_0^{t_k} J_{t_k, s} H_s (H_s m_s + r_s) ds + O(\gamma^2). \quad (55)$$

For the covariance, from

$$\dot{\Sigma}_s = H_s \Sigma_s + \Sigma_s H_s^\top + 2a_s \text{Id}.$$

Then

$$\frac{d}{ds} \left( J_{t_k, s} \dot{\Sigma}_s J_{t_k, s}^\top \right) = J_{t_k, s} \left( \dot{H}_s \Sigma_s + \Sigma_s \dot{H}_s^\top + 2\dot{a}_s \text{Id} \right) J_{t_k, s}^\top.$$

Since

$$\begin{aligned} \frac{1}{2} \ddot{\Sigma}_s - H_s \Sigma_s H_s^\top &= \frac{1}{2} \left( \dot{H}_s \Sigma_s + \Sigma_s \dot{H}_s^\top + 2\dot{a}_s \text{Id} \right) \\ &\quad + \frac{1}{2} \left( H_s^2 \Sigma_s + \Sigma_s (H_s^\top)^2 + 2a_s (H_s + H_s^\top) \right), \end{aligned}$$

(36) becomes

$$\begin{aligned} \text{Cov}[\hat{Y}_k] - \text{Cov}[Y_{t_k}] &= -\frac{\gamma}{2} \left[ J_{t_k, s} (H_s \Sigma_s + \Sigma_s H_s^\top + 2a_s \text{Id}) J_{t_k, s}^\top \right]_0^{t_k} \\ &\quad - \frac{\gamma}{2} \int_0^{t_k} J_{t_k, s} \left[ H_s^2 \Sigma_s + \Sigma_s (H_s^\top)^2 + 2a_s (H_s + H_s^\top) \right] J_{t_k, s}^\top ds + O(\gamma^2). \end{aligned} \quad (56)$$

□

## F Proof of Proposition 1

*Proof.* We first remind the notations, for  $t \in [0, T]$  and  $k \in \llbracket 0, K \rrbracket$ ,  $m_t = \mathbb{E}[Y_t]$ ,  $C_t = \text{Cov}[Y_t]$ ,  $\hat{m}_k = \mathbb{E}[\hat{Y}_k]$  and  $\hat{C}_k = \text{Cov}[\hat{Y}_k]$ . We also remind the independent evolution equations (43)-(44)- (47)-(48) that follow these quantities (see Appendix E for details):

$$\dot{m}_s = H_s m_s + r_s, \quad (57)$$

$$\hat{m}_{k+1} = \hat{m}_k + \gamma (H_{t_k} \hat{m}_k + r_{t_k}) \quad (58)$$

$$\dot{C}_s = H_s C_s + C_s H_s^\top + 2a_s \text{Id} \quad (59)$$

$$\hat{C}_{k+1} = (I + \gamma H_{t_k}) \hat{C}_k (I + \gamma H_{t_k})^\top + 2\gamma a_{t_k} \text{Id}. \quad (60)$$

Moreover, from (7),  $H_s$  co-diagonalizes with  $\Sigma_{\text{data}} = U \text{Diag}(\lambda_i) U^\top$  and  $r_s$  takes the form  $r_s = P_s \mu_{\text{data}}$  with  $P_s$  which co-diagonalizes with  $\Sigma_{\text{data}}$ . We thus get, subtracting the continuous and discrete equations, the following decomposition at time  $t_k = k\gamma$ :

$$d_{t_k}^\mu := \hat{m}_k - m_{t_k} = U \text{Diag} \left( \Delta_{t_k}^\mu(\lambda_i) \right) U^\top \mu_{\text{data}},$$

$$d_{t_k}^\Sigma := \hat{C}_k - C_{t_k} = U \text{Diag} \left( \Delta_{t_k}^\Sigma(\lambda_i) \right) U^\top$$

for some  $\Delta_{t_k}^\Sigma(\lambda_i), \Delta_{t_k}^\mu(\lambda_i) \in \mathbb{R}^d$ . We now calculate the second order expansions of  $\Delta_{t_k}^\Sigma$  and  $\Delta_{t_k}^\mu$  at  $t_k = T$ . For this, we use the second order expansions of  $d_{t_k}^\mu$  and  $d_{t_k}^\Sigma$  calculated in Appendix E, Proposition 8, for a general linear drift  $v_t(x) = H_t x + r_t$ , which we specialize with the values of  $H_t$  and  $r_t$  from (7).

First, we calculate explicitly the Jacobian matrix  $J_{t,s}$  which appears in the means and covariance decomposition of Proposition 8. Recall that  $J_{t,s}$  is the unique solution of the linear ODE:

$$\frac{dJ_{t,s}(Y)}{dt} = \nabla v_t(Y_t) J_{t,s}(Y) = H_t J_{t,s}(Y), \quad J_{s,s} = \text{Id}$$

Note that all the  $H_s$  commute in time and thus

$$J_{t,s}(Y) = \exp \left( \int_s^t H_\tau d\tau \right).$$

Using  $\Sigma_t = \eta_t^2(\Sigma_{\text{data}} + \sigma_t^2 \text{Id})$  gives

$$\frac{d}{dt} \log \Sigma_t = \Sigma_t^{-1} \frac{d}{dt} \Sigma_t = 2 \frac{\dot{\eta}_t}{\eta_t} \text{Id} + 2\eta_t^2 \sigma_t \dot{\sigma}_t \Sigma_t^{-1},$$

hence

$$H_t = \alpha \frac{\dot{\eta}_{T-t}}{\eta_{T-t}} \text{Id} - \frac{1+\alpha}{2} \frac{d}{du} \log \Sigma_u \Big|_{u=T-t}.$$

Changing variables  $u = T - \tau$ , we obtain

$$\int_s^t H_\tau d\tau = \alpha \left[ \log \eta_u \right]_{T-t}^{T-s} \text{Id} - \frac{1+\alpha}{2} \left[ \log \Sigma_u \right]_{T-t}^{T-s},$$

and therefore

$$J_{t,s} = \left( \frac{\eta_{T-s}}{\eta_{T-t}} \right)^\alpha \Sigma_{T-t}^{\frac{1+\alpha}{2}} \Sigma_{T-s}^{-\frac{1+\alpha}{2}}$$

and at final time  $t = T$

$$J_{T,s} = \eta_{T-s}^{-1} \Sigma_{\text{data}}^{\frac{1+\alpha}{2}} (\Sigma_{\text{data}} + \sigma_{T-s}^2 \text{Id})^{-\frac{1+\alpha}{2}}. \quad (61)$$

We are ready to evaluate each term of Proposition 8, (at time  $t_k = T$ ). We start with the mean expansion.

**First-order mean coefficient.** We start with (37) at time  $t_k = T$

$$d_T^{\mu,[1]} = -\frac{1}{2} \int_0^T J_T \ddot{m}_s ds$$

and we look for  $\Delta^{\mu,[1]}$  such that

$$d_T^{\mu,[1]} = U \text{Diag} \left( \Delta^{\mu,[1]} \right) U^\top \mu_{\text{data}}$$

Define

$$A_s = \frac{\dot{\eta}_s}{\eta_s}, \quad B_s(\lambda) := \frac{\sigma_s \dot{\sigma}_s}{\lambda + \sigma_s^2}, \quad N_s(\lambda) := \frac{\lambda}{\lambda + \sigma_s^2}$$

Differentiating  $\dot{m}_s = H_s m_s + r_s = -A_{T-s} m_s$ :

$$\begin{aligned} \ddot{m}_s &= (\dot{A}_{T-s} + A_{T-s}^2) m_s \\ &= (\dot{A}_{T-s} + A_{T-s}^2) \eta_{T-s} \mu_{\text{data}}. \end{aligned} \quad (62)$$

Combined with (61) and using the change of variable  $s \leftarrow T - s$ , we directly get:

$$\Delta^{\mu,[1]} = -\frac{1}{2} \int_0^T N_s(\lambda)^{\frac{1+\alpha}{2}} (\dot{A}_s + A_s^2) ds.$$

Since

$$\frac{d}{ds} N_s(\lambda)^{\frac{1+\alpha}{2}} = -(1+\alpha) B_s(\lambda) N_s(\lambda)^{\frac{1+\alpha}{2}} \quad \text{and} \quad \frac{\dot{\eta}_s}{\eta_s} = \dot{A}_s + A_s^2,$$

an integration by parts gives

$$\Delta^{\mu,[1]}(\lambda) = -\frac{1}{2} \left[ N_s(\lambda)^{\frac{1+\alpha}{2}} A_s \right]_0^T - \frac{1}{2} \int_0^T N_s(\lambda)^{\frac{1+\alpha}{2}} A_s \left( A_s + (1+\alpha) B_s(\lambda) \right) ds.$$

**Second-order mean coefficient.** We now calculate  $\Delta^{\mu,[2]}$  from (39) at time  $t_k = T$ :

$$d_T^{\mu,[2]} = \int_0^T J_{T,s} \left[ -\frac{1}{2}(\dot{H}_s + H_s^2)d_s^{\mu,[1]} + \frac{1}{4}H_s\ddot{m}_s + \frac{1}{12}\ddot{m}_s \right] ds = U \text{Diag} \left( \Delta^{\mu,[2]} \right) U^\top \mu_{\text{data}}$$

With a change of variable  $s \rightarrow T - s$ , we get

$$U \text{Diag} \left( \Delta^{\mu,[2]} \right) U^\top \mu_{\text{data}} = \int_0^T J_{T,T-s} \left[ -\frac{1}{2}(\dot{H}_{T-s} + H_{T-s}^2)d_{T-s}^{\mu,[1]} + \frac{1}{4}H_{T-s}\ddot{m}_{T-s} + \frac{1}{12}\ddot{m}_{T-s} \right] ds \quad (63)$$

Note that  $d_{T-s}^{\mu,[1]} = U \text{Diag} \left( \tilde{\Delta}_s^{\mu,[1]}(\lambda) \right) U^\top$  where we define

$$\tilde{\Delta}_s^{\mu,[1]}(\lambda) := -\frac{1}{2} \int_s^T N_u(\lambda)^{\frac{1+\alpha}{2}} (\dot{A}_u + A_u^2) du.$$

which is similar to  $\Delta^{\mu,[1]}(\lambda)$  calculated above but with an integration between time  $s$  and time  $T$ . Differentiating  $\ddot{m}_s$  (62) gives

$$\ddot{m}_s = -(\ddot{A}_{T-s} + 3A_{T-s}\dot{A}_{T-s} + A_{T-s}^3)\eta_{T-s}\mu_{\text{data}}$$

Let

$$Q_s(\lambda) := A_s + (1 + \alpha)B_s(\lambda)$$

Note that  $Q_t$  verifies  $\text{Diag} (Q_t) = U H_{T-t} U^\top$  with  $H_t$  and thus  $\frac{d}{ds} H_{T-t} = U \text{Diag} \left( \dot{Q}_t(\lambda) \right) U^\top$ . Therefore, we get from (63):

$$\begin{aligned} \Delta^{\mu,[2]}(\lambda) = \int_0^T N_s(\lambda)^{\frac{1+\alpha}{2}} \left[ -\frac{1}{2} \left( \dot{Q}_s(\lambda) + Q_s(\lambda)^2 \right) \tilde{\Delta}_s^{\mu,[1]}(\lambda) - \frac{1}{4} Q_s(\lambda) (\dot{A}_s + A_s^2) \right. \\ \left. - \frac{1}{12} (\ddot{A}_s + 3A_s\dot{A}_s + A_s^3) \right] ds. \end{aligned} \quad (64)$$

**Covariance coefficients.** Since  $H_s$ ,  $J_{T,s}$  and  $\Sigma_s$  are spectral functions of  $\Sigma_{\text{data}}$ , the covariance bias is diagonal in the eigenbasis of  $\Sigma_{\text{data}}$ . We therefore fix one eigendirection of variance  $\lambda$  and work only with the corresponding scalar quantities. We remind that  $\Sigma_s = U \text{Diag} (\lambda_s) U^\top$  with  $\lambda_s = \eta_s^2(\lambda + \sigma_s^2)$ .

**First-order covariance coefficient.** We now calculate  $\Delta^{\Sigma,[1]}$  from (38) at time  $t_k = T$ :

$$D_T^{\Sigma,[1]} = - \int_0^T J_{T,s} \left[ \frac{1}{2} \ddot{\Sigma}_s - H_s \Sigma_s H_s^\top \right] J_{T,s}^\top ds = U \text{Diag} \left( \Delta^{\Sigma,[1]} \right) U^\top$$

With a change of variable  $s \rightarrow T - s$ , and commutation of the different matrices:

$$U \text{Diag} \left( \Delta^{\Sigma,[1]} \right) U^\top = - \int_0^T J_{T,T-s}^2 \left[ \frac{1}{2} \ddot{\Sigma}_{T-s} - H_{T-s}^2 \Sigma_{T-s} \right] ds.$$

Moreover, using the previously introduced notations:

$$\begin{aligned} H_{T-s} &= -U \text{Diag} (Q_s(\lambda)) U^\top \\ J_{T,T-s}^2 \Sigma_{T-s} &= U \text{Diag} (\lambda N_s(\lambda)^\alpha) U^\top \end{aligned}$$

and differentiating  $\lambda_s$  gives

$$\begin{aligned}\dot{\lambda}_s &= 2(A_s + B_s(\lambda))\lambda_s \\ \frac{1}{2}\ddot{\lambda}_s &= \left(\dot{A}_s + \dot{B}_s(\lambda) + 2(A_s + B_s(\lambda))^2\right)\lambda_s\end{aligned}$$

Therefore,

$$\Delta^{\Sigma, [1]}(\lambda) = -\lambda \int_0^T N_s(\lambda)^\alpha \left( \dot{A}_s + \dot{B}_s(\lambda) + 2(A_s + B_s(\lambda))^2 - Q_s(\lambda)^2 \right) ds.$$

Since

$$\begin{aligned}\frac{d}{ds} N_s(\lambda)^\alpha &= -2\alpha B_s(\lambda) N_s(\lambda)^\alpha, \\ \frac{d}{ds} \left( N_s(\lambda)^\alpha (A_s + B_s(\lambda)) \right) &= N_s(\lambda)^\alpha \left( \dot{A}_s + \dot{B}_s(\lambda) - 2\alpha B_s(\lambda) (A_s + B_s(\lambda)) \right),\end{aligned}$$

an integration by parts gives

$$\Delta^{\Sigma, [1]}(\lambda) = -\lambda \left[ N_s(\lambda)^\alpha (A_s + B_s(\lambda)) \right]_0^T - \lambda \int_0^T N_s(\lambda)^\alpha \left( (A_s + B_s(\lambda))^2 - \alpha^2 B_s(\lambda)^2 \right) ds.$$

**Second-order covariance coefficient.** We now calculate  $\Delta^{\Sigma, [2]}$  from (40) at time  $t_k = T$ :

$$D_T^{\Sigma, [2]} = \int_0^T J_{T,s} \begin{bmatrix} -\frac{1}{2}(\dot{H}_s + H_s^2)D_s^{\Sigma, [1]} - \frac{1}{2}D_s^{\Sigma, [1]}(\dot{H}_s^\top + (H_s^\top)^2) \\ + \frac{1}{4}H_s\ddot{\Sigma}_s + \frac{1}{4}\ddot{\Sigma}_s H_s^\top + \frac{1}{12}\ddot{\Sigma}_s \\ - \frac{1}{2}\dot{H}_s\Sigma_s H_s^\top - \frac{1}{2}H_s\Sigma_s\dot{H}_s^\top \\ - H_s^2\Sigma_s H_s^\top - H_s\Sigma_s(H_s^\top)^2 - a_s H_s H_s^\top \end{bmatrix} J_{T,s}^\top ds = U\Delta^{\Sigma, [2]}U^\top$$

With a change of variable  $s \rightarrow T - s$ , we get

$$U\Delta^{\Sigma, [2]}U^\top = \int_0^T J_{T, T-s} \begin{bmatrix} -\frac{1}{2}(\dot{H}_{T-s} + H_{T-s}^2)D_{T-s}^{\Sigma, [1]} - \frac{1}{2}D_{T-s}^{\Sigma, [1]}(\dot{H}_{T-s}^\top + (H_{T-s}^\top)^2) \\ + \frac{1}{4}H_{T-s}\ddot{\Sigma}_{T-s} + \frac{1}{4}\ddot{\Sigma}_{T-s}H_{T-s}^\top + \frac{1}{12}\ddot{\Sigma}_{T-s} \\ - \frac{1}{2}\dot{H}_{T-s}\Sigma_{T-s}H_{T-s}^\top - \frac{1}{2}H_{T-s}\Sigma_{T-s}\dot{H}_{T-s}^\top \\ - H_{T-s}^2\Sigma_{T-s}H_{T-s}^\top - H_{T-s}\Sigma_{T-s}(H_{T-s}^\top)^2 - a_{T-s}H_{T-s}H_{T-s}^\top \end{bmatrix} J_{T, T-s}^\top ds. \quad (65)$$

Note that  $D_{T-s}^{\Sigma, [1]} = U\tilde{\Delta}_s^{\Sigma, [1]}(\lambda)U^\top$  where we define

$$\tilde{\Delta}_s^{\Sigma, [1]}(\lambda) := -\lambda \int_s^T N_u(\lambda)^\alpha \left( \dot{A}_u + \dot{B}_u(\lambda) + 2(A_u + B_u(\lambda))^2 - Q_u(\lambda)^2 \right) du.$$

which is similar to  $\Delta^{\Sigma, [1]}(\lambda)$  calculated above but with an integration between time  $s$  and time  $T$ . Moreover, using the above notations:

$$\begin{aligned} H_{T-s} &= -U \text{Diag}(Q_s(\lambda)) U^\top \\ \frac{d}{ds} H_{T-s} &= U \dot{Q}_s(\lambda) U^\top \\ a_{T-s} &= \alpha B_s(\lambda) \lambda_s \\ J_{T, T-s}^2 \lambda_s &= U \text{Diag}(\lambda N_s(\lambda)^\alpha) U^\top, \end{aligned}$$

and differentiating  $\lambda_s$  one more time gives:

$$\frac{1}{12} \lambda_s^{(3)} = \frac{1}{6} \left( \ddot{A}_s + \ddot{B}_s(\lambda) + 6(A_s + B_s(\lambda))(\dot{A}_s + \dot{B}_s(\lambda)) + 4(A_s + B_s(\lambda))^3 \right) \lambda_s.$$

Therefore, we get from (65):

$$\begin{aligned} \Delta^{\Sigma, [2]}(\lambda) &= \int_0^T \left[ - \left( \dot{Q}_s(\lambda) + Q_s(\lambda)^2 \right) \tilde{\Delta}_s^{\Sigma, [1]}(\lambda) \right. \\ &\quad + \lambda N_s(\lambda)^\alpha \left( - \frac{1}{6} \left( \ddot{A}_s + \ddot{B}_s(\lambda) + 6(A_s + B_s(\lambda))(\dot{A}_s + \dot{B}_s(\lambda)) + 4(A_s + B_s(\lambda))^3 \right) \right. \\ &\quad \left. \left. - Q_s(\lambda) \left( \dot{A}_s + \dot{B}_s(\lambda) + 2(A_s + B_s(\lambda))^2 \right) + Q_s(\lambda) \dot{Q}_s(\lambda) + 2Q_s(\lambda)^3 - \alpha B_s(\lambda) Q_s(\lambda)^2 \right) \right] ds. \quad (66) \end{aligned}$$

**Large- $\sigma_T$  simplification.** The residual terms obtained above are  $\left[ \Omega_s^\mu(\lambda) \right]_0^T$  and  $\left[ \Omega_s^\Sigma(\lambda) \right]_0^T$  with

$$\Omega_s^\mu(\lambda) := -\frac{1}{2} \left( \frac{\lambda}{\lambda + \sigma_s^2} \right)^{\frac{1+\alpha}{2}} \frac{\dot{\eta}_s}{\eta_s},$$

and

$$\Omega_s^\Sigma(\lambda) := -\lambda \left( \frac{\lambda}{\lambda + \sigma_s^2} \right)^\alpha \left( \frac{\dot{\eta}_s}{\eta_s} + \frac{\sigma_s \dot{\sigma}_s}{\lambda + \sigma_s^2} \right).$$

First, for  $s = T$ , as  $\sigma_T = \sigma_{\max} \rightarrow \infty$ , under Assumption 1(ii), we have

$$\begin{aligned} \Omega_s^\mu(\lambda) &= -\frac{1}{2} \lambda^{\frac{1+\alpha}{2}} \sigma_T^{-(1+\alpha)} \frac{\dot{\eta}_T}{\eta_T} (1 + o(1)) = o_{\sigma_{\max} \rightarrow \infty}(1), \\ \Omega_s^\Sigma(\lambda) &= -\lambda^{\alpha+1} \sigma_T^{-2\alpha} \left( \frac{\dot{\eta}_T}{\eta_T} + \frac{\dot{\sigma}_T}{\sigma_T} \right) (1 + o(1)) = o_{\sigma_{\max} \rightarrow \infty}(1). \end{aligned}$$

Moreover, as  $s \rightarrow 0$ , if  $\dot{\sigma}_s \sigma_s \rightarrow 0$  and  $\dot{\eta}_s \rightarrow 0$  (Assumption 1(ii)),  $R^\mu$  and  $R^\Sigma$  vanish in  $t \rightarrow 0$ . Thus:

$$\left[ \Omega_s^\mu(\lambda) \right]_0^T = o_{\sigma_{\max} \rightarrow \infty}(1), \quad \left[ \Omega_s^\Sigma(\lambda) \right]_0^T = o_{\sigma_{\max} \rightarrow \infty}(1).$$

□

## F.1 First-order scheduler specializations

**Variance Exploding [Song et al., 2021]** It corresponds to  $\eta_t = 1$ . Then the first and second order mean errors from Proposition 1 vanish:

$$\Delta^{\mu,[1]}(\lambda) = \Delta^{\mu,[2]}(\lambda) = 0$$

Moreover, if  $\dot{\sigma}_t \sigma_t \rightarrow 0$  as  $t \rightarrow 0$ , Assumption 1(ii) holds and the covariance error (9) simplifies to:

$$\Delta^{\Sigma,[1]}(\lambda) = (\alpha^2 - 1)\lambda^{\alpha+1} \int_0^T \frac{(\sigma_s \dot{\sigma}_s)^2}{(\lambda + \sigma_s^2)^{\alpha+2}} ds + o_{\sigma_{\max} \rightarrow \infty}(1).$$

Assume further that

$$\sigma_t = \sigma_{\max} \left( \frac{t}{T} \right)^\beta, \quad \beta > \frac{1}{2}, \quad \alpha > 0.$$

Then

$$\Delta^{\Sigma,[1]}(\lambda) = (\alpha^2 - 1) \frac{\beta^2 \sigma_{\max}^4}{T} \lambda^{\alpha+1} \int_0^1 \frac{x^{4\beta-2}}{(\lambda + \sigma_{\max}^2 x^{2\beta})^{\alpha+2}} dx + o_{\sigma_{\max} \rightarrow \infty}(1).$$

With the change of variable  $v = \frac{\sigma_{\max}^2}{\lambda} x^{2\beta}$ , we obtain

$$\Delta^{\Sigma,[1]}(\lambda) = (\alpha^2 - 1) \frac{\beta}{2T} \lambda^{1-\frac{1}{2\beta}} \sigma_{\max}^{1/\beta} \int_0^{\sigma_{\max}^2/\lambda} \frac{v^{1-\frac{1}{2\beta}}}{(1+v)^{\alpha+2}} dv + o_{\sigma_{\max} \rightarrow \infty}(1).$$

Since  $\beta > \frac{1}{2}$  and  $\alpha > 0$ ,

$$\int_0^{\sigma_{\max}^2/\lambda} \frac{v^{1-\frac{1}{2\beta}}}{(1+v)^{\alpha+2}} dv \rightarrow \text{B}\left(2 - \frac{1}{2\beta}, \alpha + \frac{1}{2\beta}\right),$$

hence

$$\Delta^{\Sigma,[1]}(\lambda) = (\alpha^2 - 1) \frac{\beta \lambda}{2T} \text{B}\left(2 - \frac{1}{2\beta}, \alpha + \frac{1}{2\beta}\right) \left(\frac{\sigma_{\max}^2}{\lambda}\right)^{\frac{1}{2\beta}} + o_{\sigma_{\max} \rightarrow \infty}(\sigma_{\max}^{1/\beta}).$$

**Variance Preserving [Song et al., 2021, Ho et al., 2020]** It corresponds to  $\eta_t = (1 + \sigma_t^2)^{-1/2}$ . Then, if  $\dot{\sigma}_t \sigma_t \rightarrow 0$  as  $t \rightarrow 0$ , Assumption 1(ii) holds and the mean (8) and covariance (9) errors simplify to

$$\Delta^{\mu,[1]}(\lambda) = -\frac{1}{2\lambda} \int_0^T \frac{(\sigma_s \dot{\sigma}_s)^2}{1 + \sigma_s^2} \left( \frac{\lambda}{\lambda + \sigma_s^2} \right)^{\frac{\alpha+3}{2}} \left( \frac{\lambda - 1}{1 + \sigma_s^2} - \alpha \right) ds + o_{\sigma_{\max} \rightarrow \infty}(1), \quad (67)$$

$$\Delta^{\Sigma,[1]}(\lambda) = -\frac{1}{\lambda} \int_0^T \left( \frac{\lambda}{\lambda + \sigma_s^2} \right)^{\alpha+2} (\sigma_s \dot{\sigma}_s)^2 \left[ \left( \frac{1 - \lambda}{1 + \sigma_s^2} \right)^2 - \alpha^2 \right] ds + o_{\sigma_{\max} \rightarrow \infty}(1) \quad (68)$$

We now further specialize when  $\alpha = 0$  for the polynomial schedule

$$\sigma_t = \sigma_{\max} \left( \frac{t}{T} \right)^\beta, \quad \beta > \frac{1}{2}.$$

Setting  $x = t/T$ , we get

$$\begin{aligned}\Delta^{\mu,[1]}(\lambda) &= -\frac{\beta^2(\lambda-1)\sqrt{\lambda}\sigma_{\max}^4}{2T} \int_0^1 \frac{x^{4\beta-2}}{(1+\sigma_{\max}^2x^{2\beta})^2(\lambda+\sigma_{\max}^2x^{2\beta})^{3/2}} dx + o(1), \\ \Delta^{\Sigma,[1]}(\lambda) &= -\frac{\beta^2(1-\lambda)^2\lambda\sigma_{\max}^4}{T} \int_0^1 \frac{x^{4\beta-2}}{(1+\sigma_{\max}^2x^{2\beta})^2(\lambda+\sigma_{\max}^2x^{2\beta})^2} dx + o(1),\end{aligned}$$

With the change of variable

$$u = \sigma_{\max}^2x^{2\beta}, \quad dx = \frac{1}{2\beta}\sigma_{\max}^{-1/\beta}u^{\frac{1}{2\beta}-1} du, \quad x^{4\beta-2} = \sigma_{\max}^{-4+\frac{2}{\beta}}u^{2-\frac{1}{\beta}},$$

we obtain

$$\begin{aligned}\Delta^{\mu,[1]}(\lambda) &= -\frac{\beta(\lambda-1)\sqrt{\lambda}}{4T} \sigma_{\max}^{1/\beta} \int_0^{\sigma_{\max}^2} \frac{u^{1-\frac{1}{2\beta}}}{(1+u)^2(\lambda+u)^{3/2}} du + o(\sigma_{\max}^{1/\beta}), \\ \Delta^{\Sigma,[1]}(\lambda) &= -\frac{\beta(1-\lambda)^2\lambda}{2T} \sigma_{\max}^{1/\beta} \int_0^{\sigma_{\max}^2} \frac{u^{1-\frac{1}{2\beta}}}{(1+u)^2(\lambda+u)^2} du + o(\sigma_{\max}^{1/\beta}).\end{aligned}$$

Since  $\beta > \frac{1}{2}$ , both integrands are integrable on  $(0, \infty)$ , so dominated convergence yields

$$\Delta^{\mu,[1]}(\lambda) = -\frac{\beta(\lambda-1)\sqrt{\lambda}}{4T} \sigma_{\max}^{1/\beta} \int_0^\infty \frac{u^{1-\frac{1}{2\beta}}}{(1+u)^2(\lambda+u)^{3/2}} du + o(\sigma_{\max}^{1/\beta}), \quad (69)$$

$$\Delta^{\Sigma,[1]}(\lambda) = -\frac{\beta(1-\lambda)^2\lambda}{2T} \sigma_{\max}^{1/\beta} \int_0^\infty \frac{u^{1-\frac{1}{2\beta}}}{(1+u)^2(\lambda+u)^2} du + o(\sigma_{\max}^{1/\beta}). \quad (70)$$

**Flow Matching [Lipman et al., 2022]** For the standard deterministic linear-interpolation Flow Matching schedule (using  $T = 1 - \varepsilon$  in order to have  $\eta_T$  and  $\sigma_T$  well defined):

$$\alpha = 0, \quad \eta_t = 1 - \frac{t}{T}, \quad \sigma_t = \frac{t}{T-t}.$$

Then  $A_t = \frac{\dot{\eta}_t}{\eta_t}$  verifies  $\dot{A}_t + A_t^2 = 0$  and thus the first-order mean formula from Proposition 1 cancels:

$$\Delta^{\mu,[1]}(\lambda) = 0.$$

For the covariance error, for  $Q_t(\lambda) := A_t + B_t(\lambda)$ , since  $\alpha = 0$ ,

$$\Delta^{\Sigma,[1]}(\lambda) = -\lambda \int_0^T (\dot{Q}_t(\lambda) + Q_t(\lambda)^2) dt.$$

We derive for the above choice of  $\eta_t$  and  $\sigma_t$ :

$$\dot{Q}_t(\lambda) + Q_t(\lambda)^2 = \frac{T^2\lambda}{(\lambda(T-t)^2 + t^2)^2}$$

Hence, the first order error becomes fully explicit:

$$\Delta^{\Sigma,[1]}(\lambda) = -\lambda^2 T^2 \int_0^T \frac{dt}{(\lambda(T-t)^2 + t^2)^2} = -\left(\frac{\lambda}{T} + \frac{(1+\lambda)\sqrt{\lambda}}{4T}\pi\right).$$

## F.2 Second-order specialization for VE

For the analysis of the optimal diffusion-term parameter  $\alpha$  of Proposition 2, we need the second-order covariance coefficient  $\Delta^{\Sigma, [2]}$  at  $\alpha = 1$  for VE ( $\eta_t = 1$ ). In this case, using the notations from the proof of Proposition 1 in Appendix F:

$$A_s = 0, \quad B_s(\lambda) = \frac{\sigma_s \dot{\sigma}_s}{\lambda + \sigma_s^2}, \quad Q_s(\lambda) = 2B_s(\lambda), \quad N_s(\lambda) = \frac{\lambda}{\lambda + \sigma_s^2}, \quad \Delta_s^{\Sigma, [1]}(1, \lambda) = -\lambda \left[ N_r(\lambda) B_r(\lambda) \right]_s^T$$

Plugging this identity into (66) yields

$$\begin{aligned} \Delta^{\Sigma, [2]}(1, \lambda) &= \int_0^T \left[ -2 \left( \dot{B}_s(\lambda) + 2B_s(\lambda)^2 \right) \Delta_s^{\Sigma, [1]}(1, \lambda) \right. \\ &\quad \left. + \lambda N_s(\lambda) \left( -\frac{1}{6} \ddot{B}_s(\lambda) - B_s(\lambda) \dot{B}_s(\lambda) + \frac{10}{3} B_s(\lambda)^3 \right) \right] ds. \end{aligned}$$

We also use the polynomial schedule  $\sigma_t = \sigma_{\max} \left( \frac{t}{T} \right)^\beta$ , and assume  $\beta > 1$ , with large  $\sigma_{\max} \rightarrow \infty$ . Set

$$z := \frac{\sigma_{\max}^2}{\lambda}, \quad x := \frac{s}{T}.$$

Then

$$B_s(\lambda) = \frac{\beta z x^{2\beta-1}}{T(1 + z x^{2\beta})},$$

and

$$\begin{aligned} \dot{B}_s(\lambda) &= \frac{\beta z x^{2\beta-2} \left( (2\beta - 1) - z x^{2\beta} \right)}{T^2 (1 + z x^{2\beta})^2}, \\ \ddot{B}_s(\lambda) &= \frac{2\beta z x^{2\beta-3}}{T^3 (1 + z x^{2\beta})^3} \left( (\beta - 1)(2\beta - 1) - (\beta + 2)(2\beta - 1) z x^{2\beta} + z^2 x^{4\beta} \right). \end{aligned}$$

Moreover,

$$\lambda N_T(\lambda) B_T(\lambda) = \frac{\beta \lambda z}{T(1 + z)^2},$$

and

$$\Delta_s^{\Sigma, [1]}(1, \lambda) = \lambda N_s(\lambda) B_s(\lambda) - \lambda N_T(\lambda) B_T(\lambda).$$

Let  $R_z(\lambda)$  denote the induced change in  $\Delta^{\Sigma, [2]}(1, \lambda)$  when  $\Delta_s^{\Sigma, [1]}(1, \lambda)$  is replaced by  $\lambda N_s(\lambda) B_s(\lambda)$  i.e. removing the second  $T$  term. Then

$$R_z(\lambda) = 2\lambda N_T(\lambda) B_T(\lambda) \int_0^T \left( \dot{B}_s(\lambda) + 2B_s(\lambda)^2 \right) ds.$$

Since  $B_0(\lambda) = 0$ ,

$$\int_0^T \dot{B}_s(\lambda) ds = B_T(\lambda) - B_0(\lambda) = \frac{\beta z}{T(1 + z)}.$$

Also,

$$\begin{aligned} \int_0^T B_s(\lambda)^2 ds &= \frac{\beta^2 z^2}{T} \int_0^1 \frac{x^{4\beta-2}}{(1 + z x^{2\beta})^2} dx \\ &= \frac{\beta}{2T} z^{1/(2\beta)} \int_0^z \frac{u^{1-\frac{1}{2\beta}}}{(1 + u)^2} du \\ &\leq \frac{\beta}{2T} B \left( 2 - \frac{1}{2\beta}, \frac{1}{2\beta} \right) z^{1/(2\beta)}, \end{aligned}$$

Hence

$$\begin{aligned} |R_z(\lambda)| &\leq 2 \frac{\beta \lambda z}{T(1+z)^2} \left( \frac{\beta z}{T(1+z)} + \frac{\beta}{T} B\left(2 - \frac{1}{2\beta}, \frac{1}{2\beta}\right) z^{1/(2\beta)} \right) \\ &\leq C_{\beta, \lambda, T} \left( z^{-1} + z^{1/(2\beta)-1} \right) \end{aligned}$$

for some constant  $C_{\beta, \lambda, T} > 0$  independent of  $z$ . And thus:

$$R_z(\lambda) = o\left(z^{1/\beta}\right) = o\left(\sigma_{\max}^{2/\beta}\right),$$

We now calculate  $\Delta^{\Sigma, [2]}(1, \lambda)$  up to  $O\left(\sigma_{\max}^{2/\beta}\right)$ . Using the change of variables  $u = zx^{2\beta}$ , we obtain

$$\begin{aligned} \Delta^{\Sigma, [2]}(1, \lambda) &= \frac{\lambda}{6T^2} z^{1/\beta} \int_0^z \frac{u^{-1/\beta}}{(1+u)^4} \left( -(\beta-1)(2\beta-1) - 2(\beta-1)(2\beta-1)u \right. \\ &\quad \left. + (10\beta^2 + 3\beta - 1)u^2 \right) du + o\left(z^{1/\beta}\right). \end{aligned} \quad (71)$$

Since  $\beta > 1$ , the integral converges at 0 and at  $+\infty$ , so the upper integral limit  $z$  can be replaced by  $+\infty$  up to  $o(1)$ . Now using  $B$  the Beta function, we use

$$I_k(\beta) := \int_0^\infty \frac{u^{k-\frac{1}{\beta}}}{(1+u)^4} du = B\left(k+1 - \frac{1}{\beta}, 3 - k + \frac{1}{\beta}\right), \quad k = 0, 1, 2.$$

and the identities:

$$\begin{aligned} I_0(\beta) &= \frac{(\beta+1)(2\beta+1)}{(\beta-1)(2\beta-1)} B\left(3 - \frac{1}{\beta}, 1 + \frac{1}{\beta}\right), \\ I_1(\beta) &= \frac{\beta+1}{2\beta-1} B\left(3 - \frac{1}{\beta}, 1 + \frac{1}{\beta}\right), \\ I_2(\beta) &= B\left(3 - \frac{1}{\beta}, 1 + \frac{1}{\beta}\right). \end{aligned}$$

Therefore, the terms of (71) can be simplified using  $B\left(3 - \frac{1}{\beta}, 1 + \frac{1}{\beta}\right)$ :

$$\begin{aligned} & -(\beta-1)(2\beta-1)I_0(\beta) - 2(\beta-1)(2\beta-1)I_1(\beta) + (10\beta^2 + 3\beta - 1)I_2(\beta) \\ &= \left( -(\beta+1)(2\beta+1) - 2(\beta^2-1) + 10\beta^2 + 3\beta - 1 \right) B\left(3 - \frac{1}{\beta}, 1 + \frac{1}{\beta}\right) \\ &= 6\beta^2 B\left(3 - \frac{1}{\beta}, 1 + \frac{1}{\beta}\right). \end{aligned}$$

Substituting this identity into (71) gives

$$\Delta^{\Sigma, [2]}(1, \lambda) = C^{(2)}(\beta) \frac{\lambda}{T^2} \left( \frac{\sigma_{\max}^2}{\lambda} \right)^{\frac{1}{\beta}} + o\left(\sigma_{\max}^{2/\beta}\right), \quad (72)$$

with

$$C^{(2)}(\beta) := \beta^2 B\left(3 - \frac{1}{\beta}, 1 + \frac{1}{\beta}\right) > 0. \quad (73)$$

## G Optimization of diffusion parameters

### G.1 Proof of Proposition 2

*Proof.* Consider first a general objective of the form

$$\mathcal{E}(\alpha, \gamma) = \mathcal{E}^{[0]}(\alpha) + \gamma \mathcal{E}^{[1]}(\alpha) + O(\gamma^2).$$

Assume that  $\alpha_*^{[0]}$  is a nondegenerate local minimizer of  $\mathcal{E}^{[0]}$ , namely

$$\partial_\alpha \mathcal{E}^{[0]}(\alpha_*^{[0]}) = 0, \quad \partial_{\alpha\alpha} \mathcal{E}^{[0]}(\alpha_*^{[0]}) > 0.$$

Then the implicit function theorem gives

$$\alpha^*(\gamma) = \alpha_*^{[0]} + \gamma \alpha_*^{[1]} + O(\gamma^2)$$

with

$$\partial_\alpha \mathcal{E}(\alpha_*(\gamma), \gamma) = 0.$$

Expanding this identity gives

$$0 = \partial_{\alpha\alpha} \mathcal{E}^{[0]}(\alpha_*^{[0]}; \vartheta) \alpha_*^{[1]} \gamma + \partial_\alpha \mathcal{E}^{[1]}(\alpha_*^{[0]}) \gamma + O(\gamma^2),$$

hence

$$\alpha^*(\gamma) = \alpha_*^{[0]} - \gamma \frac{\partial_\alpha \mathcal{E}^{[1]}(\alpha_*^{[0]})}{\partial_{\alpha\alpha} \mathcal{E}^{[0]}(\alpha_*^{[0]})} + O(\gamma^2).$$

Let's derive the higher order error  $E^{[1]}$  in our case. For VE, there is no error on the mean at first and second orders, thus

$$\|\mathbb{E}[Y_k] - \mu_{\text{data}}\|^2 = o(\gamma^4)$$

Moreover, as detailed in Appendix D.1, the Bures distance between covariance expands at order  $\gamma^3$  as:

$$\begin{aligned} \mathcal{E}(\alpha, \gamma) := \text{FD}(p_{\text{data}}, \text{Law}(\hat{Y}_K)) &= \frac{\gamma^2}{4} \sum_{i=1}^d \frac{\Delta^{\Sigma, [1]}(\alpha, \lambda_i)^2}{\lambda_i} \\ &+ \gamma^3 \sum_{i=1}^d \left( \frac{\Delta^{\Sigma, [1]}(\alpha, \lambda_i) \Delta^{\Sigma, [2]}(\alpha, \lambda_i)}{2\lambda_i} - \frac{\Delta^{\Sigma, [1]}(\alpha, \lambda_i)}{8\lambda_i^2} \right) + o(\gamma^4). \end{aligned}$$

In correspondence with  $\mathcal{E}(\alpha, \gamma) = \mathcal{E}^{[0]}(\alpha) + \gamma \mathcal{E}^{[1]}(\alpha) + O(\gamma^2)$ , the leading-order is

$$\mathcal{E}^{[0]}(\alpha) := \frac{\gamma^2}{4} \sum_{i=1}^d \frac{\Delta^{\Sigma, [1]}(\alpha, \lambda_i)^2}{\lambda_i}$$

and, using (10) its minimizer is  $\alpha_*^{[0]} = 1$ . The higher order error is

$$\mathcal{E}^{[1]}(\alpha) := \gamma^2 \sum_{i=1}^d \left( \frac{\Delta^{\Sigma, [1]}(\alpha, \lambda_i) \Delta^{\Sigma, [2]}(\alpha, \lambda_i)}{2\lambda_i} - \frac{\Delta^{\Sigma, [1]}(\alpha, \lambda_i)^3}{8\lambda_i^2} \right)$$

Since  $\Delta^{\Sigma,[1]}(\alpha_*^{[0]}, \lambda_i) = 0$ , one has

$$\partial_{\alpha\alpha}\mathcal{E}^{[0]}(\alpha_*^{[0]}) = \frac{\gamma^2}{2} \sum_{i=1}^d \frac{1}{\lambda_i} (\partial_{\alpha}\Delta^{\Sigma,[1]}(\alpha_*^{[0]}, \lambda_i))^2$$

which is positive. and

$$\partial_{\alpha}\mathcal{E}^{[1]}(\alpha_*^{[0]}) = \frac{\gamma^2}{2} \sum_{i=1}^d \frac{1}{\lambda_i} \partial_{\alpha}\Delta^{\Sigma,[1]}(\alpha_*^{[0]}, \lambda_i) \Delta^{\Sigma,[2]}(\alpha_*^{[0]}, \lambda_i)$$

Overall we get:

$$\alpha^*(\gamma) = 1 - \gamma \frac{\sum_{i=1}^d \frac{1}{\lambda_i} \partial_{\alpha}\Delta^{\Sigma,[1]}(\alpha_*^{[0]}, \lambda_i) \Delta^{\Sigma,[2]}(\alpha_*^{[0]}, \lambda_i)}{\sum_{i=1}^d \frac{1}{\lambda_i} (\partial_{\alpha}\Delta^{\Sigma,[1]}(\alpha_*^{[0]}, \lambda_i))^2} + O(\gamma^2). \quad (74)$$

For the Variance Exploding case with power law noise schedule  $\sigma_t = \sigma_{max} \left(\frac{t}{T}\right)^{\beta}$ , we have seen in (11) that

$$\Delta^{\Sigma,[1]}(\alpha, \lambda) = (\alpha^2 - 1) \frac{\beta\lambda}{2T} B\left(2 - \frac{1}{2\beta}, \alpha + \frac{1}{2\beta}\right) \left(\frac{\sigma_{max}^2}{\lambda}\right)^{\frac{1}{2\beta}} + o_{\sigma_{max} \rightarrow \infty}(\sigma_{max}^{1/\beta}).$$

giving

$$\partial_{\alpha}\Delta^{\Sigma,[1]}(1, \lambda) = \frac{1}{T} \lambda C^{(1)}(\beta) \left(\frac{\sigma_{max}^2}{\lambda}\right)^{\frac{1}{2\beta}} + o_{\sigma_{max} \rightarrow \infty}(\sigma_{max}^{1/\beta}).$$

with  $C^{(1)}(\beta) := \beta B\left(2 - \frac{1}{2\beta}, 1 + \frac{1}{2\beta}\right) > 0$ . Now, from the calculations of section F.2:

$$\Delta^{\Sigma,[2]}(1, \lambda) = C^{(2)}(\beta) \frac{\lambda}{T^2} \left(\frac{\sigma_{max}^2}{\lambda}\right)^{\frac{1}{\beta}} + o\left(\sigma_{max}^{2/\beta}\right)$$

where

$$C^{(2)}(\beta) := \beta^2 B\left(3 - \frac{1}{\beta}, 1 + \frac{1}{\beta}\right) > 0.$$

We thus get

$$\alpha^*(\gamma) = 1 - \gamma \left( \frac{C^{(2)}(\beta)}{C^{(1)}(\beta)} \frac{\sigma_{max}^{\frac{1}{\beta}}}{T} \frac{\sum_{i=1}^d (\lambda_i)^{1-\frac{3}{2\beta}}}{\sum_{i=1}^d (\lambda_i)^{1-\frac{1}{\beta}}} + o\left(\sigma_{max}^{\frac{1}{\beta}}\right) \right) + O(\gamma^2)$$

Since both  $C^{(1)}(\beta)$  and  $C^{(2)}(\beta)$  are positive, the first-order correction is negative, so the perturbative optimum shifts below 1. □

## G.2 Proof of Proposition 3

*Proof.* First note that for polynomial  $\sigma_t$  with  $\beta > 1$  and for

$$\eta_s(c) = \left(\frac{c}{c + \sigma_s^2}\right)^{1/2}$$

Assumption 1(ii) is satisfied. Thus, starting from the large- $\sigma_{\max}$  form of (9), the first-order covariance error in one eigendirection of variance  $\lambda$  is

$$\begin{aligned}\Delta^{\Sigma, [1]}(\lambda; c) &= -\lambda \int_0^T \left( \frac{\dot{\eta}_s(c)}{\eta_s(c)} + \frac{\sigma_s \dot{\sigma}_s}{\lambda + \sigma_s^2} \right)^2 ds + o_{\sigma_{\max} \rightarrow \infty}(1) \\ &= -\lambda(c - \lambda)^2 \int_0^T \left( \frac{\sigma_s \dot{\sigma}_s}{(\lambda + \sigma_s^2)(c + \sigma_s^2)} \right)^2 ds + o_{\sigma_{\max} \rightarrow \infty}(1).\end{aligned}$$

We therefore look for the parameter  $c$  that minimizes the corresponding large- $\sigma_{\max}$  objective

$$\begin{aligned}\mathcal{E}(c) &= \sum_i \frac{1}{\lambda_i} \Delta^{\Sigma, [1]}(\lambda_i; c)^2 \\ &= \sum_i \frac{1}{\lambda_i} \left[ \lambda_i(c - \lambda_i)^2 \int_0^T \left( \frac{\dot{\sigma}_s \sigma_s}{(\lambda_i + \sigma_s^2)(c + \sigma_s^2)} \right)^2 ds + o_{\sigma_{\max} \rightarrow \infty}(1) \right]^2\end{aligned}$$

In the case  $\sigma_t = \sigma_{\max} \left(\frac{t}{T}\right)^\beta$ , with the change of variable  $u = \sigma_s^2$ , this expansion becomes

$$\Delta^{\Sigma, [1]}(\lambda_i; c) = \frac{\beta \sigma_{\max}^{1/\beta}}{2T} \lambda_i \left[ h\left(\frac{c}{\lambda_i}\right) + O_{\beta \rightarrow \infty}\left(\frac{1}{\beta}\right) \right] + o_{\sigma_{\max} \rightarrow \infty}\left(\sigma_{\max}^{1/\beta}\right)$$

with

$$h(z) := \frac{z+1}{z-1} \log(z) - 2, \quad g(z) := h(z)^2.$$

so that, at leading order in  $\sigma_{\max}$ ,

$$\mathcal{E}(c) = \frac{\beta^2 \sigma_{\max}^{2/\beta}}{4T^2} \sum_i \lambda_i \left[ g\left(\frac{c}{\lambda_i}\right) + O_{\beta \rightarrow \infty}\left(\frac{1}{\beta}\right) \right] + o_{\sigma_{\max} \rightarrow \infty}\left(\sigma_{\max}^{2/\beta}\right).$$

We now assume a finite power-law spectrum

$$\lambda_i = \lambda_{\max} i^{-p}, \quad i = 1, \dots, d, \quad p > 0.$$

Setting  $\tau := c/\lambda_{\max}$ , the objective becomes

$$\mathcal{E}(c) = \frac{\beta^2 \sigma_{\max}^{2/\beta}}{4T^2} \lambda_{\max} \sum_{i=1}^d i^{-p} \left[ g(\tau i^p) + O_{\beta \rightarrow \infty}\left(\frac{1}{\beta}\right) \right] + o_{\sigma_{\max} \rightarrow \infty}\left(\sigma_{\max}^{2/\beta}\right).$$

**Remark 2.** The above formulation shows that very small eigenvalues  $\lambda_i$  have little effect on the objective  $\mathcal{E}(c)$ . Indeed, for  $\lambda_i \ll c$ , we have  $g(c/\lambda_i) \sim \log^2(c/\lambda_i)$ , so the weighted contribution  $\lambda_i g(c/\lambda_i)$  scales as  $\lambda_i \log^2(c/\lambda_i)$  and therefore vanishes as  $\lambda_i \rightarrow 0$ .

Ignoring the lower-order  $O_{\beta \rightarrow \infty}(\beta^{-1})$  and  $o_{\sigma_{\max} \rightarrow \infty}(\sigma_{\max}^{2/\beta})$  terms, minimizing  $\mathcal{E}(c)$  is equivalent to minimizing

$$\Psi_p(\tau) := \sum_{i=1}^d i^{-p} g(\tau i^p), \quad \tau > 0. \quad (75)$$

Hence any minimizer satisfies  $c^* = \lambda_{\max} \tau_p^*$  for some minimizer  $\tau_p^*$  of  $\Psi_p$ . We now prove that the minimizer  $\tau_p^*$  is unique and belongs in  $(0, 1)$ , before characterizing its evolution with  $p$ . Recall that

$$\Psi_p(\tau) := \sum_{i=1}^d i^{-p} g(\tau i^p), \quad g(z) = \left[ \frac{z+1}{z-1} \log z - 2 \right]^2,$$

where  $g(1)$  is defined by continuity as  $g(1) = 0$ . We use the logarithmic change of variables

$$\tau = e^s, \quad z = e^x.$$

and define

$$\phi(x) := g(e^x) = \left[ x \coth \left( \frac{x}{2} \right) - 2 \right]^2.$$

Let

$$r(y) := y \coth y - 1$$

such that

$$\phi(x) = 4r \left( \frac{x}{2} \right)^2.$$

We now show that  $\phi$  is strictly convex.

$$r'(y) = \frac{\sinh y \cosh y - y}{\sinh^2 y},$$

Let  $N(y) := \sinh y \cosh y - y$ .  $N(0) = 0$ , and for  $y > 0$ ,

$$N'(y) = \cosh^2 y + \sinh^2 y - 1 = 2 \sinh^2 y > 0.$$

Thus  $N(y) > 0$  for every  $y > 0$ . Since also  $\sinh^2 y > 0$ , we conclude that  $r'(y) > 0$  for every  $y > 0$ . By symmetry,  $r$  is even, so  $r(y) \geq 0$  for all  $y$ , with equality only at  $y = 0$ . Moreover,

$$r''(y) = \frac{2}{\sinh^2(y)} r(y)$$

Hence, for  $y \neq 0$ ,

$$\frac{d^2}{dy^2} r(y)^2 = 2r'(y)^2 + 2r(y)r''(y) = 2r'(y)^2 + \frac{4r(y)^2}{\sinh^2(y)} > 0.$$

Thus  $y \mapsto r(y)^2$  is strictly convex, and therefore  $\phi$  is strictly convex. Now define

$$\tilde{\Psi}_p(s) := \Psi_p(e^s) = \sum_{i=1}^d i^{-p} \phi(s + p \log i).$$

Each function

$$s \mapsto \phi(s + p \log i)$$

is strictly convex, and all weights  $i^{-p}$  are positive. Therefore  $\tilde{\Psi}_p$  is strictly convex on  $\mathbb{R}$ . Furthermore, we have  $\tilde{\Psi}_p(s) \rightarrow +\infty$  when  $|s| \rightarrow \infty$ . Consequently,  $\tilde{\Psi}_p$  admits a unique minimizer  $s_p^* \in \mathbb{R}$  and thus  $\Psi_p$  has a unique minimizer  $\tau_p^* = e^{s_p^*}$  in  $(0, \infty)$ .

Finally, since  $\phi$  is even and strictly convex, we have  $\phi'(x) > 0$  for  $x > 0$  and therefore,

$$\tilde{\Psi}'_p(0) = \sum_{i=1}^d i^{-p} \phi'(p \log i) > 0,$$

Finally,  $\tilde{\Psi}_p$  is strictly convex, thus its unique minimizer satisfies  $s_p^* < 0$  and  $0 < \tau_p^* < 1$  thus

$$0 < \tau_p^* < 1.$$

□

We now give insights on the evolution of  $p \rightarrow \tau_p^*$ . The first-order optimality condition is

$$\Psi'_p(\tau) = \sum_{i=1}^d g'(\tau i^p) = 0.$$

Differentiating the identity  $\Phi(\tau_p^*, p) = 0$  with respect to  $p$  gives

$$\frac{d\tau_p^*}{dp} = -\tau_p^* \frac{\sum_{i=1}^d i^p (\log i) g''(\tau_p^* i^p)}{\Psi''_p(\tau_p^*)}.$$

By strict convexity of  $\phi$  (see the above proof), we get that  $\Psi''_p(\tau_p^*) > 0$  and since  $\tau_p^* > 0$ :

$$\text{sign}\left(\frac{d\tau_p^*}{dp}\right) = -\text{sign}\left(\sum_{i=1}^d i^p (\log i) g''(\tau_p^* i^p)\right).$$

The sign of the above sum is however difficult to follow analytically. Figure G.1 plots the evolution of  $\tau_p^*$  and its derivative  $\frac{d\tau_p^*}{dp}$  with respect to  $p$ , for different values of  $d$ . Note that, across very large  $d$ , we get  $\frac{d\tau_p^*}{dp} < 0$  and thus  $\tau_p^*$  is decreasing for  $p \lesssim 0.9$ .

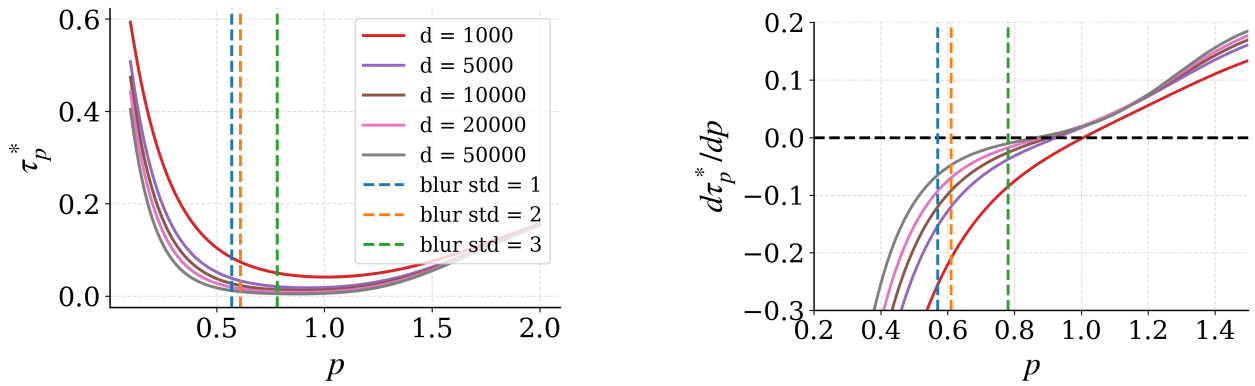


Figure G.1: Evolution of the minimizer  $\tau_p^*$  of  $\Psi_p(\tau)$  (75) w.r.t  $p$  (left) and of its derivative  $\frac{d\tau_p^*}{dp}$  w.r.t  $p$  (right). The plot is done for different values of the dimension  $d$  appearing on the sum. We also draw vertical lines for the values of  $p$  we got for the posterior sampling experiment detailed in Section 5 (for this experiment  $d = 12288$ ).

**Relation with the posterior sampling experiment** In the posterior sampling experiment of Figure 2, the fitted power-law exponents are  $p \approx 0.57, 0.61,$  and  $0.83$  for the three blur levels (see the table in Figure 2). Figure G.1 shows that, for  $d = 12288$  and throughout this range of  $p$ , the minimizer  $\tau_p^*$  decreases as  $p$  increases, equivalently  $\frac{d\tau_p^*}{dp} < 0$ . Since Proposition 3 gives  $c_\eta^* = \lambda_{\max}\tau_p^*$ , this implies that the normalized optimum  $c_\eta^*/\lambda_{\max} = \tau_p^*$  also decreases with  $p$  and, for fixed  $\lambda_{\max}$ , so does  $c_\eta^*$ . This is consistent with Figure 2 (bottom), where the minimizer of the curves plotted against  $c_\eta/\lambda_{\max}$  shifts to the left as the posterior spectrum becomes steeper.

### G.3 Proof of Proposition 4

*Proof.* In the variance exploding case, the first-order mean error vanishes. Starting from (9), the first-order covariance error in one eigendirection of variance  $\lambda$  becomes

$$\Delta^{\Sigma, [1]}(\lambda) = -\lambda \int_0^T \left( \frac{\lambda}{\lambda + \sigma_s^2} \right)^\alpha \left[ \frac{d}{ds} \left( \frac{\sigma_s \dot{\sigma}_s}{\lambda + \sigma_s^2} \right) + (1 - 2\alpha - \alpha^2) \left( \frac{\sigma_s \dot{\sigma}_s}{\lambda + \sigma_s^2} \right)^2 \right] ds. \quad (76)$$

The one-dimensional leading order Fréchet error is proportional to  $\Delta^{\Sigma, [1]}(\lambda)^2$ , so it is minimized as soon as  $\Delta^{\Sigma, [1]}(\lambda) = 0$ . We therefore look for a schedule that cancels the full integrand in (76). Define

$$B_t(\lambda) := \frac{\sigma_t \dot{\sigma}_t}{\lambda + \sigma_t^2}, \quad q_\alpha := 1 - 2\alpha - \alpha^2.$$

Then (76) rewrites as

$$\Delta^{\Sigma, [1]}(\lambda) = -\lambda \int_0^T \left( \frac{\lambda}{\lambda + \sigma_s^2} \right)^\alpha \left( \dot{B}_s(\lambda) + q_\alpha B_s(\lambda)^2 \right) ds.$$

Since  $\left( \frac{\lambda}{\lambda + \sigma_t^2} \right)^\alpha > 0$ , cancelling the full integrand in (76) is equivalent to

$$\dot{B}_t(\lambda) + q_\alpha B_t(\lambda)^2 = 0. \quad (77)$$

If  $q_\alpha = 0$ , then  $B_t(\lambda)$  is constant. Since

$$\frac{d}{dt} \log \left( 1 + \frac{\sigma_t^2}{\lambda} \right) = 2B_t(\lambda),$$

the function  $\log(1 + \sigma_t^2/\lambda)$  is affine, and the boundary condition  $\sigma_T = \sigma_{\max}$  gives

$$1 + \frac{(\sigma_t^*)^2}{\lambda} = \left( 1 + \frac{\sigma_{\max}^2}{\lambda} \right)^{t/T}.$$

Hence

$$(\sigma_t^*)^2 = \lambda \left[ \left( 1 + \frac{\sigma_{\max}^2}{\lambda} \right)^{t/T} - 1 \right].$$

Now, if  $q_\alpha \neq 0$ , define

$$P_t(\lambda) := \left( 1 + \frac{\sigma_t^2}{\lambda} \right)^{q_\alpha/2}.$$

Since  $\dot{P}_t(\lambda) = q_\alpha B_t(\lambda) P_t(\lambda)$ , condition (77) rewrites as

$$\ddot{P}_t(\lambda) = 0,$$

i.e.  $P_t(\lambda)$  affine. Using the boundary conditions:

$$P_0(\lambda) = 1, \quad P_T(\lambda) = \left(1 + \frac{\sigma_{\max}^2}{\lambda}\right)^{q_\alpha/2},$$

we get

$$P_t^*(\lambda) = 1 + \frac{t}{T} \left( \left(1 + \frac{\sigma_{\max}^2}{\lambda}\right)^{q_\alpha/2} - 1 \right).$$

and in terms of  $\sigma_t$ :

$$(\sigma_t^*)^2 = \lambda \left[ \left(1 + \frac{t}{T} \left( \left(1 + \frac{\sigma_{\max}^2}{\lambda}\right)^{q_\alpha/2} - 1 \right) \right)^{2/q_\alpha} - 1 \right]. \quad (78)$$

□

**Remark 3.** Note that the above  $\sigma_t^*$  is obtained by canceling the integrand from the first-order covariance error (9) and not using the simplification (11) obtained under  $\sigma_{\max} \rightarrow \infty$  using Assumption 1(ii). Indeed, as  $t \rightarrow 0$ , the above solution (78) behaves as  $\sigma_t = O(\sqrt{t})$  and thus does not satisfy the assumption  $\xi_t = \dot{\sigma}_t \sigma_t \rightarrow 0$ .

#### G.4 Optimal noise schedule for VP

**Proposition 9** (Single-eigendirection optimal noise schedule for VP). *With the rescaling  $\eta_t = \left(\frac{c}{c + \sigma_t^2}\right)^{1/2}$ ,  $\mu_{\text{data}} = 0$  and  $\alpha = 0$ , the following schedule cancels the first-order one-dimensional Fréchet error:*

$$\sigma_t^*(\lambda)^2 = \frac{c\lambda(1 - z_t^2)}{\lambda z_t^2 - c}, \quad z_t := 1 + \frac{t}{T} \left( \sqrt{\frac{c(\lambda + \sigma_{\max}^2)}{\lambda(c + \sigma_{\max}^2)}} - 1 \right).$$

*Proof.* Choose a constant  $c > 0$  and set

$$\eta_t = \left(\frac{c}{c + \sigma_t^2}\right)^{1/2}.$$

Assume  $\alpha = 0$ . In one dimension, the centered first-order Fréchet error is proportional to  $\Delta^{\Sigma, [1]}(\lambda)^2$ , so it is minimized when  $\Delta^{\Sigma, [1]}(\lambda) = 0$ . For this rescaling family,

$$A_t = -\frac{\sigma_t \dot{\sigma}_t}{c + \sigma_t^2}, \quad B_t(\lambda) = \frac{\sigma_t \dot{\sigma}_t}{\lambda + \sigma_t^2}.$$

Proposition 1 then gives

$$\Delta^{\Sigma, [1]}(\lambda) = -\lambda \int_0^T \left( \dot{A}_s + \dot{B}_s(\lambda) + (A_s + B_s(\lambda))^2 \right) ds.$$

Define

$$z_t := \sqrt{\frac{c(\lambda + \sigma_t^2)}{\lambda(c + \sigma_t^2)}}.$$

Then

$$\frac{\dot{z}_t}{z_t} = A_t + B_t(\lambda).$$

Therefore

$$\Delta^{\Sigma, [1]}(\lambda) = -\lambda \int_0^T \frac{\ddot{z}_s}{z_s} ds.$$

Hence cancelling the full integrand is equivalent to

$$\ddot{z}_t = 0.$$

Therefore  $z_t$  is affine. Using  $\sigma_0 = 0$  and  $\sigma_T = \sigma_{\max}$  yields

$$z_t^* = 1 + \frac{t}{T} \left( \sqrt{\frac{c(\lambda + \sigma_{\max}^2)}{\lambda(c + \sigma_{\max}^2)}} - 1 \right) = z_t.$$

Since

$$z_t^2 = \frac{c(\lambda + \sigma_t^2)}{\lambda(c + \sigma_t^2)},$$

solving for  $\sigma_t^2$  gives

$$(\sigma_t^*)^2 = \frac{c\lambda(1 - z_t^2)}{\lambda z_t^2 - c}.$$

When  $\sigma_{\max} = \infty$ , this reduces to

$$z_t = 1 + \frac{t}{T} \left( \sqrt{\frac{c}{\lambda}} - 1 \right).$$

Finally, when  $\lambda = c$ , one has  $z_t \equiv 1$ , hence  $\Delta^{\Sigma, [1]}(c) = 0$  for every schedule.  $\square$

**Remark 4.** Note again that the above  $\sigma_t^*$  is obtained by canceling the integrand from the first-order covariance error (9) and not using the simplification (11) obtained under  $\sigma_{\max} \rightarrow \infty$  using Assumption 1(ii). As for VE, as  $t \rightarrow 0$ , the above solution (78) behaves as  $\sigma_t = O(\sqrt{t})$  and thus does not satisfy the assumption  $\xi_t = \dot{\sigma}_t \sigma_t \rightarrow 0$ .

## H On the relation with Lipschitz constant optimization [Chen et al. \[2025\]](#)

To control the discretization error of ODE diffusion sampling ( $\alpha = 0$ ), [Chen et al. \[2025\]](#) proposed optimizing parameters by minimizing an average squared local Lipschitzness of the drift along the trajectory:

$$\min \int_0^T \mathbb{E} \left[ \|\nabla v_s(Y_s)\|^2 \right] ds. \quad (79)$$

**Connection with the general weak error formula.** The objective (79) is a natural surrogate for our weak error expansion (4). Indeed, defining

$$L_s(Y_s) := \|\nabla v_s(Y_s)\|,$$

we have the pointwise bounds

$$\|(v_s \cdot \nabla)v_s(Y_s)\| \leq L_s(Y_s) \|v_s(Y_s)\|, \quad \|J_{t,s}(Y)\| \leq \exp\left(\int_s^t L_\tau(Y_\tau) d\tau\right).$$

Thus, decreasing the local Jacobian norm can reduce both the local acceleration term and its amplification by the flow.

However, this Lipschitz-type quantity does not capture the time-derivative contribution  $\partial_s v_s$  appearing in the material derivative of the velocity. Moreover, the above inequalities are norm-based upper bounds: they replace the multi-dimensional geometric action of  $\nabla v_s$  and  $J_{t,s}$  by operator-norm estimates. Consequently, the Lipschitz objective may be conservative. In particular, the first-order weak error can vanish even when the local Lipschitz factor is not small.

**Comparison in the Gaussian case.** This distinction becomes even more explicit in the Gaussian setting. For  $\alpha = 0$ , the first-order covariance error in Proposition 1 reads

$$\Delta^{\Sigma, [1]}(\lambda) = -\lambda[A_s + B_s(\lambda)]_0^T - \lambda \int_0^T (A_s + B_s(\lambda))^2 ds.$$

For  $\alpha = 0$ , the linear drift (7) has the form

$$v_t(x) = H_t x + r_t, \quad H_t = U \text{Diag}(\Delta_t^H(\lambda)) U^\top,$$

where

$$\Delta_{T-t}^H(\lambda) = -\frac{\dot{\eta}_t}{\eta_t} - \frac{\dot{\sigma}_t \sigma_t}{\lambda + \sigma_t^2} = -(A_t + B_t(\lambda)).$$

Therefore,

$$\Delta^{\Sigma, [1]}(\lambda) = -\lambda[\Delta_s^H(\lambda)]_0^T - \lambda \int_0^T (\Delta_s^H(\lambda))^2 ds.$$

Under the endpoint conditions in Assumption 1(ii), and in the large terminal-noise regime  $\sigma_T \rightarrow \infty$ , the boundary term vanishes, yielding

$$\Delta^{\Sigma, [1]}(\lambda) = -\lambda \int_0^T (\Delta_s^H(\lambda))^2 ds + o(1).$$

Hence the covariance contribution to the target Fréchet objective (12) becomes

$$\min \sum_i \lambda_i \left( \int_0^T (\Delta_s^H(\lambda_i))^2 ds \right)^2.$$

By contrast, in the Gaussian case the averaged Lipschitz objective (79) reduces to

$$\min \int_0^T \lambda_{\max}(H_s)^2 ds = \min \int_0^T (\Delta_s^H(\lambda_{\min}))^2 ds.$$

Thus, the Lipschitz objective is governed only by the most contractive spectral direction, corresponding to  $\lambda_{\min}$ . Our Fréchet objective, instead, depends on the whole spectrum through the weights  $\{\lambda_i\}$ . In this sense, our criterion is more geometry-aware: it accounts for the full covariance structure rather than only the extremal eigenvalue controlling the operator norm.

# I Experiments

## I.1 Experimental setup

For empirical image sampling, we use the DeepInverse library [Tachella et al., 2025] and the diffusion models from [Karras et al., 2022], trained on CIFAR-10, FFHQ, and ImageNet. The CIFAR-10 model generates  $32 \times 32$  images, whereas the FFHQ and ImageNet models generate  $64 \times 64$  images. The CIFAR-10 and FFHQ models use the NCSN architecture from [Song and Ermon, 2019], while the ImageNet model uses the ADM architecture [Dhariwal and Nichol, 2021].

Each model was trained with a specific rescaling schedule  $\eta_t$ —VE for CIFAR-10 and FFHQ, and VP for ImageNet. However, at each model evaluation, we re-normalize the input and output to match our target rescaling  $\eta_t$ . We assume that the choice of  $\sigma_t$  used during training does not affect the quality of the score estimate. We use  $\sigma_{\max} = 80$  during sampling (which is smaller or equal to the maximum training value).

To estimate FID, we use 30,000 generated images and 30,000 reference images. Uncertainty is reported as 95% bootstrap confidence intervals, computed using 256 resamples of the generated and reference features.

Figure I.1 (left) shows the spectra of the empirical covariance estimated on each dataset.

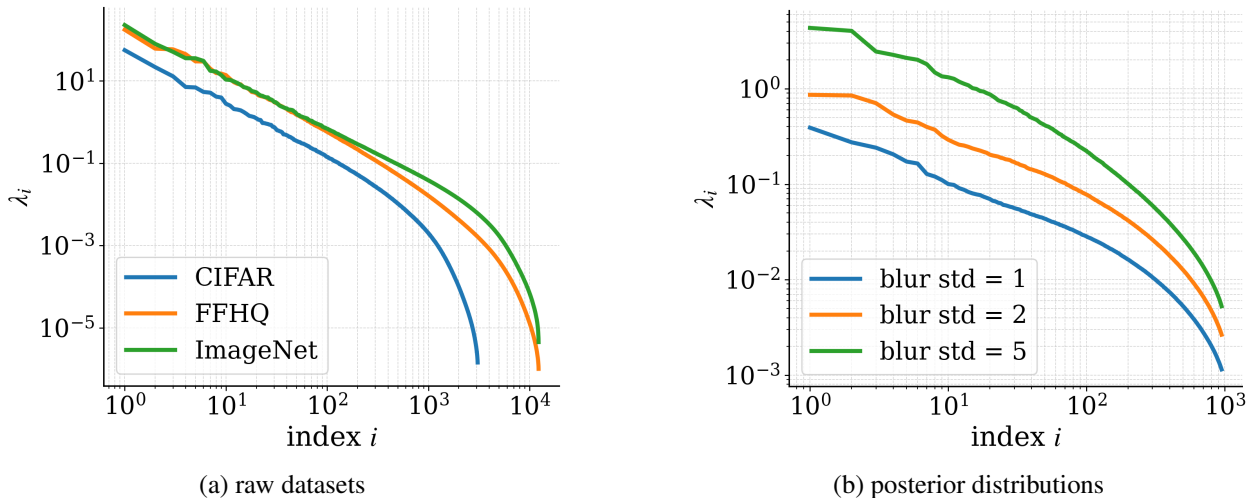


Figure I.1: Empirical covariance spectra used in the experiments: raw image datasets for unconditional sampling (a), and FFHQ posterior distributions obtained with Gaussian blur of varying standard deviation (b).

All experiments are performed on single NVIDIA H100 or A100 GPUs.

## I.2 Posterior sampling experiment

In Section 5, we also consider posterior sampling problems of the form  $p(x | y)$ , where  $y = k * x + w$  is a blurred and noisy observation of an FFHQ image  $x$  (see Figure I.4); here  $k$  is a Gaussian blur kernel with varying standard deviation and  $w$  is Gaussian noise with standard deviation 0.05.

To sample from  $p(x | y)$  without retraining a dedicated posterior model, we use the moment-matching method of Rozet et al. [2024]. At each step of the sampling algorithm (3), in order to compute the score of the posterior

$$\nabla_{x_t} \log p(x_t|y) = \nabla_{x_t} \log p(x_t) + \nabla_{x_t} \log p(y|x_t)$$

using a single pretrained score model for  $\nabla \log p(x_t)$ , this method proposes an approximation of the term

$$\begin{aligned} \nabla_{x_t} \log p(y|x_t) &= \nabla_{x_t} \log \int p(y|x_0)p(x_0|x_t)dx_0 \\ &= \frac{\int p(y|x_0)\nabla_{x_t}p(x_0|x_t)dx_0}{p(y|x_t)} \end{aligned}$$

They propose to approximate  $p(x_0|x_t)$  in the above identity by a Gaussian  $\mathcal{N}(\mathbb{E}[x_0|x_t], \text{Cov}[x_0|x_t])$  with mean and covariance given by the first and second-order Tweedie formulas. See [Rozet et al. \[2024\]](#) for more details. Note that this approximation is exact when the data distribution  $p_{\text{data}}$  is Gaussian. In practice, computing  $\nabla_{x_t} \log p(y | x_t)$  requires at each sampling step to compute the Jacobian of the score model and to compute the inverse of the moment-matched measurement covariance. This covariance inversion is handled only approximately with a single conjugate-gradient step.

Because posterior sampling is substantially more expensive, we estimate the empirical Fréchet distance from 1,000 generated samples. For each compared parameter value ( $c_\eta$  in Section 5), the reference statistics are computed from posterior samples generated with the same parameter  $c_\eta$ , using 500 discretization steps. For the theoretical curves, we use a single reference mean and covariance estimated by aggregating posterior reference samples across the entire  $c_\eta$  range. The corresponding empirical spectra are plotted in [Figure I.1](#) (right).

### I.3 More details on the optimal diffusion-term parameter $\alpha$

We show in [Figure I.2](#) the empirical (a,b) and the theoretical (c) Fréchet errors, decomposed along each eigendirection of the data covariance  $\Sigma_{\text{data}}$ . By [Proposition 1](#), this decomposition is exact in the Gaussian case. For the empirical errors, we project the empirical covariance of the generated samples onto the eigenbasis of the dataset (empirical) covariance. We report this per-eigendirection error using spectra extracted from Inception space in (a) and image space in (b). The theoretical curve in (c) is computed using the empirical dataset spectrum extracted in image space.

The spectral trend predicted by [Proposition 2](#) and illustrated in (c) remains clearly visible in both empirical curves: directions associated with smaller eigenvalues are minimized at smaller values of  $\alpha$ , whereas high-variance directions favor larger values of  $\alpha$ . As expected, the image-space Fréchet error agrees more closely with the theory, since both use the same reference spectrum. Although the Inception-space transformation is not represented in the theory, the same qualitative trend is still observed.

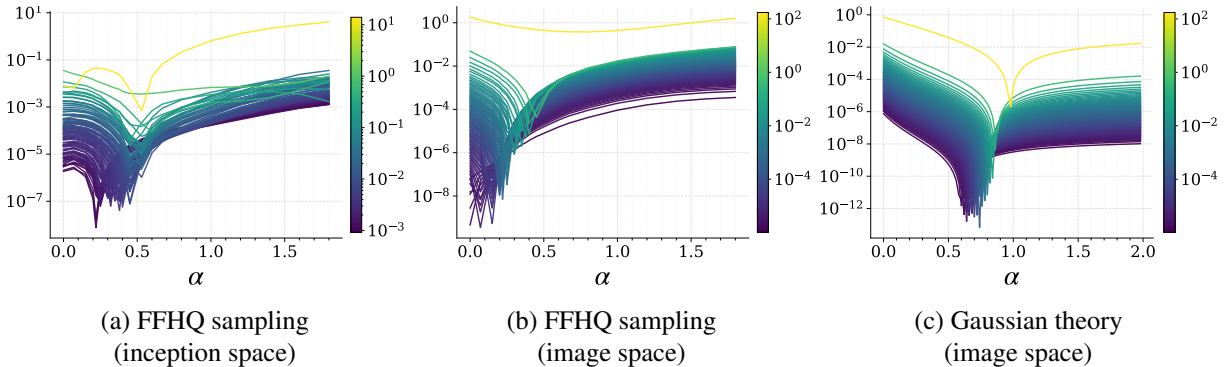


Figure I.2: Per-eigendirection Fréchet error w.r.t  $\alpha$  for FFHQ sampling with VE and  $K = 100$ . Empirical errors are projected onto the data covariance eigenbasis in Inception space (a) and image space (b); Gaussian theory is shown in image space (c). Colors indicate eigenvalues  $\lambda_i$ .

Figure I.3 shows examples of FFHQ samples generated with  $K = 100$  steps. Each column uses a different  $\alpha$  and each row uses the same random seed. Note that  $\alpha$  gives over-smoothed images that look close to the mean of the FFHQ dataset. Increasing  $\alpha$  increases variability and eventually creates visual artifacts for large  $\alpha$ . As explained in Section 5, this visual behavior can be explained by our first-order Gaussian theoretical error: using Proposition 1 the generated variance along an eigendirection  $\lambda$  is:

$$\text{Var}_\lambda(Y_K) = \lambda + \gamma \Delta^{\Sigma, [1]}(\lambda, \alpha) + o(\gamma)$$

For VE, using (10),  $\Delta^{\Sigma, [1]}(\lambda, \alpha)$  is non-decreasing in  $\alpha$ , negative for  $0 \leq \alpha < 1$  and positive for  $\alpha > 1$ . Thus, we get that  $\alpha = 0$  minimizes the generated variance  $\text{Var}_\lambda(Y_K)$  in every direction  $\lambda$ , and thus produces samples that are closer to the mean.



Figure I.3: FFHQ samples for increasing  $\alpha$  with VE and  $K = 100$  steps. Small  $\alpha$  yields smoother, mean-seeking samples, while larger  $\alpha$  increases variability.

#### I.4 Variance Exploding with $\alpha = 0$ is adequate for (posterior) mean estimation

The above observation can be particularly insightful for posterior mean estimation. In the context of image inverse problems, diffusion models can be used to sample from conditional distributions  $p(x|y)$  where  $y$  is the observed degraded image. In this situation, the goal is often to estimate  $\mathbb{E}[x|y]$  rather than sampling from the full posterior. This mean is better estimated by averaging when samples concentrate as much as possible around it. In this section, we show that one can exploit the discretization error to make the samples collapse toward  $\mu_{\text{data}}$ , i.e., to minimize

$$\mathcal{V}_K(\alpha) := \mathbb{E} \|\hat{Y}_K - \mu_{\text{data}}\|^2 = \text{Tr}(\hat{\Sigma}_K) + \|\hat{\mu}_K - \mu_{\text{data}}\|^2.$$

Note that  $\mathcal{V}_K$  combines the effect of the residual spread of the sampled law around its own mean and the bias of the sampled mean relative to the target mean. Under the Gaussian data assumption, using the notations of

Proposition 1, we get the following expansion:

$$\mathcal{V}_K = \text{Tr}(\Sigma_{\text{data}}) + \gamma \sum_{i=1}^d \Delta^{\Sigma, [1]}(\lambda_i) + \gamma^2 \left[ \sum_{i=1}^d \Delta^{\mu, [1]}(\lambda_i)^2 (U^\top \mu_{\text{data}})_i^2 + \sum_{i=1}^d \Delta^{\Sigma, [2]}(\lambda_i) \right] + O(\gamma^3). \quad (80)$$

Equation (80) shows that, when the above first and second order coefficients are negative, discretization error (i.e. using a positive stepsize  $\gamma$ ) can reduce the distance to the mean. At first order in  $\gamma$ , this distance is only controlled by the covariance error, and the mean error contributes only at order  $\gamma^2$ . At first order, the parameters that minimize  $\mathcal{V}_K$  are thus those that minimize the total first-order covariance correction  $\sum_{i=1}^d \Delta^{\Sigma, [1]}(\lambda_i)$ .

In the Variance Exploding case, (10) shows that the first-order covariance correction is minimized at  $\alpha = 0$ . Hence, within the VE family, the deterministic reverse ODE is the best first-order choice for concentrating samples around the data mean. Compared to Variance Preserving (VP), for a fixed noise schedule, if  $\lambda_i \leq 1$  for all  $i$ , then direct comparison of (11) and (68) shows that VE with  $\alpha = 0$  yields a larger first-order covariance correction than any VP choice  $\alpha \geq 0$ , and therefore a smaller first-order value of  $\mathcal{V}_K$ . Moreover, for VE (and not for VP), the mean error  $\Delta^{\mu, [1]} = 0$  which also cancels the second-order mean effect.

To illustrate this, we perform deblurring posterior sampling using the Moment Matching method described in Section I.2. Figure I.4 shows posterior samples obtained with VE, using  $K = 50$  discretization steps and different values of  $\alpha$ . For small values of  $\alpha$ , the variability across samples is low: the samples are concentrated around the estimated posterior mean. In contrast, larger values of  $\alpha$  produce substantially more variability across samples. Thus,  $\alpha = 0$  makes it possible to estimate the posterior mean with very few samples. However, this posterior mean tends to be smoother than the original image, which is a classical limitation of posterior-mean estimation in image restoration [Blau and Michaeli, 2018, Kawar et al., 2021].

### I.5 More details on the optimal rescaling schedule $\eta_t$

Figure I.5 shows the empirical (a,b) and the theoretical (c) Fréchet errors from Figure 2 (top), but here decomposed along each eigendirection of the data covariance  $\Sigma_{\text{data}}$ . See Section I.3 for more details on the per- $\lambda_i$  computations.

On the theoretical Figure (c), for each eigendirection, the curve is minimized near  $c_\eta \approx \lambda_i$ , consistently with the first-order cancellation condition (13) at  $\alpha = 0$ . Thus, large-variance directions favor larger values of  $c_\eta$ , while low-variance directions favor smaller ones. This spectral ordering is also visible in the empirical decompositions (a,b), although the curves are noisier in Inception space.

This non-uniform behavior across eigendirections also explains the evolution of the optimal  $c^*$  observed Figure 2 for an anisotropic spectrum: datasets with larger effective scale favor larger optimal  $c_\eta$ , while a steeper spectrum shifts the normalized optimum  $c_\eta/\lambda_{\text{max}}$  toward smaller values.

### I.6 More details on the optimal noise schedule $\sigma_t$

Figure I.6 complements the discussion in Section 5 by showing the dependence on the polynomial exponent  $\beta$  together with its spectral decomposition. First, note the strong resemblance between the empirical and theoretical curves. In particular, both empirical and theoretical errors decrease sharply when moving away from the nearly linear schedule  $\beta = 1$ , and then exhibit a broad minimum at moderate exponents. The location of this minimum changes only mildly across CIFAR-10, FFHQ, and ImageNet, matching the prediction of the Gaussian theoretical curves. Figures (c) and (d) also illustrate the discussion in Section 5 at the eigendirection level. For moderately large  $\beta$ , the per-eigendirection error varies only mildly across different  $\lambda_i$  values.

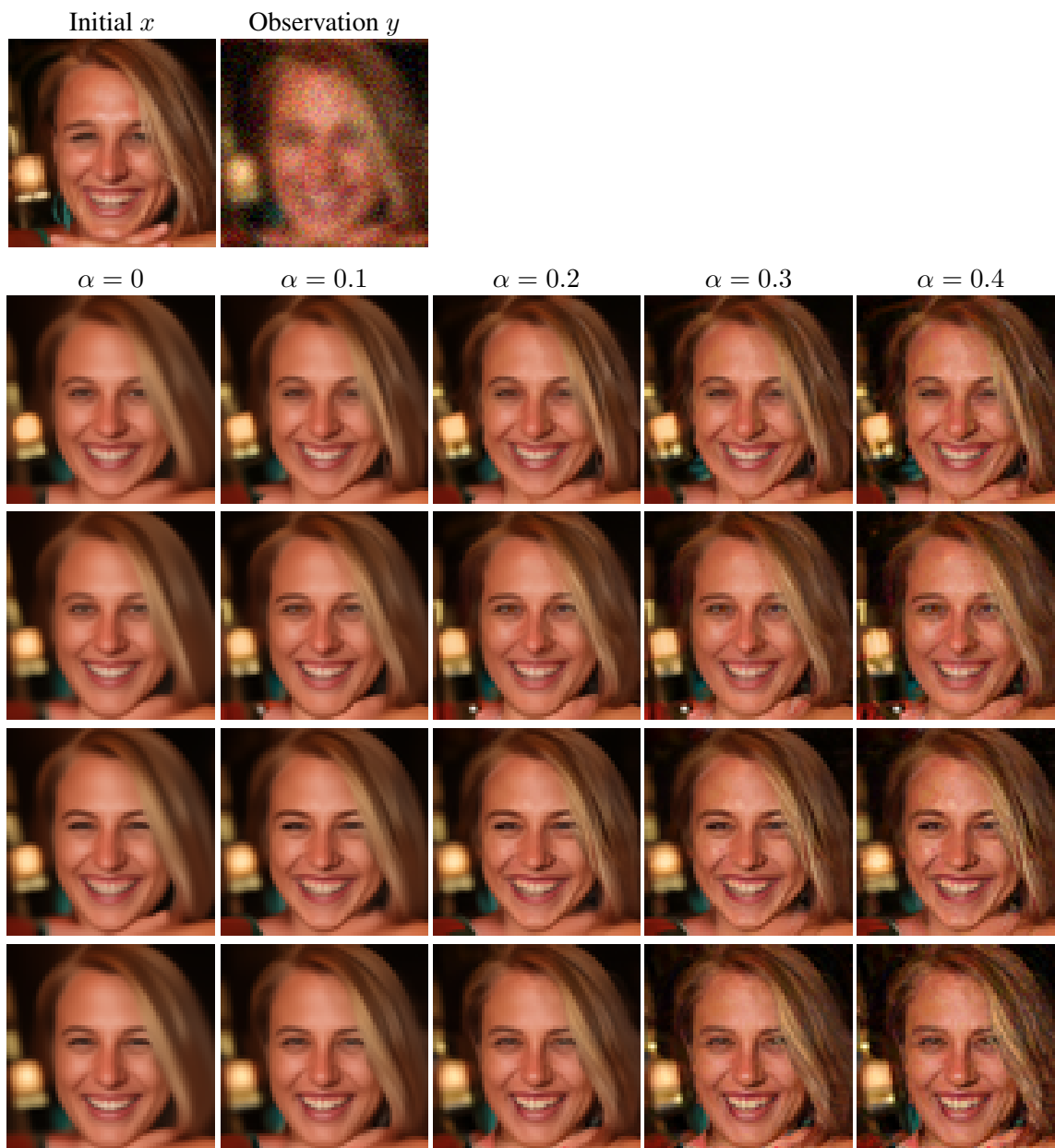


Figure I.4: Deblurring posterior samples for increasing  $\alpha$  with VE and  $K = 50$  steps. Each row corresponds to a different seed. The observation has been obtained by  $y = k * x + w$  with  $k$  a Gaussian blur kernel with standard deviation 1.5 and  $w$  a Gaussian noise with standard deviation 0.05. See Section I.2 for more details on the posterior sampling algorithm.

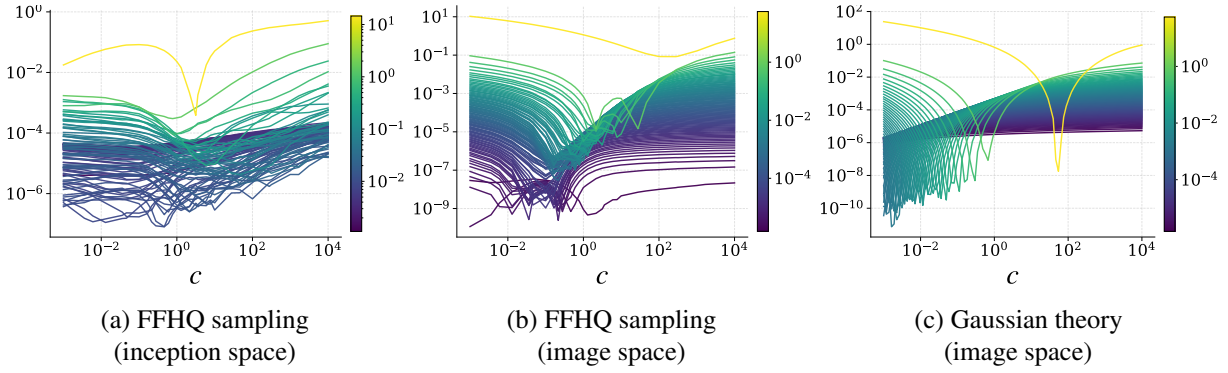


Figure I.5: Per-eigendirection Fréchet error w.r.t  $c_\eta$  for FFHQ sampling with VE and  $K = 100$ . Empirical errors are projected onto the data covariance eigenbasis in Inception space (a) and image space (b); Gaussian theory is shown in image space (c). Colors indicate eigenvalues  $\lambda_i$ .

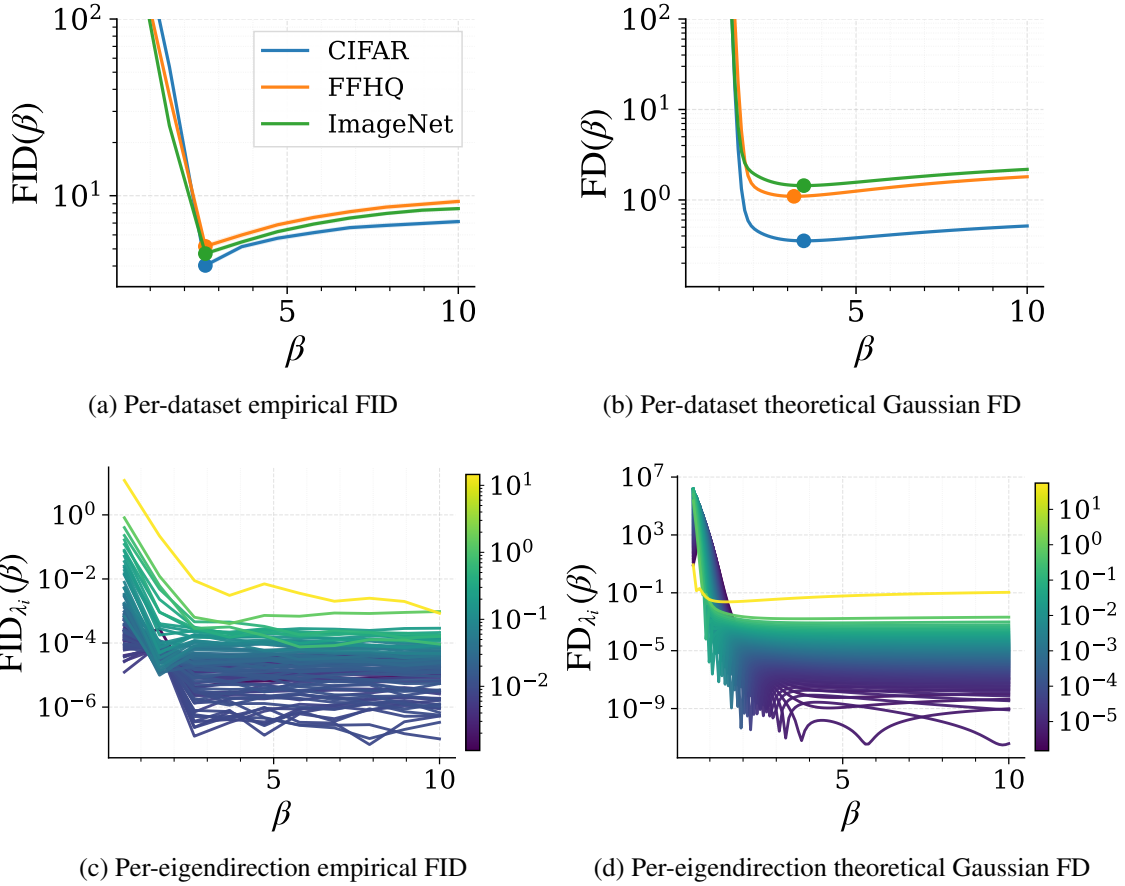


Figure I.6: Discretization error as a function of the polynomial noise exponent  $\beta$  for image sampling across CIFAR-10, FFHQ, and ImageNet, using the variance exploding schedule with  $\alpha = 0.25$  and  $K = 100$  discretization steps: empirical FID in (a) and the corresponding Gaussian theory Fréchet Distance (FD) in (b). We show below the corresponding errors split per eigendirection  $\lambda_i$ .